2012

Spatial variation analysis of salinity to determine fluid flow pathways and reservoir compartmentalization in a deepwater Gulf of Mexico field

William Jacob Daugherty
Louisiana State University and Agricultural and Mechanical College, wdaugh2@tigers.lsu.edu

SPATIAL VARIATION ANALYSIS OF SALINITY TO DETERMINE FLUID FLOW PATHWAYS AND RESERVOIR COMPARTMENTALIZATION IN A DEEPWATER GULF OF MEXICO FIELD

A Thesis

Submitted to the Graduate Faculty of the
Louisiana State University
and Agricultural and Mechanical College
in partial fulfillment of the
requirements for the degree of
Master of Science

in

The Department of Geology and Geophysics

by
William Jacob Daugherty
B.S. Austin Peay State University, 2009
August 2012

DEDICATION

This thesis is first and foremost dedicated to my loving wife Morgan who has been my rock throughout our entire relationship. Without her encouragement and patience I would not have been able to achieve certain goals in my life and I will forever be thankful to her. This thesis is also dedicated to my parents, Bill and Susan Daugherty, who have helped mold me into the man I am today. Without them I would not have the foundation in life that they helped create. Lastly this thesis is dedicated to my professors at Austin Peay State University and Louisiana State University for putting up with me and teaching me the fundamentals of being a great geologist.

ACKNOWLEDGEMENTS

I would like to acknowledge ATP Oil and Gas and TGS for donating the data presented in this thesis. I would also like to thank Clark Walraven, geologist at ATP Oil and Gas, who was able to help me with any and all questions I had regarding the complexities of the study area. I would also like to thank Dr. Jeffrey Nunn, my committee advisor, as well as my committee members Dr. Jeffrey Hanor and Dr. Stephen Sears. Andre Revil was also helpful in the writing of this thesis by providing feedback and answers to questions I had regarding the calculations involved in this study.

TABLE OF CONTENTS

ABSTRACT

Variations in salinity have been documented in previous studies onshore Louisiana in the Wilcox group (Funayama and Hanor 1995) as well as offshore Louisiana on the continental shelf (Bruno and Hanor 2003 and Steen et al. 2011). These studies were conducted using various methods to estimate pore water salinity and make inferences about possible fluid flow pathways and compartmentalization of reservoirs in order to better understand the complex hydrogeology of the Gulf of Mexico. Similar variations in salinity were documented in this study located in a deepwater salt withdrawal minibasin located on the upper slope of the Gulf of Mexico. Data that supported this study included digital well logs, 2D seismic lines and whole core analysis. Using a dual conductance model outlined in Revil et al. (1998) this study was able to calculate salinity from digital gamma ray, deep resistivity and density porosity well logs. This technique allowed for the estimation of salinity where there was well log coverage creating a salinity well log similar to standard well logs used in industry. Variations in salinity were documented between each section of the study area as well in each wellbore and correlated to structures such as salt and faults in order to make inferences about possible fluid flow pathways. Two hydrogeologic regimes, a hydropressured and overpressured regime, were described in each wellbore and illustrated the vertical and lateral variations in salinity across the study area. The hydropressured regime exhibited salinities that were approximately equal to normal marine salinity and the overpressured regime had multiple variations in salinities within each well. These hydrogeologic regimes and their associate salinity profiles are the result of complex fluid migration pathways associated with salt structures and faulting in the Gulf of Mexico.

CHAPTER 1. INTRODUCTION

The salinity of pore fluids has been studied in areas such as the Wilcox onshore Louisiana (Funayama and Hanor 1995) and the continental shelf offshore Louisiana (Bruno and Hanor 2003, Hanor and Mercer 2010, Steen et al. 2011, McCammon 2012) to better understand the source of the fluids and the mechanisms that transport them. Pore fluids for sediments deposited in marine environments, such as those found in this study, should have an original salinity close to seawater at the time of deposition (approximately 35 g/L). However, significant variations in salinity have been observed (Funayama and Hanor 1995, Bruno and Hanor 2003, Steen et al. 2011). These salinities are sometimes as much as ten times normal marine salinity. Mechanisms for fluid flow in the Gulf of Mexico include the dissolution of salt and subsequent brine migration (Bruno and Hanor 2003) and migration of fluids along fault planes (Lin and Nunn 1997). These mechanisms for fluid flow have been documented in offshore studies around salt domes (Nikiel and Hanor 1999, Bruno and Hanor 2003, Steen et al. 2011). The purpose of this study is to document variations in salinity for a deep water field in the Gulf of Mexico to expand on research of the hydrogeology of the Gulf of Mexico from previous studies (Hanor and Mercer 2010, McCammon 2012). A method for estimating salinity from the gamma ray, deep resistivity and density porosity logs (Revil et al. 1998) was used in this study. Core data was used in this study to calculate the cation exchange capacity of clays within the study area as well as quality check the Revil et al. (1998) method of estimating salinity. The use of multiple wellbores across the study area as well as structure contour maps and 2D seismic lines will be used to identify fluid flow pathways and possible compartmentalization of reservoirs.

CHAPTER 2. GEOLOGIC SETTING

2.1. Introduction

The location of this study is in the southwestern corner of the Mississippi Canyon protraction area of the northern Gulf of Mexico (Fig. 1). The wells within the study area are located in approximately 3000 feet of water and were drilled to a total depth of approximately 17,000 ft. in Upper Miocene aged rocks. Well locations are shown in Figure 2. For this study, the wells have been divided into three sections (Figs. 3-5) based on geographic location and proximity to known salt structures at depth. This location was chosen to study the spatial distribution of pore fluid salinity around an allochthonous salt body to better understand the complex hydrogeology of the Gulf of Mexico and make inferences about compartmentalization. This is important to understand the mechanisms of fluid flow around salt structures as well as barriers to flow such as faults or low permeability zones. The exact location of this study area is proprietary.

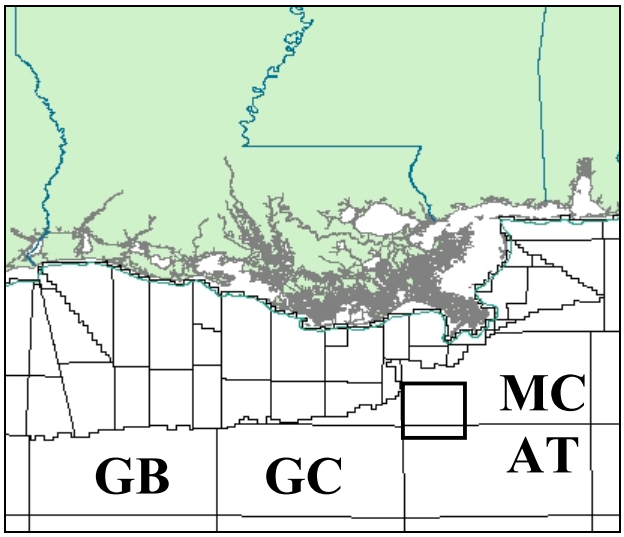

Figure 1. Map of the Gulf of Mexico protraction areas and approximate location of study area (black square). MC=Mississippi Canyon, AT=Atwater Valley, GC=Green Canyon, GB=Garden Banks

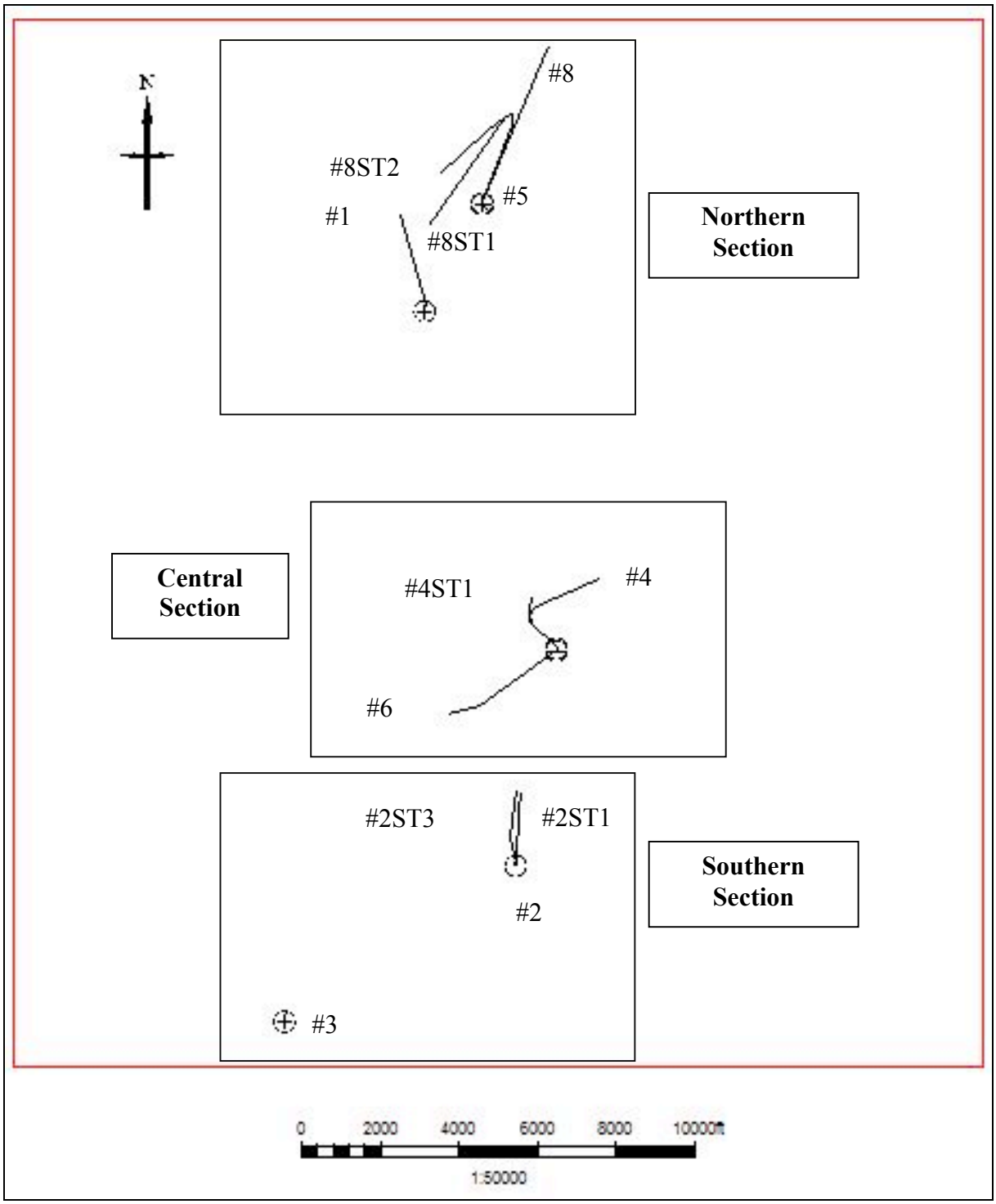

Figure 2. Map showing well locations and the three sections that comprise the study area. Circles with plus sign represent surface location of the well. Black line indicates directional path of the well. Well labels are at the bottom location of the well.

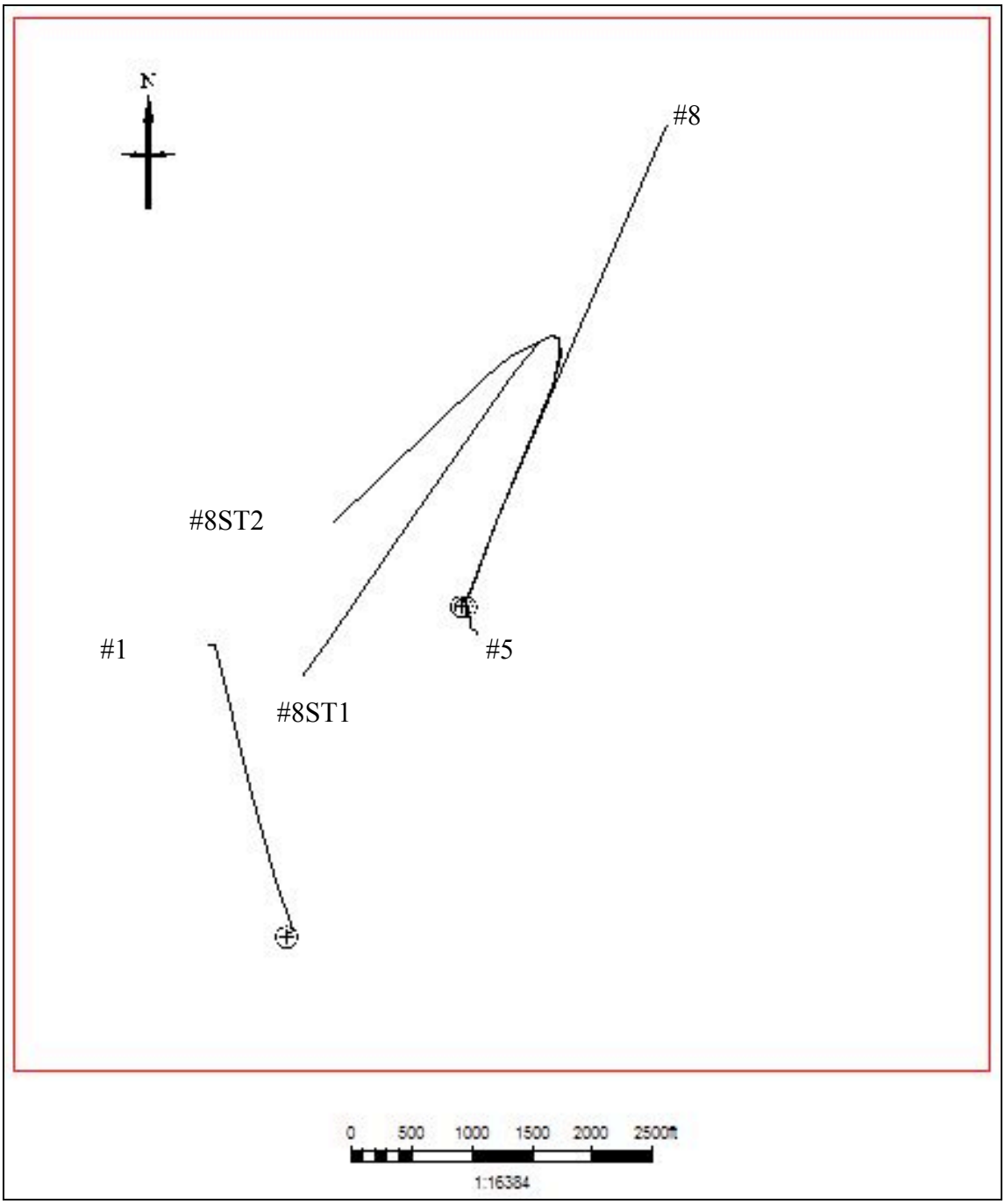

Figure 3. Map of wells in the northern section of the study area Circles with plus sign represent surface location of the well. Black line indicates directional path of the well. Well labels are at the bottom location of the well.

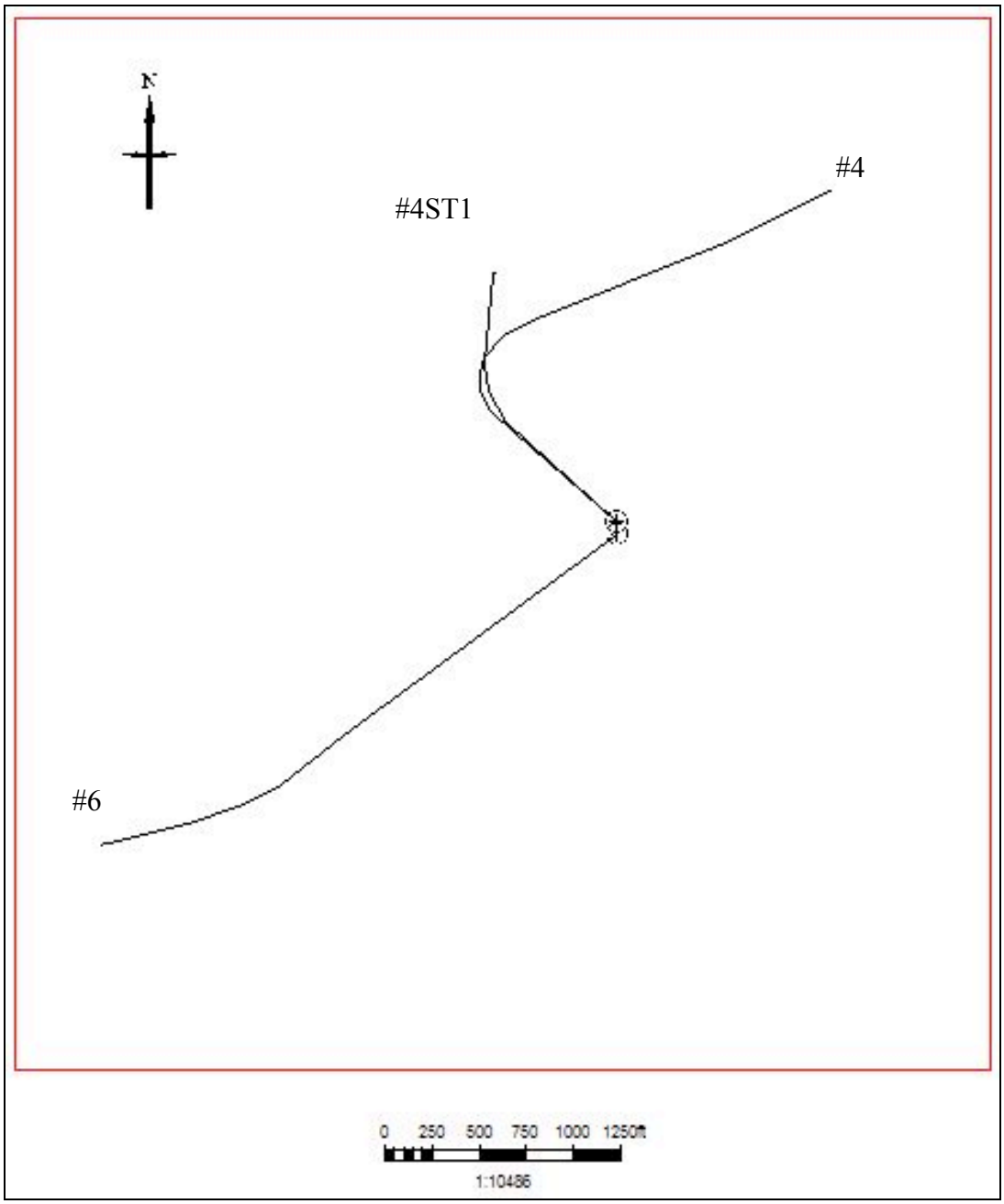

Figure 4. Map of wells in the central section of the study area Circles with plus sign represent surface location of the well. Black line indicates directional path of the well. Well labels are at the bottom location of the well.

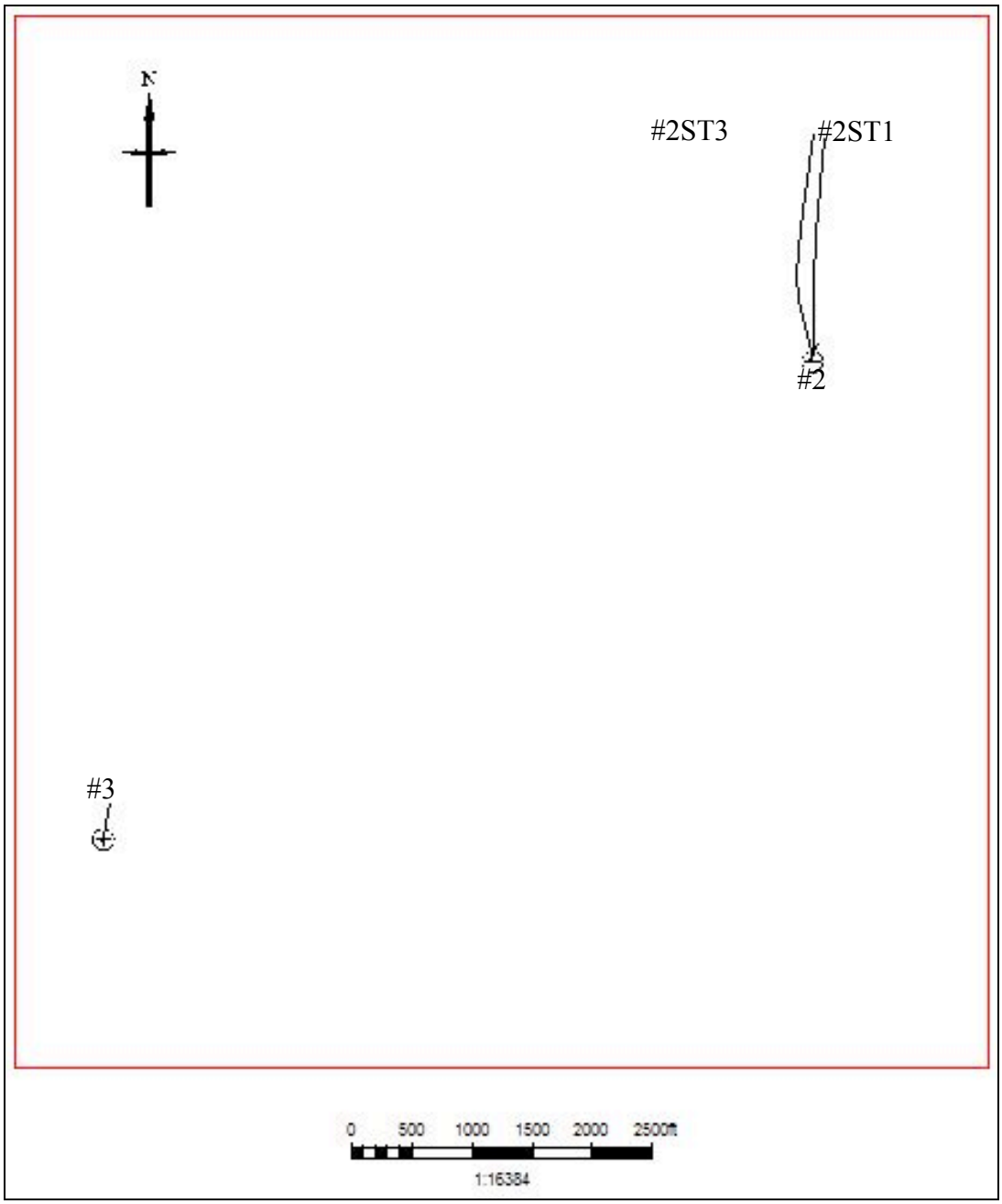

Figure 5. Map of wells in the southern section of the study area Circles with plus sign represent surface location of the well. Black line indicates directional path of the well. Well labels are at the bottom location of the well.

2.2. Gulf of Mexico Basin History

The history of the Gulf of Mexico can be divided into two tectonic phases (Salvador 1987 and Buffler 1991). The first phase (Fig. 6 A) occurred during the Late Triassic when tensional stresses dominated the area that would become the present day Gulf of Mexico as a result of the breakup of the supercontinent Pangea. These tensional stresses created a series of grabens and half grabens that accumulated non-marine sediments from the adjacent horst blocks. The Gulf of Mexico was still an emergent landmass during this time except the western edge where an embayment of the Pacific Ocean existed. Tensional stresses and subsequent sedimentation continued into the Early Jurassic. The Middle Jurassic (Fig. 6 B) saw the formation of the vast evaporite deposits, commonly referred to as the Louann salt, that are associated with the Gulf of Mexico basin. During the Middle Jurassic, the Pacific Ocean extended into the Gulf of Mexico basin where it filled topographic lows created by the graben systems established during the Late Triassic and Early Jurassic. The thickness of the salt layer varies and where it is thickest represents active subsidence of the graben systems established in the Late Triassic (Salvador 1987). Based on reconstructions by Salvador (1987) the original salt thickness ranged from a few meters to over 4000 meters.

The second tectonic phase occurred during the Late Jurassic (Fig. 6 C). Continued rifting of the Gulf of Mexico basin occurred creating oceanic crust and causing the Yucatan platform to rotate and drift towards its current position. The Gulf of Mexico basin also experienced further subsidence, which resulted in occasional influx of Pacific Ocean waters. Access of waters from the Pacific Ocean became restricted during the Late Jurassic just as the connection between the Gulf of Mexico and the Atlantic Ocean was opening. The structural and geographic features of the Gulf of Mexico as seen today were all present by the close of the Jurassic (Salvador 1987).

Primary sedimentation during the Middle Jurassic to Lower Cretaceous consisted of shallow marine carbonate platforms that rimmed the northern Gulf of Mexico basin (Fig. 6 D). During this time interval the deepest part of the basin was subsiding rapidly causing the deposition of deep-water shales and marls that were to become the source rocks for the deep-water Gulf of Mexico (Weimer et al. 1998).

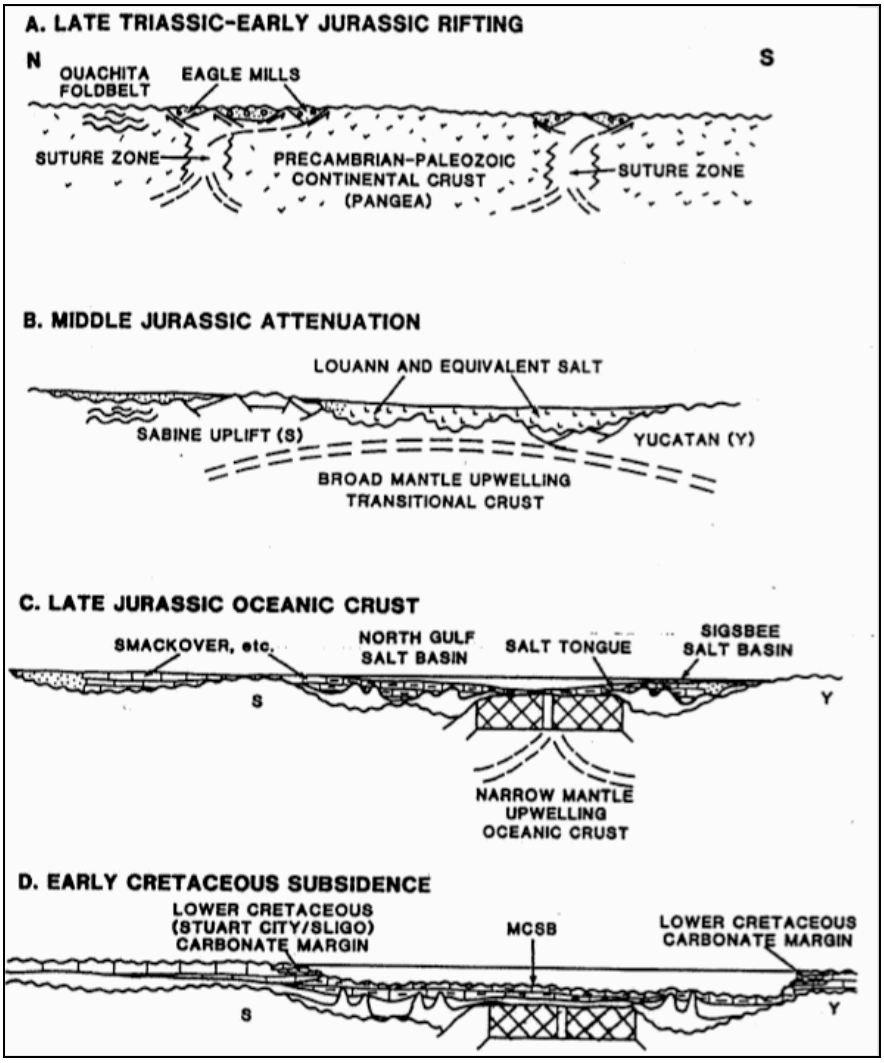

Figure 6. Cross section oriented from north to south depicting the structural evolution of the Gulf of Mexico basin. (from Buffler 1991).

The Gulf of Mexico originated in the Late Triassic due to the breakup of Pangea, but it was Cenozoic deposition that continued the evolution of the basin. According to Galloway et al. (2000), the northern Gulf of Mexico Cenozoic history is interpreted from the influence of eight

sedimentary input systems, shore-zone shelf, slope and basinal systems. The names of the sedimentary input systems are the Norma, Rio Grande, Carrizo, Corsair, Houston, Red River, Central Mississippi and East Mississippi systems and can be seen in figure 7. The eastern and southeastern Gulf of Mexico was primarily deprived of clastic sedimentation therefore carbonate sedimentation dominated. For a full discussion of the Cenozoic depositional history of the Gulf of Mexico the reader is referred to Galloway et al. (2000).

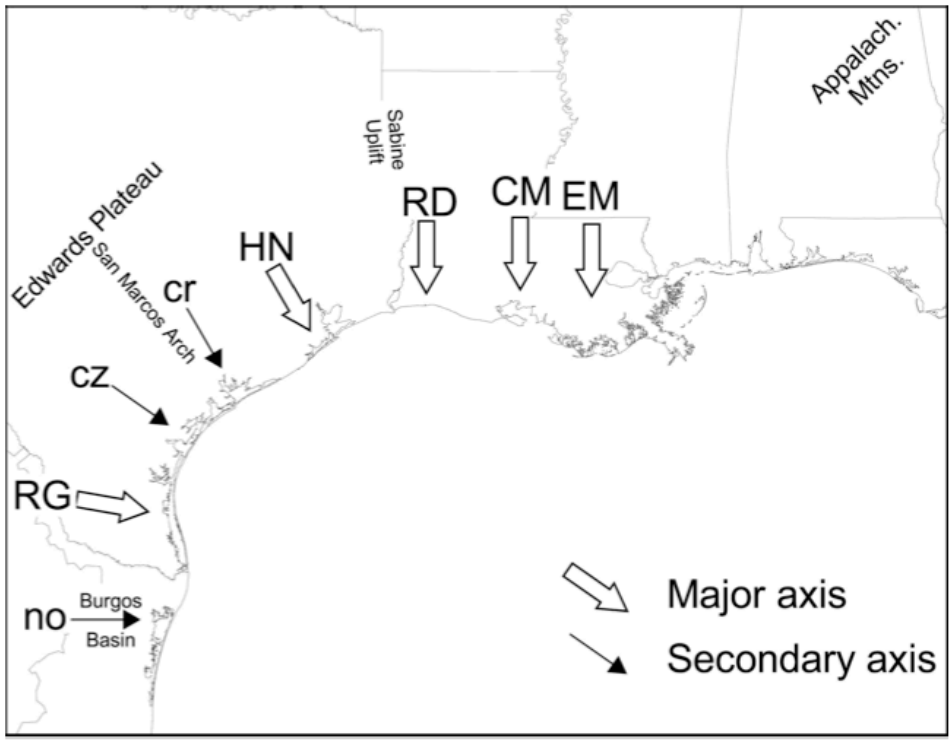

Figure 7: Basin-margin structural features and principal (caps) and secondary (lower case) Cenozoic sediment dispersal axes of the Gulf of Mexico basin: no = Norias; RG = Rio Grande; cz = Carrizo; cr = Corsair; HN = Houston; RD = Red River; CM = Central Mississippi; EM = East Mississippi (from Galloway et al. 2000).

2.3 Study Area Sequence Stratigraphy and Depositional Environments

Within the study area there are approximately 11 depositional sequences that were interpreted using biostratigraphic data from the #5 well. This well is in the northern section of the study area (Fig. 3) in approximately 3000 feet of water. The data included calcareous nannoplankton and foraminifera biostratigraphic datums with abundance and diversity

information for the foraminifera microfossils. This data can be used to infer sequence boundaries and condensed sections, which can then be used to correlate strata between partially isolated minibasins in the Gulf of Mexico (Crews et al. 2000). The nannoplankton and foraminifera datums were assigned ages and placed within their depositional sequences according to Crews et al. (2000) as seen in figure 8. The depositional sequences discussed in this section were picked by this author using a combination of microfossil age and the abundance and diversity curves from the #5 well.

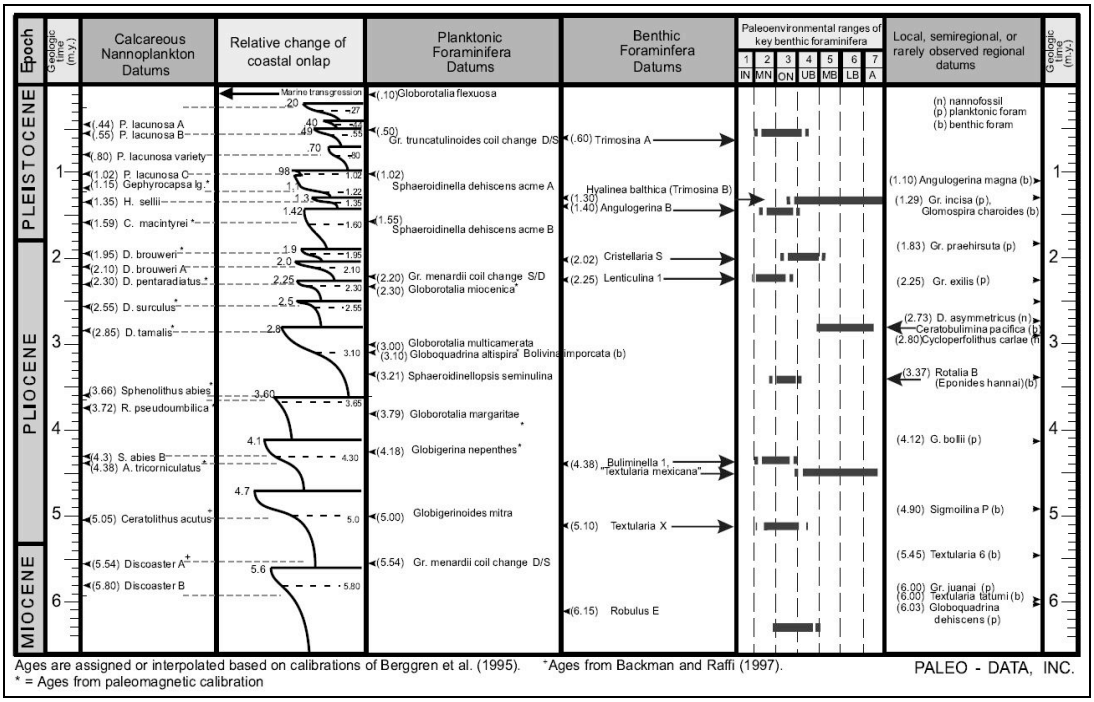

Figure 8. Biostratigraphic datums and coastal onlap curve for the northern Gulf of mexico (from Crews et al. 2000).

The 11 depositional sequences in the study area extend from Late Miocene through Pleistocene with the oldest sequence starting at 5.6 Ma and the youngest at 1.3 Ma. Each sequence represents a period of time when there was a relative fall in sea level (lowstand systems tract), a relative rise in sea level (transgressive systems tract) and a high level of sea level (highstand systems tract) with each tract consisting of predictable facies. These tracts are the fundamental elements of sequence stratigraphy (see Van Wagoner et al. 1988 for details).

During the Pliocene and Pleistocene about one-half of the drainage area of the North American continent deposited sediments into the Gulf of Mexico (Pulham 1993). This caused large accumulations of sediments in some areas and continued the active deformation of the Jurassic Louann Salt. This deformation of the Louann salt created partially isolated salt withdrawal minibasins on the upper slope that became the focus of turbidite depositional systems. These turbidite systems were capable of transporting large amounts of sediment to the upper and lower slope minibasins. Correlation between minibasins can be difficult therefore it is necessary to build a sequence stratigraphic framework in order to properly correlate strata to other parts of the northern Gulf of Mexico (Crews et al. 2000).

In this study area the depositional sequences were interpreted based on foraminifera and calcareous nannoplankton datums in order to give a detailed description of sediment dispersal patterns and depositional environments of the northern Gulf of Mexico upper slope. Well log data is sparse in the 5.6-4.1 Ma sequences therefore it is acknowledged that they are present in the study area, but they are not discussed in detail. The thickest sequence is the 4.10-3.6 Ma sequence representing approximately 2100 ft. of sediment. Interpreted sequence boundaries for this section can be seen in Figure 9. Sequence boundaries were picked based on a low abundance and diversity of microfossils following the approximate position of microfossil abundance and diversity peak, which coincide with condensed sections. Condensed sections in deepwater settings are characterized by abundance and diversity peaks of microfossils due to low amounts of sediment input during sea level highstands.

The interpreted depositional environments associated with these sequences are channel fill sands, overbank deposits and hemipelagic shales (Fig. 10) based on gamma ray signature from previous studies in the Gulf of Mexico (Weimer et al. 1998 Part B Table 2), abundance and

diversity data and core data. The channel fill sands and overbank deposits associated with the main hydrocarbon producing reservoir in this study is interpreted by this author to be part of the levee system of a large depositional turbidite channel located in the #3 well (Fig. 11). Log responses for depositional turbidite channels exhibit a bell shaped fining upwards gamma ray log response and overbank deposits have a high frequency "serrated" log response due to alternating sands and shales.

The 3.6-1.42 Ma sequences are the thinnest sequences in well #5 seen in figure 12. These five depositional sequences correspond to an approximately 500 foot section in the #5 well that exhibits a lower gamma ray signature. This is due to high amounts of calcareous nannofossils associated with multiple sequences and their respective condensed sections being stacked over a short interval (Crews et al. 2000). This interval correlates to a similar interval recognized in Green Canyon (Crews et al. 2000) and is interpreted in this study as a series of stacked sequences due to reduced rates of sedimentation associated with the main deltaic depocenter shifting further to the west (Pulham 1993). The 1.42-1.3 Ma sequence boundary is considerably thicker than the previous stacked sequences suggesting that by this time the main deltaic depocenter shifted back to the east feeding turbidite systems that delivered sediment to the upper slope. Younger sequences were not interpreted due to the lack of biostratigraphic data.

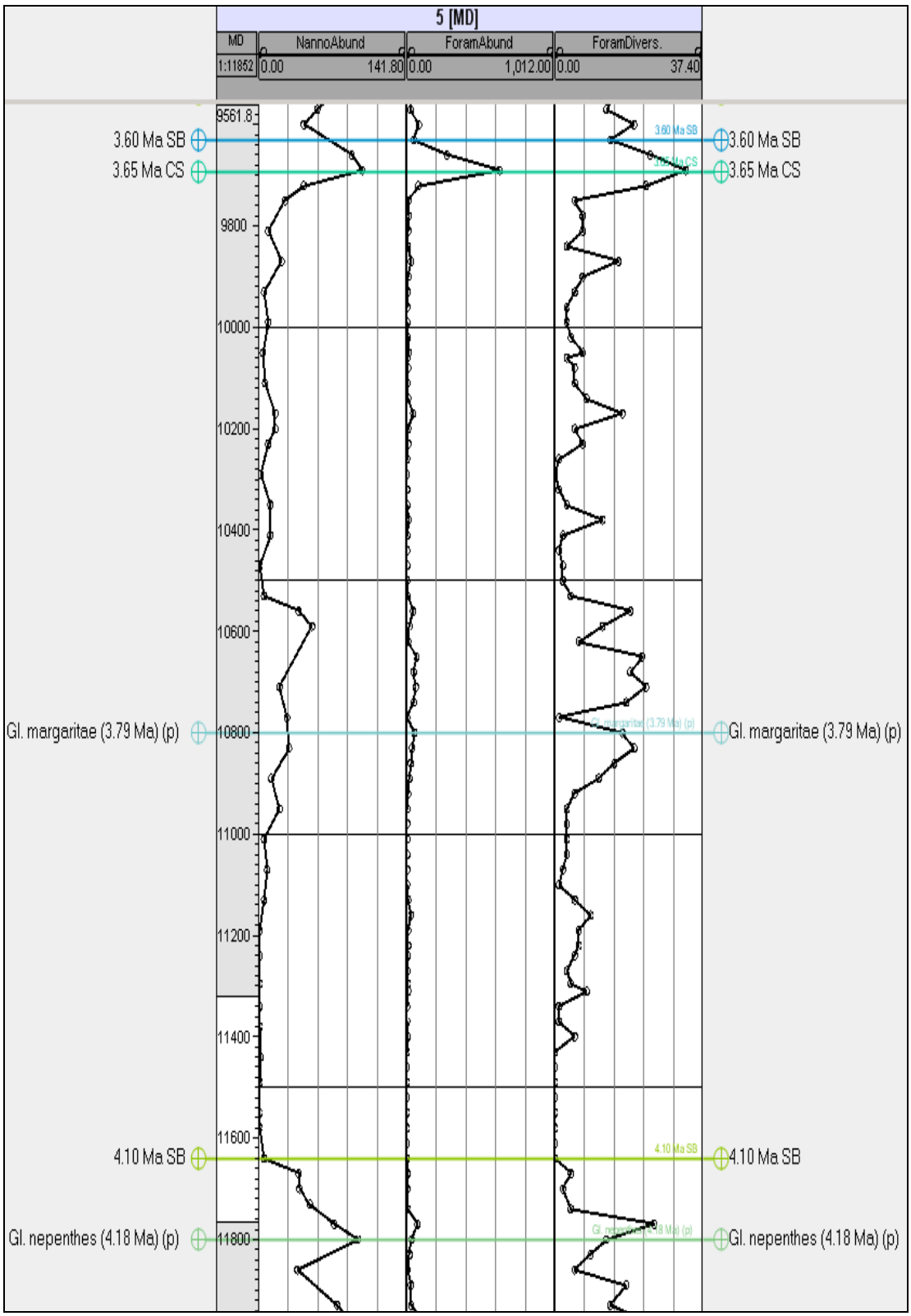

Figure 9. Well #5 4.10-3.60 Ma depositional sequence. Curves from left to right are nannofossil abundance, foraminifera abundance and foraminifera diversity. SB=sequence boundary, CS=condensed section, (p)= planktonic foraminifera datum.

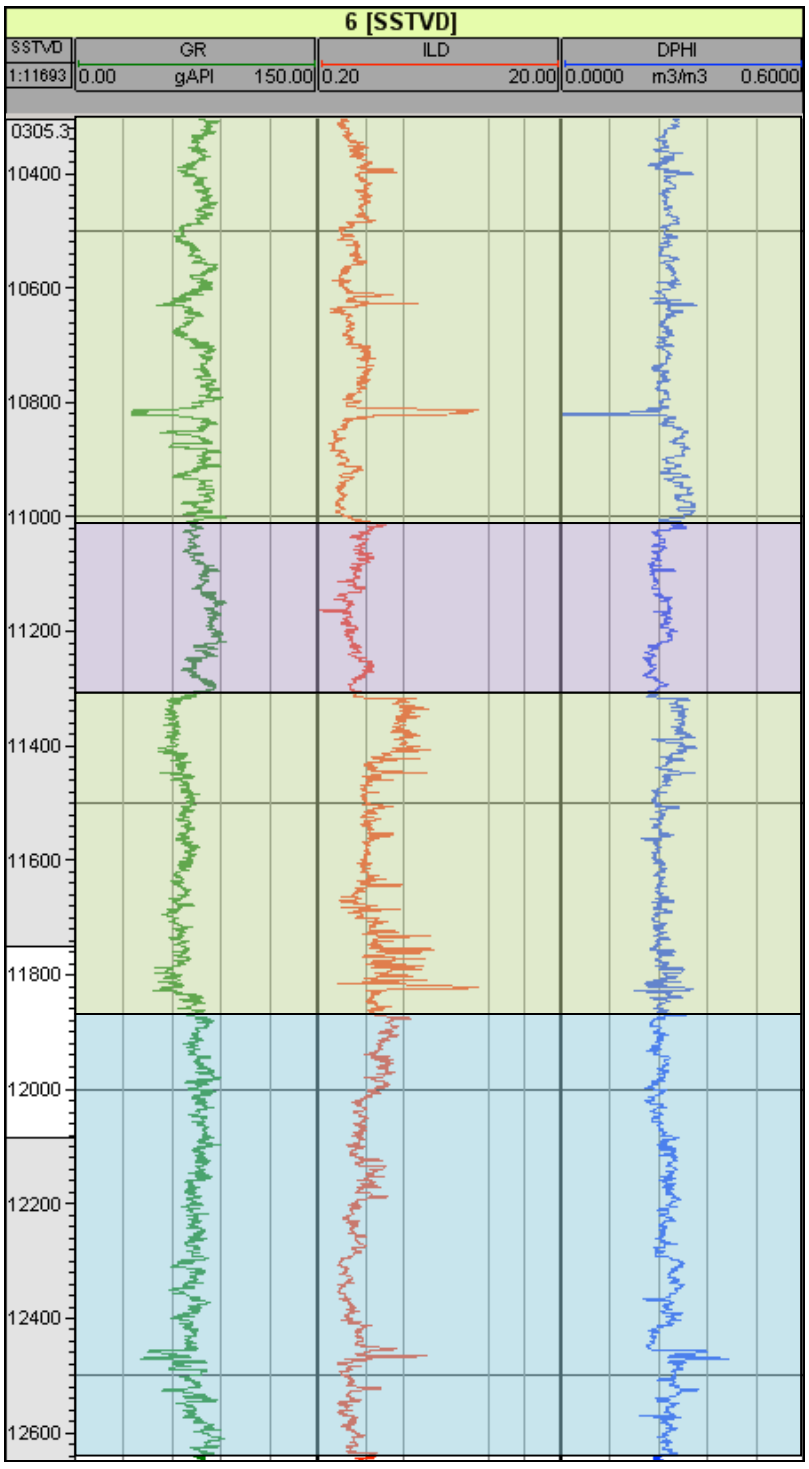

Figure 10. Example of well log interpretation of depositional environments for the #6 well. Well logs from left to right are gamma ray, deep resistivity and density porosity. Channel fill and overbank deposits (green box), Slope failure mudstones (purple box), Hemipelagic shales and overbank deposits (blue box).

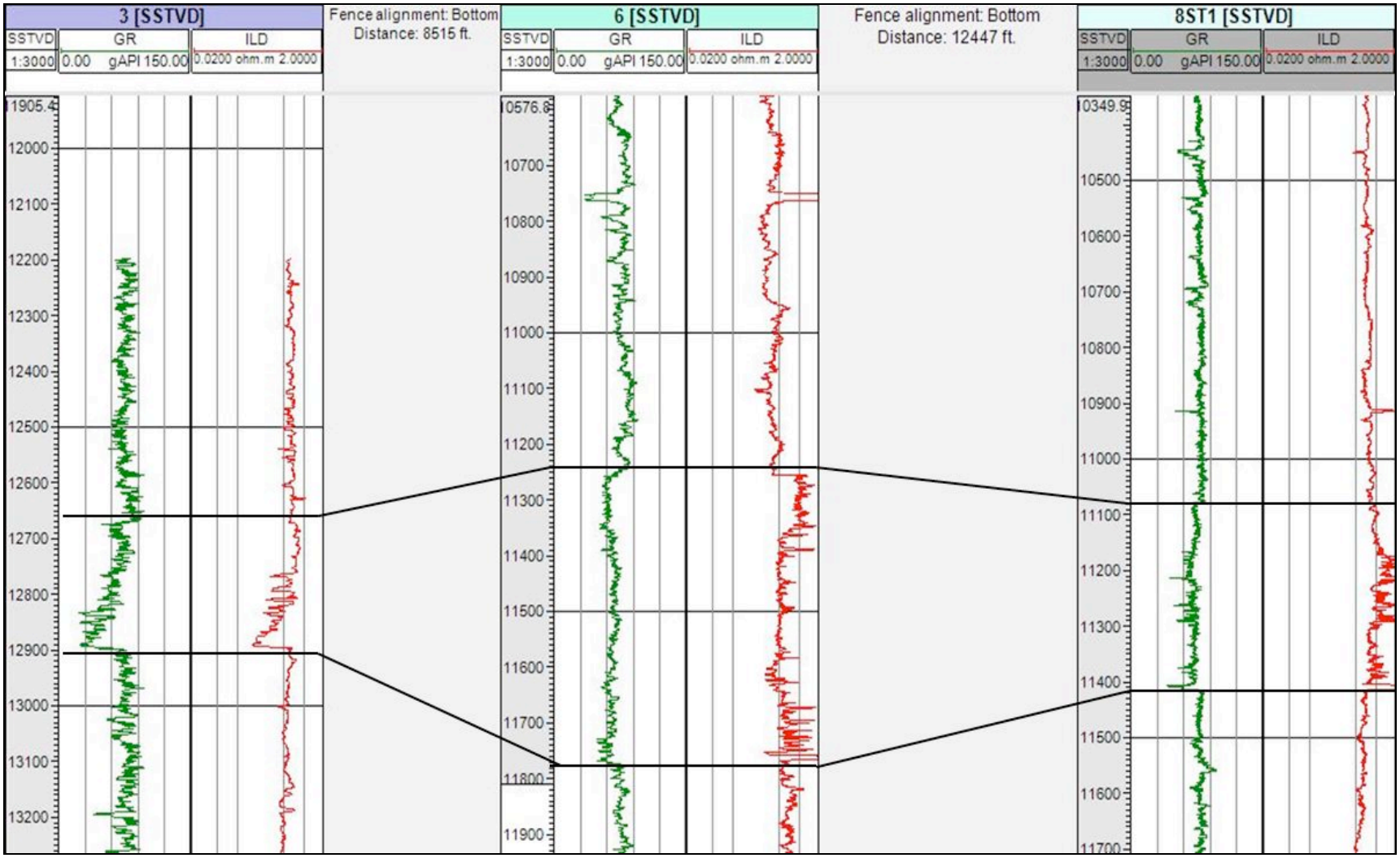

Figure 11. Well log cross section illustrating the depositional turbidite channel in the #3 well and associated overbank deposits in wells #6 and #8ST1.

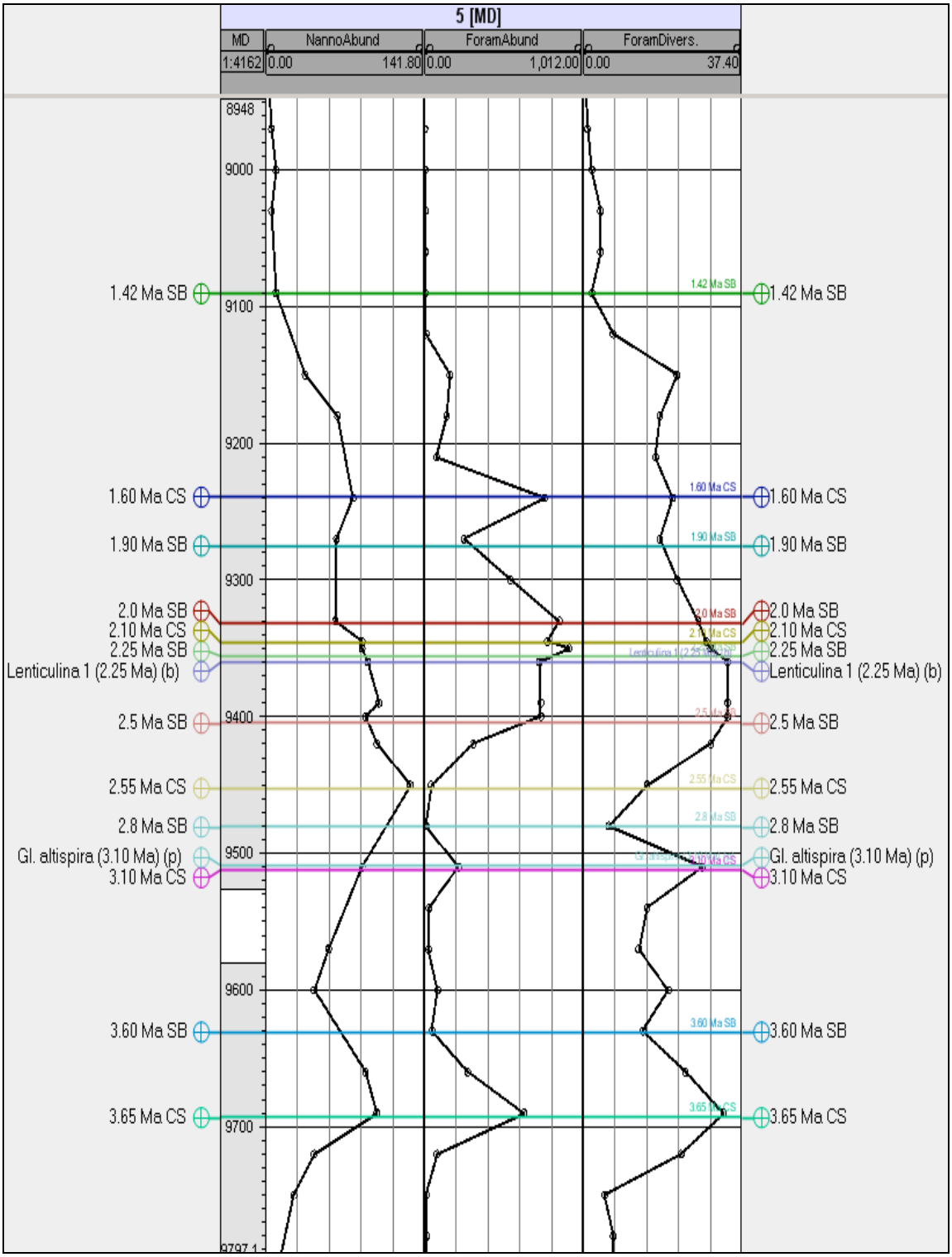

Figure 12. Well #5 3.6-1.42 Ma stacked depositional sequences. Curves from left to right are nannofossil abundance, foraminifera abundance and foraminifera diversity. Sequence boundaries are interpreted based on location of condensed sections. SB=sequence boundary, CS=condensed section, (p)= planktonic foraminifera datum

CHAPTER 3. DATA AND METHODS

3.1 Previous Studies

Variations in salinity have been used in numerous previous studies to better understand the complex hydrogeology of the Gulf of Mexico basin. The salinity of pore fluids have been estimated using the spontaneous potential (SP) response from well logging tools (Funayama and Hanor 1995, Nikiel and Hanor 1999, Bruno and Hanor 2003, Steen et al. 2011), direct pore fluid analysis (Hanor 1999, Szalkowski and Hanor 2003), and a method that uses a combination of gamma ray, resistivity and porosity well logs (Revil et al. 1998, Spears 2000, Little 2003, Hanor and Mercer 2010). The method outlined in Revil et al. (1998) was chosen for this study with a correction for hydrocarbon presence found in Waxman and Smits (1968). The Revil et al. (1998) method uses a dual conductance model to partition the bulk conductivity of sediment filled with an aqueous solution between the surface conductance of clay minerals and the conductance of the electrolyte solution in the pore space. This allows for the estimation of salinity within the pore space of the sediments. The volume and types of clay present in sediments is important in this study because of the effect that clays have on conventional resistivity logging tools. This method allowed the creation of a continuous predicted log of salinity based on the gamma ray, deep resistivity and porosity logs found in each wellbore. This method is preferred over the SP method because the SP method only works in sand units. The study area contains hydrocarbon-producing reservoirs therefore a correction introduced by Waxman and Smits (1968) was implemented in order to determine the salinity of those intervals and to quality check the above methods with production data.

3.2 Data types used

Data used in this study consists of multiple deviated wellbores that contain LWD (logging while drilling) well logs, conventional cores with core analysis taken from two wells, sidewall cores, 2D seismic lines, and production data. The conventional cores used in this study were analyzed by Core Laboratories (Houston, Texas) and provide important data such as porosity, water saturation, grain density, and clay content. This information was used to quality check the Revil et al. (1998) method because of the accuracy of the core measurements compared to logging tools. Two-dimensional seismic lines used in this study were specifically chosen to illustrate structures such as salt bodies and faults throughout the study area and their relation to the salinity profiles calculated in each well. The presence of these structures is important because they are potential fluid flow pathways or sources of saline fluids (Bray and Hanor 1990, Funayama and Hanor 1995, Nikiel and Hanor 1999, Bruno and Hanor 2003, Szalkowski and Hanor 2003, Hanor and Mercer 2010, Steen et al. 2011). Production data from the study area is limited, but the wells that have produced water data have salinity measurements in parts per million (ppm) from the production interval. These measurements can be compared to the salinity calculations using the Revil et al. (1998) method and Waxman and Smits (1968) correction for hydrocarbons to check for accuracy of each method.

3.3 CEC and Clay Weight Fraction – Revil et al. (1998) and this study

The Revil et al (1998) method has been utilized in previous studies (Spears 2000, Little 2003, Hanor and Mercer 2010). These studies used parameters (e.g., cation exchange capacity) outlined in Revil et al. (1998) for the Eugene Island area as representative of the entire Gulf of Mexico. In this study core data is available to verify

the accuracy of the Revil et al. (1998) method by providing input parameters (e.g., cation exchange capacity) that are specific to the study area.

Revil et al. (1998) described the cation exchange capacity of clay grains as the maximum number of surface exchangeable cations per unit mass of sediment expressed in milliequivalents per gram (meq/g) of sediment. The cation exchange capacity is only important for clay minerals. CEC for quartz grains is negligible (Ellis 1987). Salinity is estimated by measuring the bulk conductivity of a pore space saturated with a fluid minus the surface conductivity of clay grains (Bussian 1983). Revil et al. (1998) calculated a cation exchange capacity (see appendix, eq. 1) of 0.0793 meq/g φw, where φw is the clay weight fraction derived from the gamma ray log. This value was designated as a close approximation for sediments derived from the Mississippi River sediment input system. This calculation was found to be an error in this study. The correct value is 0.43246 meq/g φw. The clay types presented in Revil et al. (1998) and taken from core analysis in this study (Fig. 13) are similar and contain similar percentages of mixed layer clays therefore, the cation exchange capacity values for the #4ST1 and #5 wells are in close agreement with those in Revil et al (1998). Well #6 is significantly different than the other wells in this study and from Revil et al (1998) because the core was taken at a deeper depth than the other wells. The apparent complete illitization of smectite in this well at approximately 80 degrees Celsius could be due to an influx of potassium rich fluids that migrated up faults that terminate in much deeper overpressured sediments as has been found in the studies of the Jeanne d' Arc Basin offshore Eastern Canada (Abid and Hesse 2007) and the East Slovak Basin (Honty et al. 2004). The low fraction of smectite has a large impact on CEC due to its electrical properties compared to other clay

minerals. This is evident is Tables 1-4. The cation exchange capacities calculated by Revil et al (1998) and this study can be seen in tables 1-4.

The determination of clay weight fraction presented in Revil et al. (1998) assumes that the gamma ray tool is a linear function of clay content and if the clay mineralogy is known then the volume of clay present can be calculated.

	MINERALOGY OF WHOLE ROCK SAMPLE (WEIGHT %)							MINERALOGY OF CLAY FRACTION (RELATIVE %)			
Depth (ft)	Qtz	Ksp	Plag	Cal	Dol	Pyr	Clay	Ill/Smec*	Ill&Mica	Kaol	Chl
11,451.8	65	10	15	0	1	1	8	61	26	9	3
11,465.4	65	10	16	1	1	0	8	64	24	8	4
11,467.8	68	8	16	0	1	0	8	62	27	7	5
11,468.5	71	8	14	0	1	0	5	69	20	7	5
11,781.5	56	11	17	0	1	1	14	58	30	7	5
11,807.3	77	7	7	1	0	1	8	60	24	10	7
11,821.3	73	10	13	0	0	0	5	55	29	9	7
Min:	56	7	7	0	0	0	5	55	20	7	3
Max:	77	11	17	1	1	1	14	69	30	10	7
Avg:	68	9	14	0	1	1	8	61	26	8	5

*Mixed-layer illite/smectite contains 75-80% smectite layer

KEY:

Qtz = Quartz
Ksp = K-feldspar
Plag = Plagioclase
Cal = Calcite
Dol = Dolomite
Pyr = Pyrite
Clay = Total Clay
Ill/Smec = Mixed-layer Illite/Smectite
Ill&Mica = Illite and Mica
Kaol = Kaolinite
Chl = Chlorite

Figure 13. Table showing the mineralogy of the whole rock sample and clay fraction determined by x-ray diffraction in the #4ST1 well used to calculate CEC (from Core Laboratories Houston, Texas).

Table 1. Cation exchange capacities (CEC) for individual clay types and total CEC from data provided in Revil et al. (1998). CEC is in milliequivalents per gram of sediment. MLC = mixed layer clays (75% smectite 25% illite).

Clay Type	Fraction Clay	CEC (meq/g)
Illite/Smectite (MLC)	0.645	0.42441
Illite	0.0175	0.001575
Kaolinite	0.155	0.00465
Chlorite	0.1825	0.001825
	Total	0.43246

Table 2. Calculated cation exchange capacities (CEC) for individual clay types and total CEC for well #4ST1 this study. CEC is in milliequivalents per gram of sediment. Data provided by Core Laboratories (Houston, Texas). MLC = mixed layer clays (80% smectite 20% illite).

Clay Type	Fraction Clay	CEC (meq/g)
Illite/Smectite (MLC)	0.61	0.40138
Illite & Mica	0.26	0.0234
Kaolinite	0.08	0.0024
Chlorite	0.05	0.0005
	Total	0.42768

Table 3. Calculated cation exchange capacities (CEC) for individual clay types and total CEC for well #5 this study. CEC is in milliequivalents per gram of sediment. Data provided by Core Laboratories (Houston, Texas). MLC = mixed layer clays (80% smectite 20% illite).

Clay Type	**Fraction Clay**	**CEC (meq/g)**
Illite/Smectite (MLC)	0.54	0.35532
Illite & Mica	0.32	0.0288
Kaolinite	0.07	0.0021
Chlorite	0.07	0.0007
	Total	0.38692

Table 4. Calculated cation exchange capacities (CEC) for individual clay types and total CEC for well #6 this study. CEC is in milliequivalents per gram of sediment. Note that no mixed layer clays are present in the #6 well. Data provided by Core Laboratories (Houston, Texas).

Clay Type	**Fraction Clay**	**CEC (meq/g)**
Smectite	0.19	0.152
Illite	0.76	0.0684
Kaolinite	0.03	0.0009
Chlorite	0.02	0.0002
	Total	0.2205

The method used in Revil et al. (1998) provided an approximation of clay content, but did not match closely with the core data for this study. An alternative clay weight fraction calculation (see appendix, eq. 2) that assumes the gamma ray tool is a non-linear function of clay content and corrects for Tertiary aged rocks (Larionov 1969) was used for this study.

3.4 Porosity Determination

The porosity of sediments decrease as the effective stress in a sedimentary basin increases (Revil et al. 1998). During normal compaction pore water is expelled and porosity decreases with depth. When pore fluids are not expelled during compaction due to high sedimentation rates the sediments maintain a higher porosity and fluid overpressure is generated.

Most wells drilled in the Gulf of Mexico have the gamma ray and resistivity logs, but the porosity tool is either not run or more often than not it is only run in a specific section of the well. This section of the well is usually the interval that contains hydrocarbon bearing reservoirs. In order to study the salinity profiles of each well from surface to total depth (TD) the gaps in porosity coverage were filled by constructing a porosity versus depth curve specific to density porosity data in the #6 well. The Revil et al. (1998) method can be implemented when the gamma ray and resistivity logs are the only logs available, but an estimate of porosity must be used. This was done in a previous study by utilizing a single porosity versus depth curve (Hanor and Mercer 2010). This study created a porosity versus depth relationship for both sands and shales because each lithology could not be assigned an accurate estimated porosity based on one porosity vs. depth curve. This process was done by selecting sand and shale average

porosities from the density porosity curve and plotting them against depth (Fig. 14). The sand and shale sections were chosen based on gamma ray signature and thickness. This method has been used in sandstone and carbonate reservoirs throughout the Gulf of Mexico (Ehrenberg and Nadeau 2005, Ehrenberg et al. 2008, Ehrenberg et al. 2009) and produced consistent results in other wells that only had partial density porosity coverage. The equations that described the porosity vs. depth for sands and shales are shown below.

$$\Phi_{Sand} = -3E\text{-}5x + .3954 \quad (1)$$

$$\Phi_{Shale} = -8E\text{-}5x + .4371 \quad (2)$$

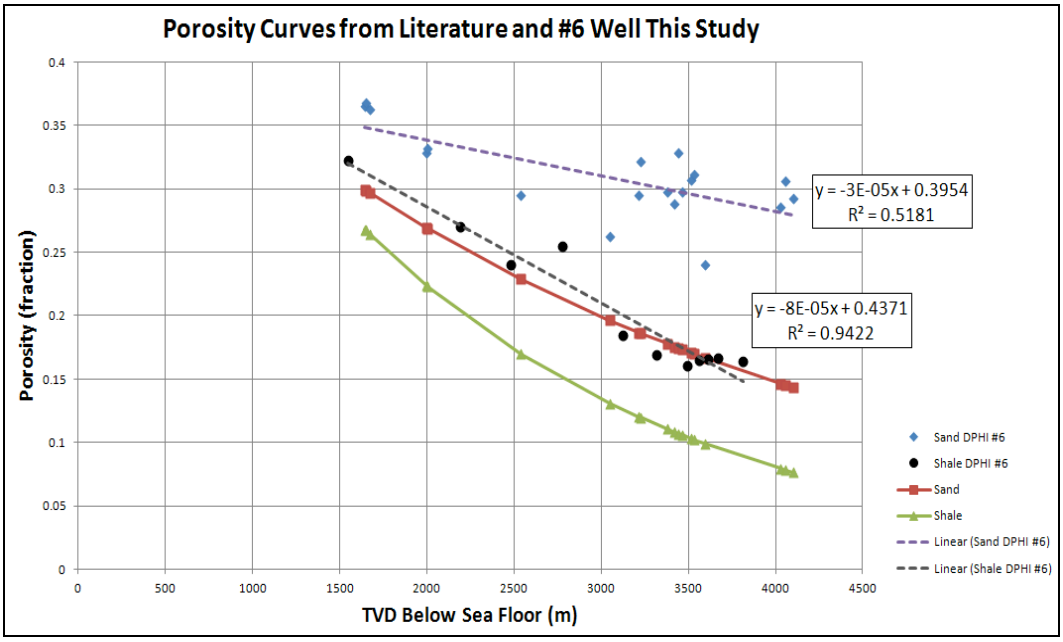

Figure 14. Porosity vs. depth plot for the #6 well. Normal compaction shale curve (green line) and sand curve (red line) underestimate porosity for the study area because the study area is overpressured at a shallow depth. A linear regression line provides the best fit for the shale (black dots) and sand (blue triangles) porosities.

3.5 Determination of overpressure

The onset of overpressure in this study area was analyzed by converting the drilling mud weights into a geostatic ratio in order to look at the variation of pore pressure gradients. Overpressure in previous studies (Beall and Fisher 1969, Overton and

Zanier 1970, Steen et al. 2011) has been associated with the presence of salinity reversals with increasing depth. As shales are further compacted and subjected to increasing temperatures the clay bound water within the clay mineral lattice can be released resulting in fresher pore waters being injected into adjacent permeable units lowering the salinity, but increasing the salinity within the shales (Beall and Fisher 1969). Correlating these salinity reversals with overpressured sediments was important to better understand the hydrogeology of the Gulf of Mexico. These types of salinity profiles are also seen in this study. The geostatic ratio was calculated for each well that contained drilling mud weight data. The calculation for geostatic ratio is

$$Geostatic\ Ratio = 0.052 * Mud\ Weig\ \ t\ (ppg) \tag{3}$$

where mud weight is in pounds per gallon (ppg). A geostatic ratio of 0.45 psi/ft is considered hydrostatically pressured, whereas 0.60 psi/ft or greater is considered overpressured. The wells that contained mud weight data were used to calculate geostatic ratio and approximate the top of overpressure (Fig. 15). In this study area the top of the onset of overpressure is at approximately 8000' subsea true vertical depth (SSTVD).

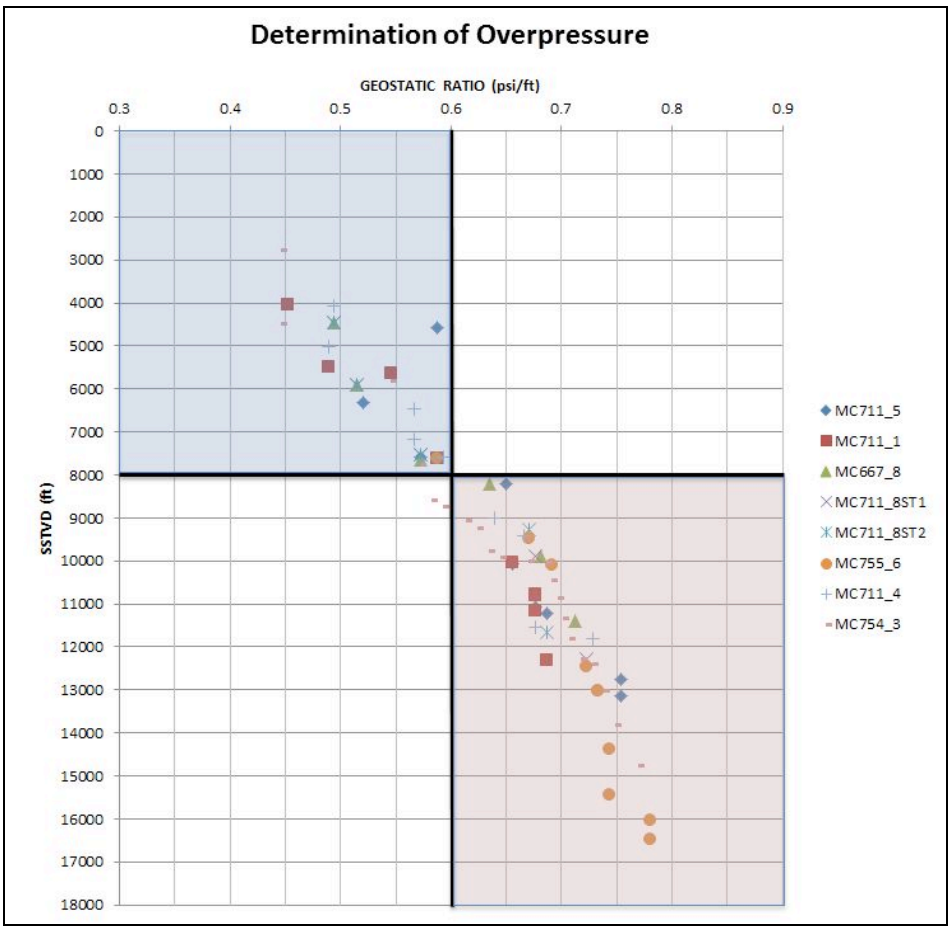

Figure 15. Graph of geostatic ratios for all wells within the study area that contained mud weight data. Two zones of pressure exist within the study area. The hydropressured zone (shaded blue) and the overpressured zone (shaded red). The top of overpressure is at approximately 8000' SSTVD.

3.6 Calibration of Revil et al. (1998) method with core data

In order to check the accuracy of the method outlined in Revil et al. (1998), salinity measurements from well log data were compared with core analysis. The #6 well located in the center section of the study area (Fig. 4) was chosen because of the location of a conventional core through a thick wet sand section (Fig. 16). Data used to calculate salinity from well logs data was taken from the gamma ray, deep resistivity and density porosity log at depths that were also taken for core analysis. The core data that was used in this comparison were porosity and clay weight fraction. The core data was also used for Archie's (1942) equation with saturation and cementation exponents of 2 and 1.88

respectively based on special core analysis provided by Core Laboratories. Core data and well log data were used to estimate salinity using the Revil et al. (1998) method and compared to the results calculated from Archie's (1942) equation. This method allowed for a comparison of salinity values produced from the Revil et al. (1998) method using only data from well logs, the Revil et al. (1998) method using a combination of conventional core data and well logs, and Archie's (1942) equation using data from cores such as water saturation. Comparison of the three different methods showed that the Revil et al. (1998) method provided results that were within +/- 2 g/L (Fig. 17) and could be used to calculate salinity for this study area.

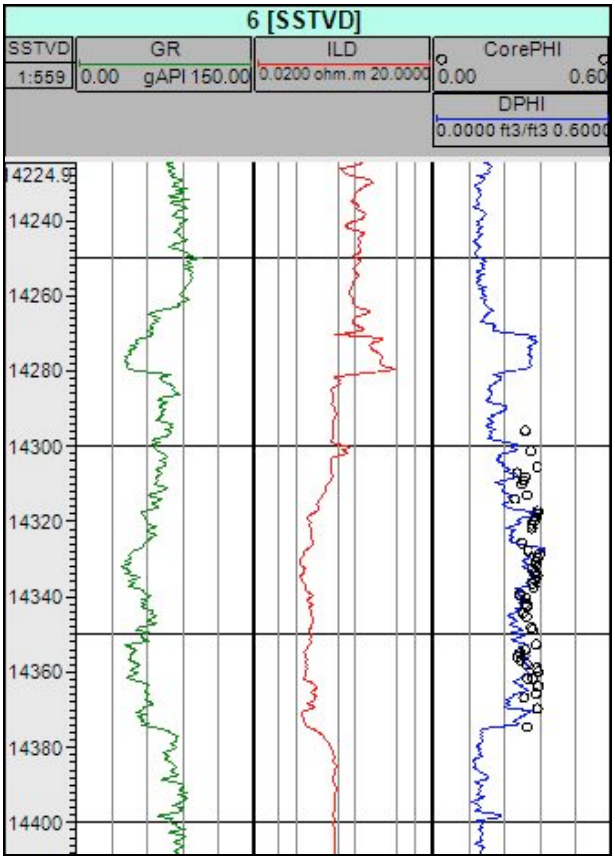

Figure 16. Sand section used for quality checking of the Revil et al. (1998) method with core data. Curves from left to right are gamma ray, deep resistivity, density porosity and core porosity (black circles).

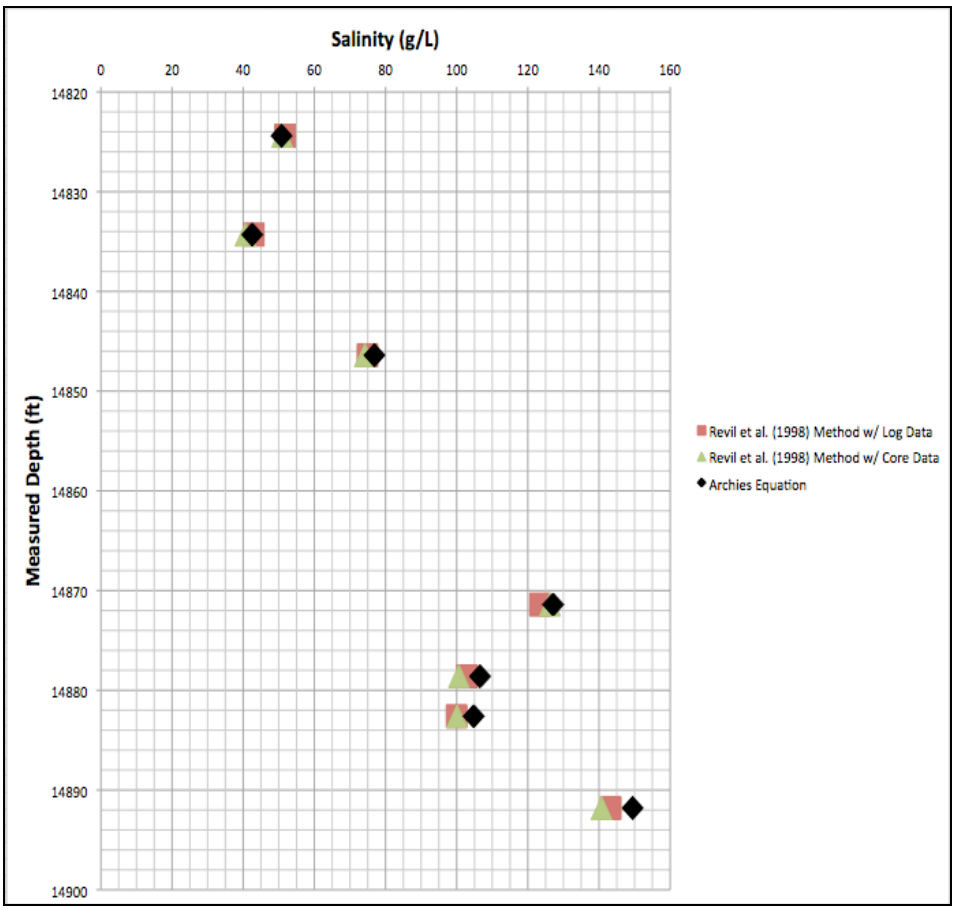

Figure 17. Comparison of salinities from the #6 well calculated from the Revil et al. (1998) method using only well logs (red squares), the Revil et al. (1998) method using a combination of core data and well logs (green triangles), and Archie's (1942) equation using core data such as water saturation (black diamonds).

The method described in Revil et al. (1998) and Waxman and Smits (1968) was also quality checked using data from cores taken in hydrocarbon bearing intervals. This allowed for the correction of hydrocarbons to be applied and then compared to production data. The Revil et al. (1998) as well as the Waxman and Smits (1968) correction for hydrocarbons equations can be found in the appendix. Two of the wells within the study area were cored through a hydrocarbon bearing interval illustrated in figure 18 from the #4ST1 well. The information obtained from the cores were water saturation and core porosity derived from core plugs rather than conventional logging tools.

The salinity profile produced using these variables can be seen in figure 18. There is good agreement with these methods when compared to areas that have high water saturations, but areas that do not have high saturations or significant vertical variations in water saturation produce scatter in the salinity data. This is most likely due to the highly laminated nature of this reservoir where bed thickness is less than a foot. A core photo of a portion of the reservoir interval can be seen in figure 19. Even though the hydrocarbon bearing interval has significant scatter in the data it still correlates to produced water salinity of approximately 200 g/L or greater.

Core was also taken in the #5 well through the same hydrocarbon bearing reservoir seen in figure 20. The cored section in this well has the same highly laminated stratigraphy as the #4ST1 well. The estimates of salinity using the Revil et al. (1998) method and the Waxman and Smits (1968) correction for hydrocarbons can be seen in figure 20. The estimated salinity from core data closely resembles the salinity derived just using the Revil et al. (1998) method except where the water saturation is less than 100 percent. The results of using both methods are in close agreement with produced water salinity of approximately 115 g/L.

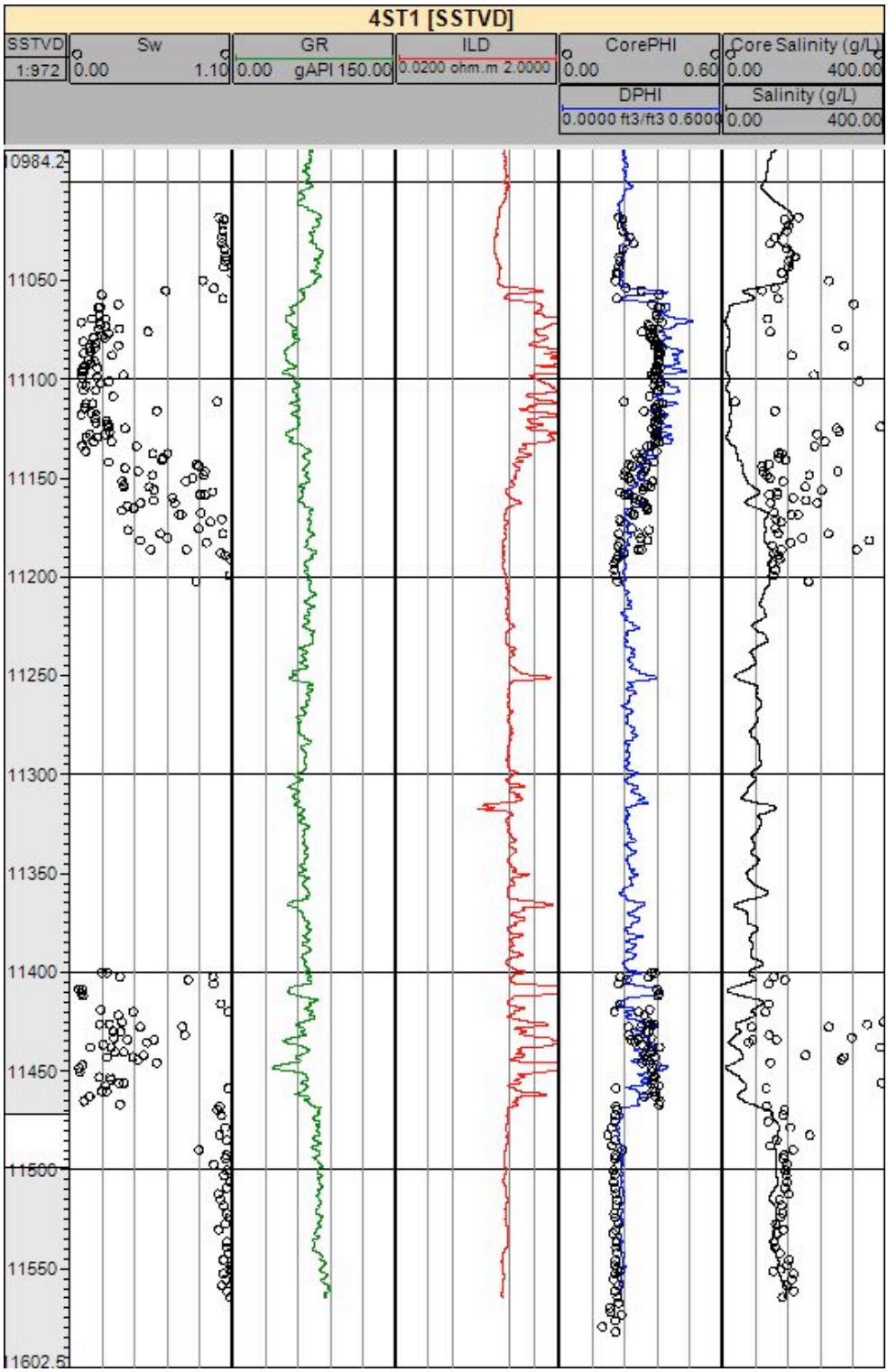

Figure 18. #4ST1 cored hydrocarbon interval. Log tracks from left to right are water saturation, gamma ray, deep resistivity, density porosity (blue line) with core porosity (black circles) overlain, and salinity calculated using the Revil et al. (1998) method (black line) with the correction for hydrocarbons salinity (black circles) overlain.

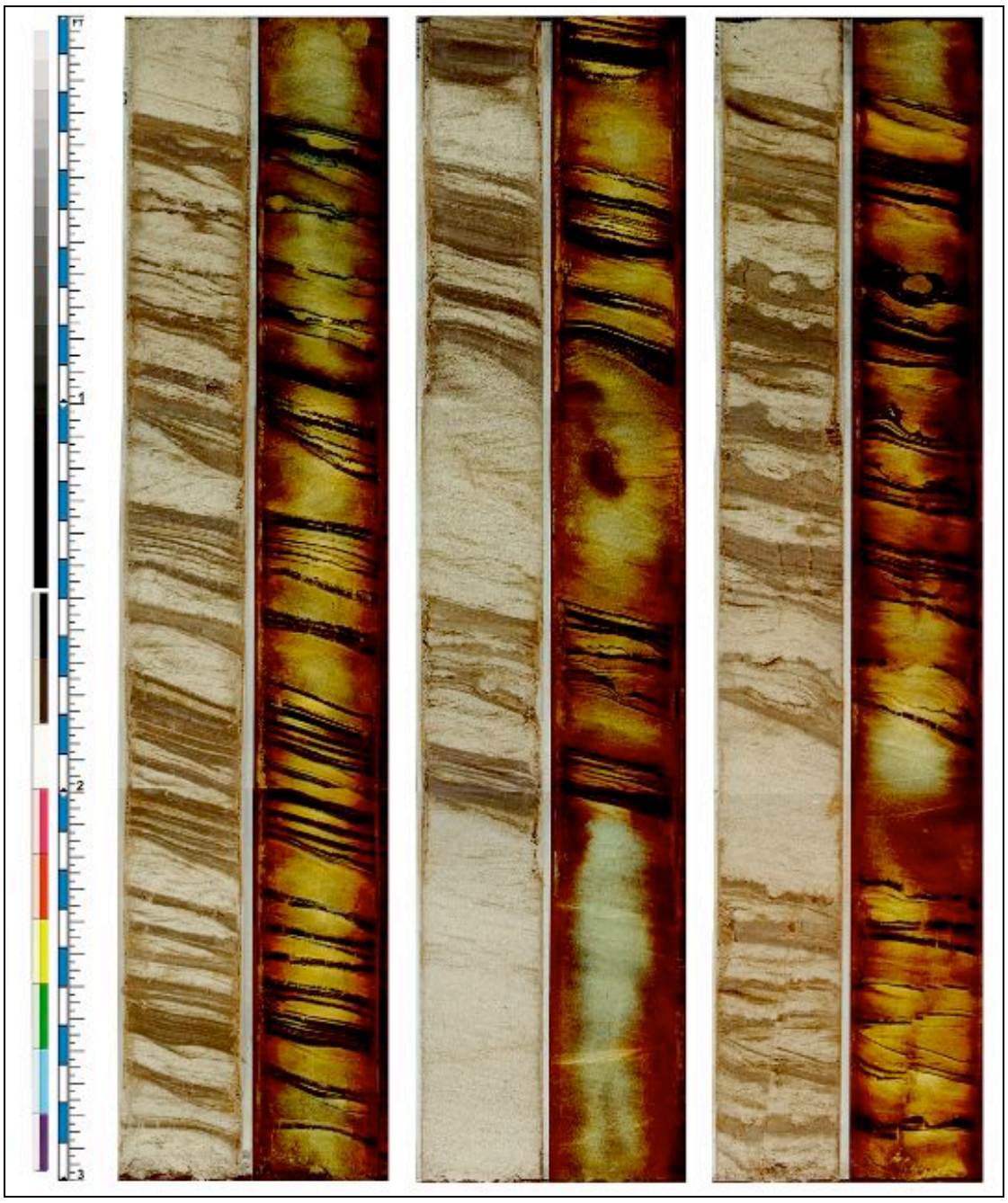

Figure 19. 9 foot section of core taken in the #4ST1 illustrating the highly laminated nature of the reservoir interval. (Provided by Core Laboratories Houston, Texas).

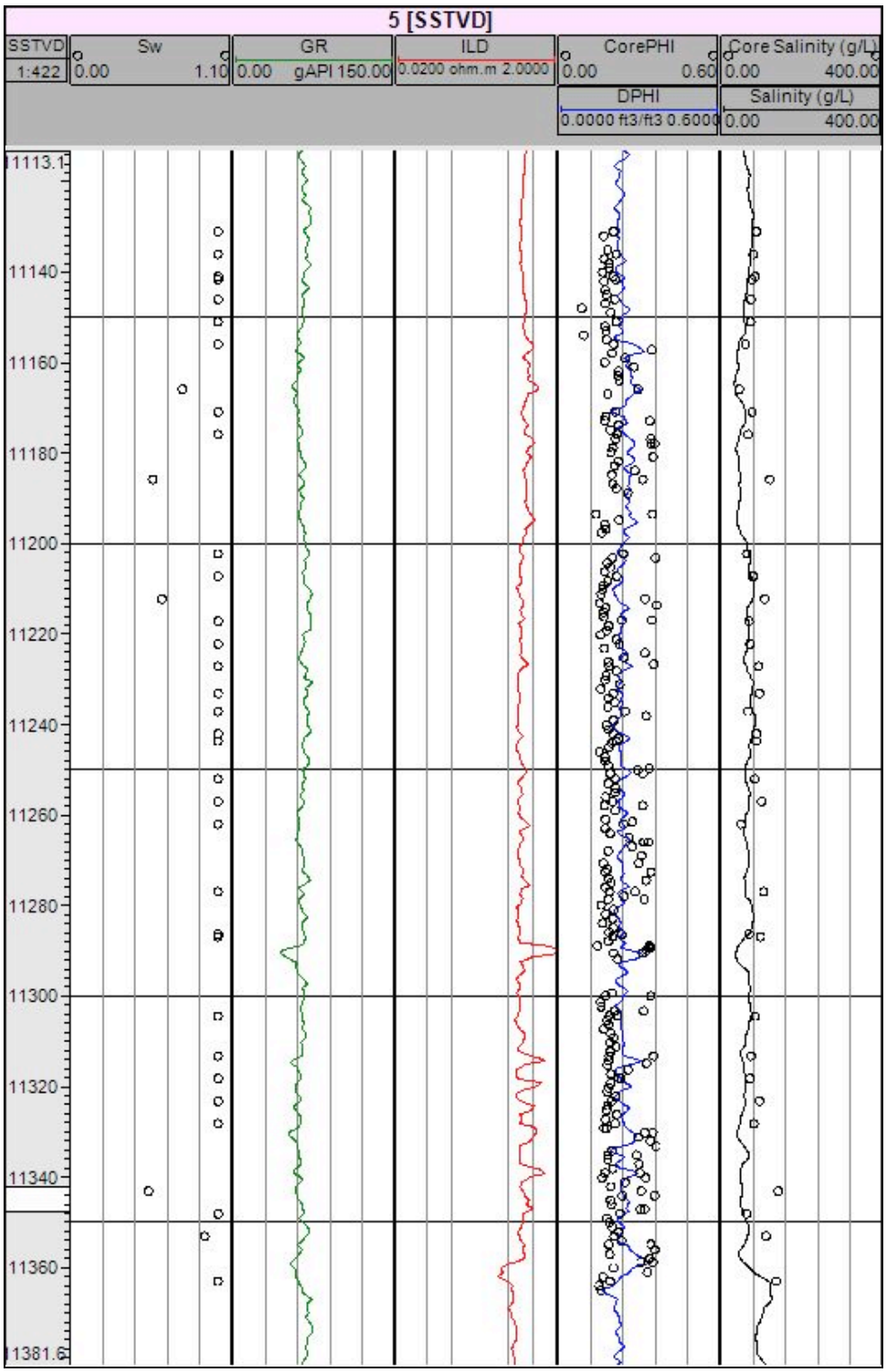

Figure 20. #5 cored hydrocarbon interval. Log tracks from left to right are water saturation, gamma ray, deep resistivity, density porosity (blue line) with core porosity (black circles) overlain, and salinity calculated using the Revil et al. (1998) method (black line) with the correction for hydrocarbons salinity (black circles) overlain.

The calculations outlined by Revil et al. (1998) have proved to be accurate when determining the salinity of pore waters for the #6 well and therefore were applied to all the wells within the study area with or without core data. The wells that do not have core data were assigned CEC values based on the closest available core data. The wells in the northern section of the study area (Fig. 3) were assigned similar CEC values as the #5 well and wells in the central and southern portion of the field (Fig. 4 & 5 respectively) were assigned CEC values similar to the #4ST1 well. The #6 well was assigned two different CEC values throughout the length of the wellbore. The interval from the beginning of the well until approximately 80 degrees Celsius was assigned the value associated with the #4ST1 and the rest of the well was assigned the CEC value found in the cored section of the #6 well. This was done because there was a documented change in CEC in the #6 well at approximately 80 degrees Celsius. For reasons discussed earlier and not focused on in this study the #6 well provides evidence of low temperature complete illitization of smectite at approximately 80 degrees Celsius. This was only done for the #6 well due to its proximity to salt and the #4 and #4ST1 wells do not reach 80 degrees Celsius in their respective wellbores.

The Revil et al. (1998) method with the Waxman and Smits (1968) correction for hydrocarbons provides an approximation of estimated salinity in intervals that have water saturation provided by core analysis even though there is scatter in the data. Wells that have hydrocarbon bearing intervals that do not contain well specific water saturations were ignored in this study due to the unreliability of assumed water saturations across the study area.

CHAPTER 4. RESULTS

Estimates of salinity from the Revil et al. (1998) method were analyzed according to depth and the proximity to salt. Results are discussed for each of the three sections of the study area (Fig. 2).

4.1 Northern section of study area

4.1.1 Overview

The wells located in the northern section of the study area (Fig. 3) include the #8, #8ST1, #8ST2, #1 and #5 and had salinities that ranged from approximately 35 g/L to 200 g/L. The highest salinities in these three wells were located in an interval between approximately 8000' and 9000' SSTVD. All but one of the wells contain hydrocarbon bearing reservoirs which have incorrect estimates of salinity due to high resistivity of hydrocarbons. These intervals were ignored in this study except for in the #5 well, which was described in chapter 3.6. The #8 well calculated salinity results will be discussed in detail here because it best represents the northern section of the study area (Fig. 3) and all other well profiles can be found in the discussion section.

4.1.2 Well #8 Salinity Profile

Well #8 has a salinity profile that extends from approximately 4200' to 11400' SSTVD. The Revil et al. (1998) method produced salinities ranging from approximately 35 g/L near the sea floor to 110 g/L near total depth. The salinity profile contains four distinct zones (Fig. 23) of salinity. Zone 1 is characterized by salinities ranging from 35g/L to 60 g/L. Zone 2 contains salinities ranging from 70 g/L to 90 g/L. Zone 3 has

lower salinities of approximately normal marine water (35 g/L). Zone 4 contains an increase of salinity from 35 g/L to 110 g/L with depth.

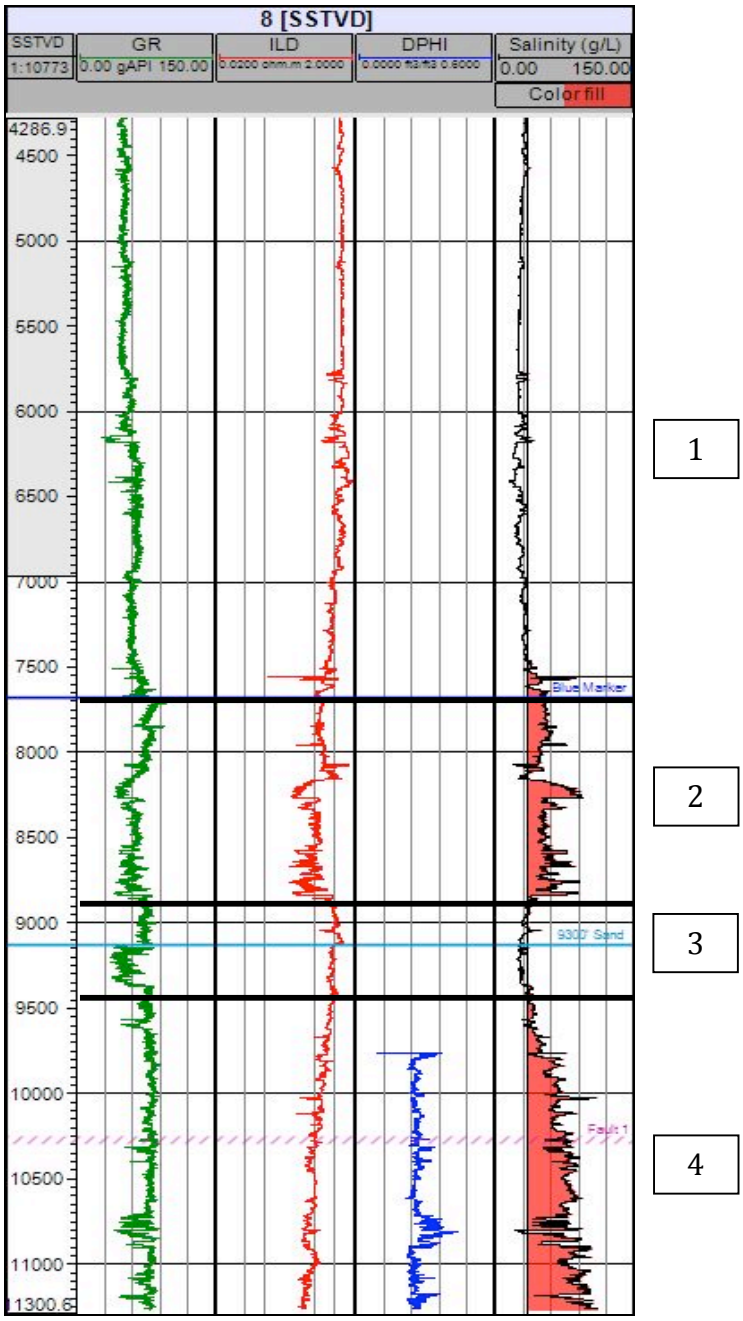

Figure 21. Well #8 salinity profile divided into four zones separated by thick black horizontal lines. Zone 1 is characterized by salinities ranging from 35g/L to 60 g/L. Zone 2 contains salinities ranging from 70 g/L to 90 g/L. Zone 3 has lower salinities of approximately normal marine water (35 g/L). Zone 4 contains a slow increase of salinity from 35 g/L to 110 g/L. Curve filling represents salinities higher than normal marine seawater (35 g/L). Logs from left to right are gamma ray, deep resistivity, density porosity and salinity.

4.2 Central section of study area

4.2.1 Overview

The wells located in the central part of the study area (Fig. 5) include the #4, #4ST1 and the #6. These wells were the closest to a known salt structure and had elevated salinities compared to wells in other sections with salinities from approximately 35 g/L to 350 g/L. The #6 and #4 wells had the most complete well log coverage of estimated salinity values, but also had spikes in the logging tool data due to drilling mud invasion, shale and marl lithologies and high deviations in the wellbore. Due to the complicated salinity profiles within this section of the study area all three wells are presented.

4.2.2 Well #4 Salinity Profile

The #4 well ranges in salinity from 35 g/L nearest the sea floor to over 300 g/L at TD (Fig. 22). This well is closest to the salt structure in the study area (Fig. 23). Just like the #8 well in the northern section the #4 well is made up of distinct salinity zones. The first zone has salinities that are approximately equal to the salinity of normal marine waters. The second zone contains spikes in the logging data caused by drilling mud invasion, shale and marl lithologies and high deviations in the wellbore. The third zone contains multiple salinity reversals followed by zone four which shows a gradual increase in salinity from 160 g/L to over 300 g/L. Zone three contains a hydrocarbon bearing interval that is excluded from this study due to lack of core data in this well (Fig. 22).

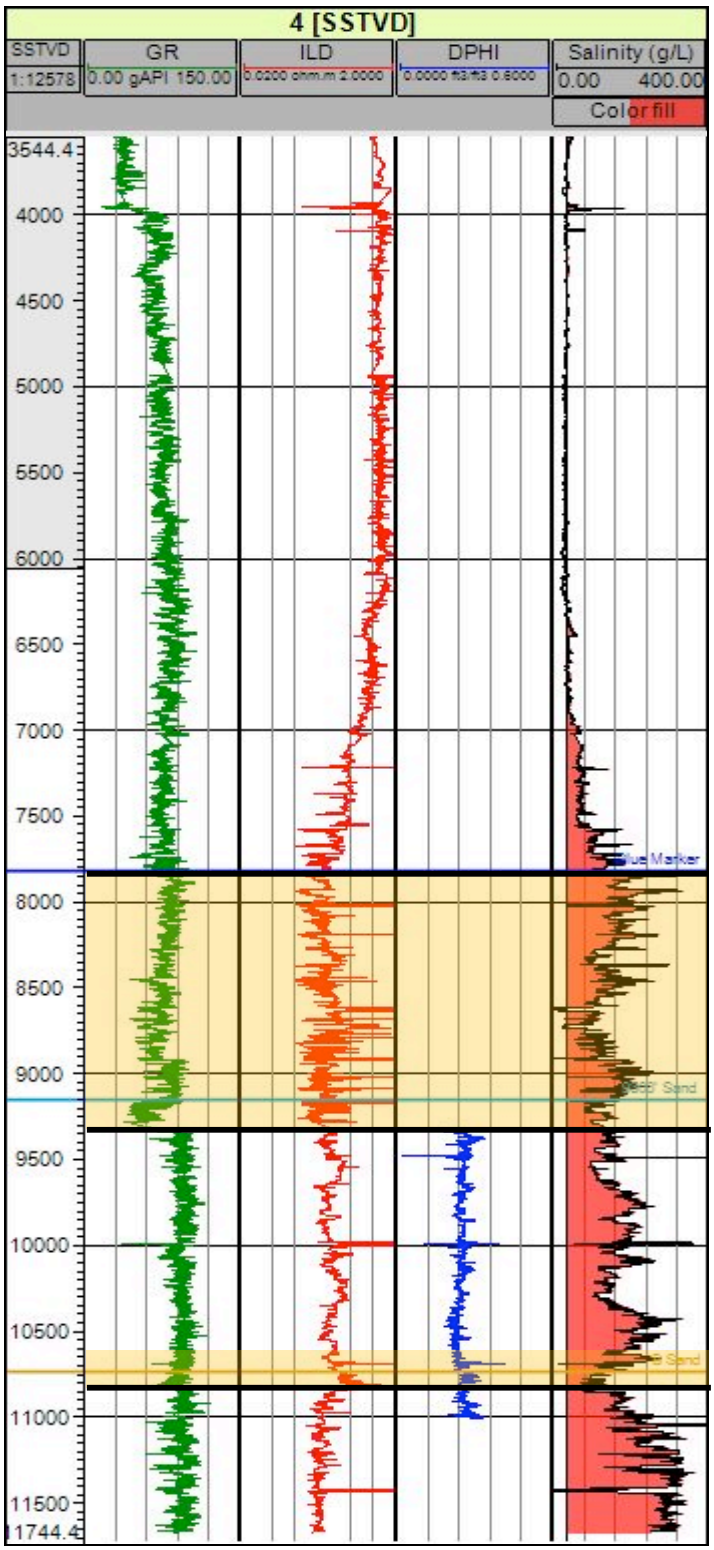

Figure 22. Well #4 salinity profile divided into four zones separated by thick black horizontal lines. Logs from left to right are gamma ray, deep resistivity, density porosity and salinity. Spiking of logging tool zone and hydrocarbon interval excluded from this study is highlighted in orange.

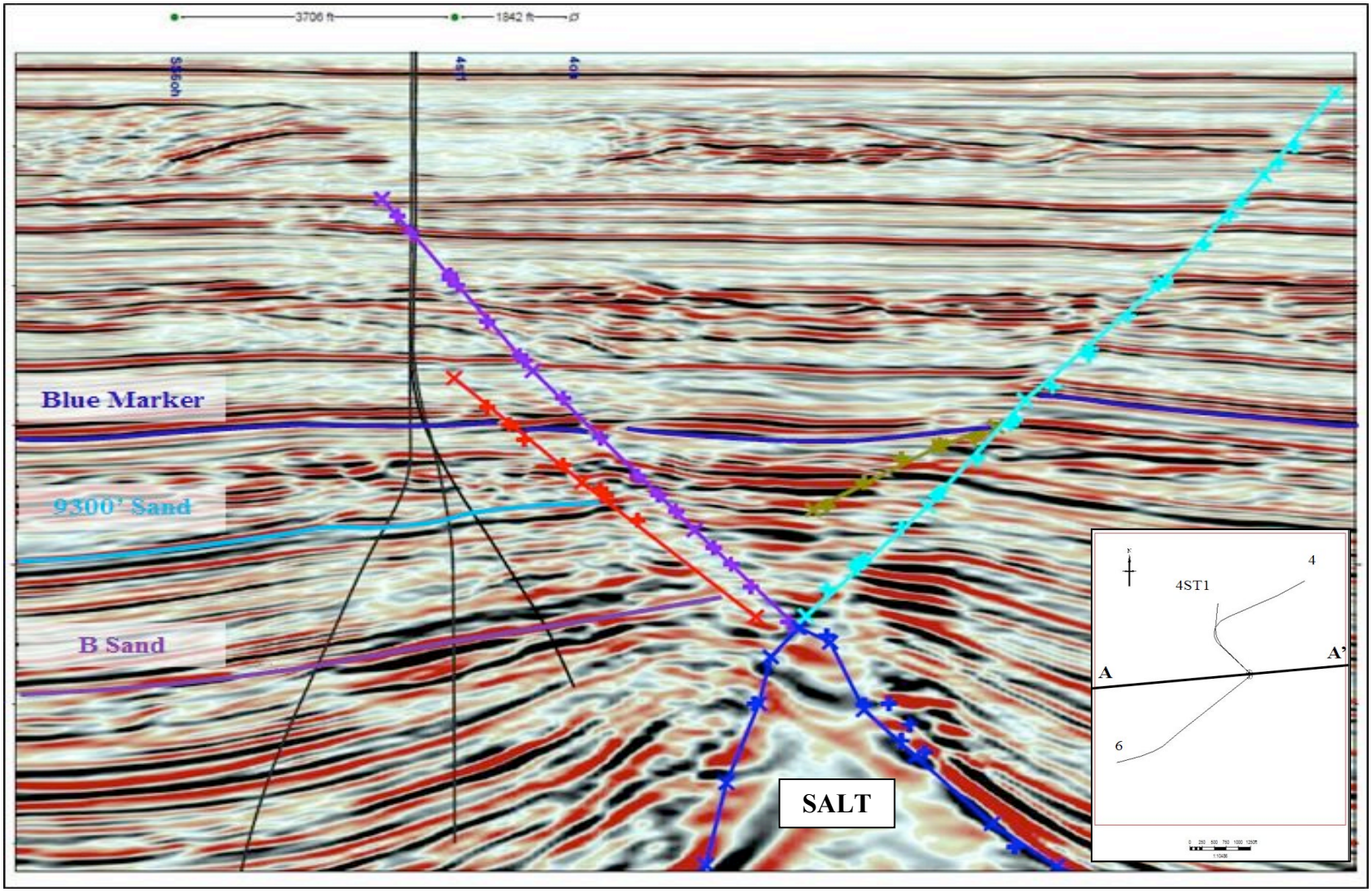

Figure 23. Seismic cross section illustrating the #6 well (left), #4ST1 (middle) and the #4 well (right). Note the #4 wells proximity to salt. Key horizons are labeled. Lines with cross hatches are faults. Line is oriented southwest to northeast in central section of study area. (Seismic data courtesy of TGS).

4.2.3 Well #4ST1 Salinity Profile

The #4ST1 well is located just downdip from the #4 well (Fig. 23) and penetrates the same stratigraphy. The salinity profile for the #4ST1 well is located in figure 24. This well does not have the same logging tool errors associated with the #4 and #6 wells and provides accurate salinity estimates for similar zones seen in other wells. The first zone has salinities that are approximately between 80 g/L and 170 g/L. The second zone illustrates a salinity reversal with salinities in the range of 80 g/L to 160 g/L. The third zone in this well exhibits a relatively steady salinity of 160 g/L. There are slight variations in salinity in this interval due to the alternating sand and shale lithologies. The third zone contains a hydrocarbon bearing interval that has apparent salinity values that are very low (see Chapter 3.6).

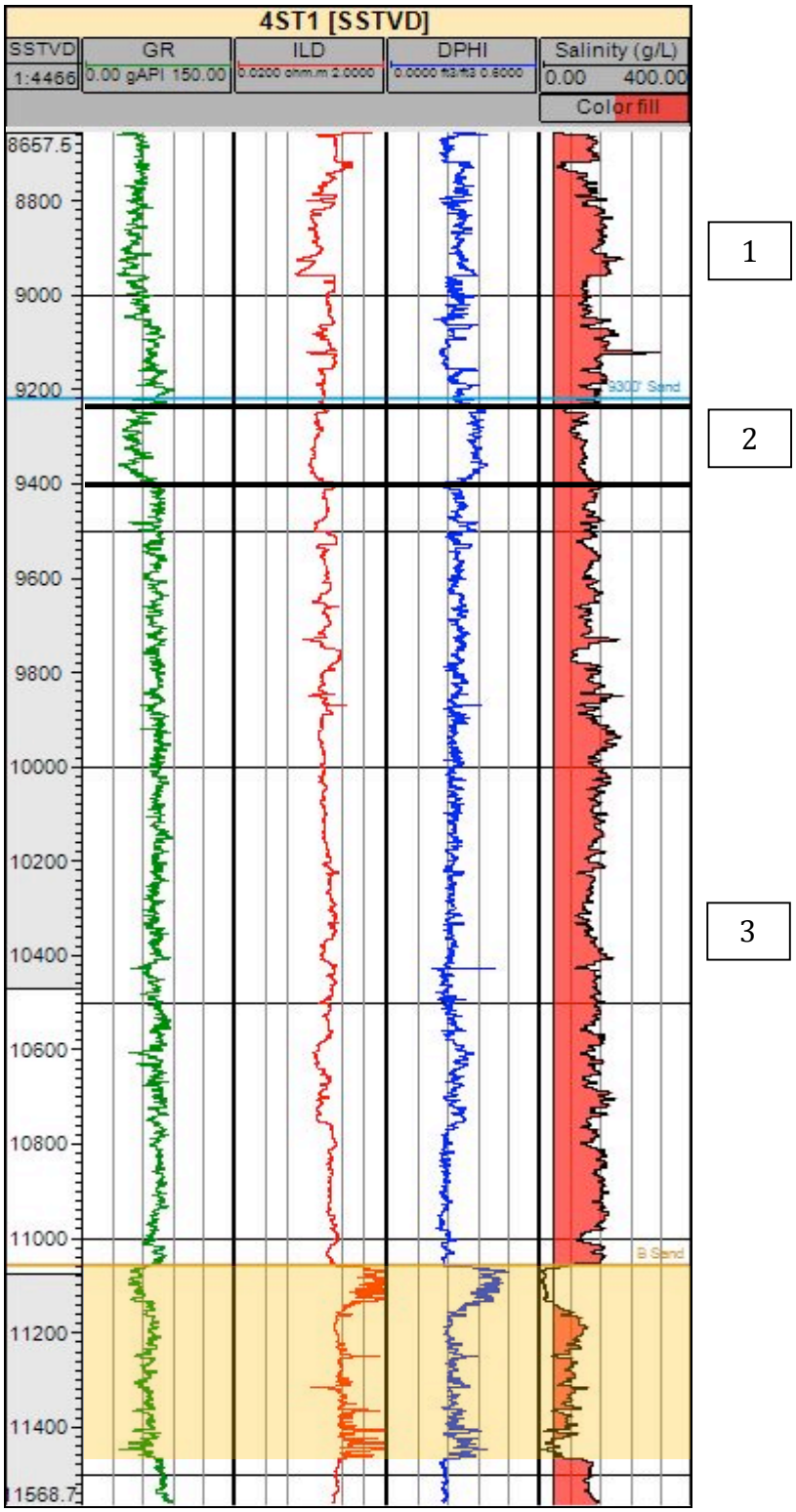

Figure 24. Well #4ST1 salinity profile divided into zones separated by thick black horizontal lines. Logs from left to right are gamma ray, deep resistivity, density porosity and salinity. Shaded zone doesn't represent true estimate of salinity due to hydrocarbon presence (see Chapter 3.6 for hydrocarbon zone salinity values).

4.2.4 Well #6 Salinity Profile

The #6 well is located downdip from the #4 and #4ST1 wells and is the deepest well in the study area. This well has multiple zones of salinity (Fig. 25) and exhibits similar salinity values (approximately 35 g/L) near the sea floor surface as other wells in zone one. The second zone contains the same spiking of logging tool response as in the #4 well and therefore contains errors in estimated salinity. Zone three ranges in salinity from 120 g/L to 160 g/L and is followed by zone four that averages approximately 120 g/L throughout the zone. Zone five contains a hydrocarbon bearing zone that lacks sufficient core data to calculate salinity using the Revil et al. (1998) method with the Waxman and Smits (1968) correction for hydrocarbons. Therefore it was excluded in this study. The sixth zone gradually increases in salinity from 80 g/L to 160 g/L. The seventh zone contains alternating sand and shale lithologies that will be explained in the following chapter, but range in salinity from 160 g/L to 240 g/L.

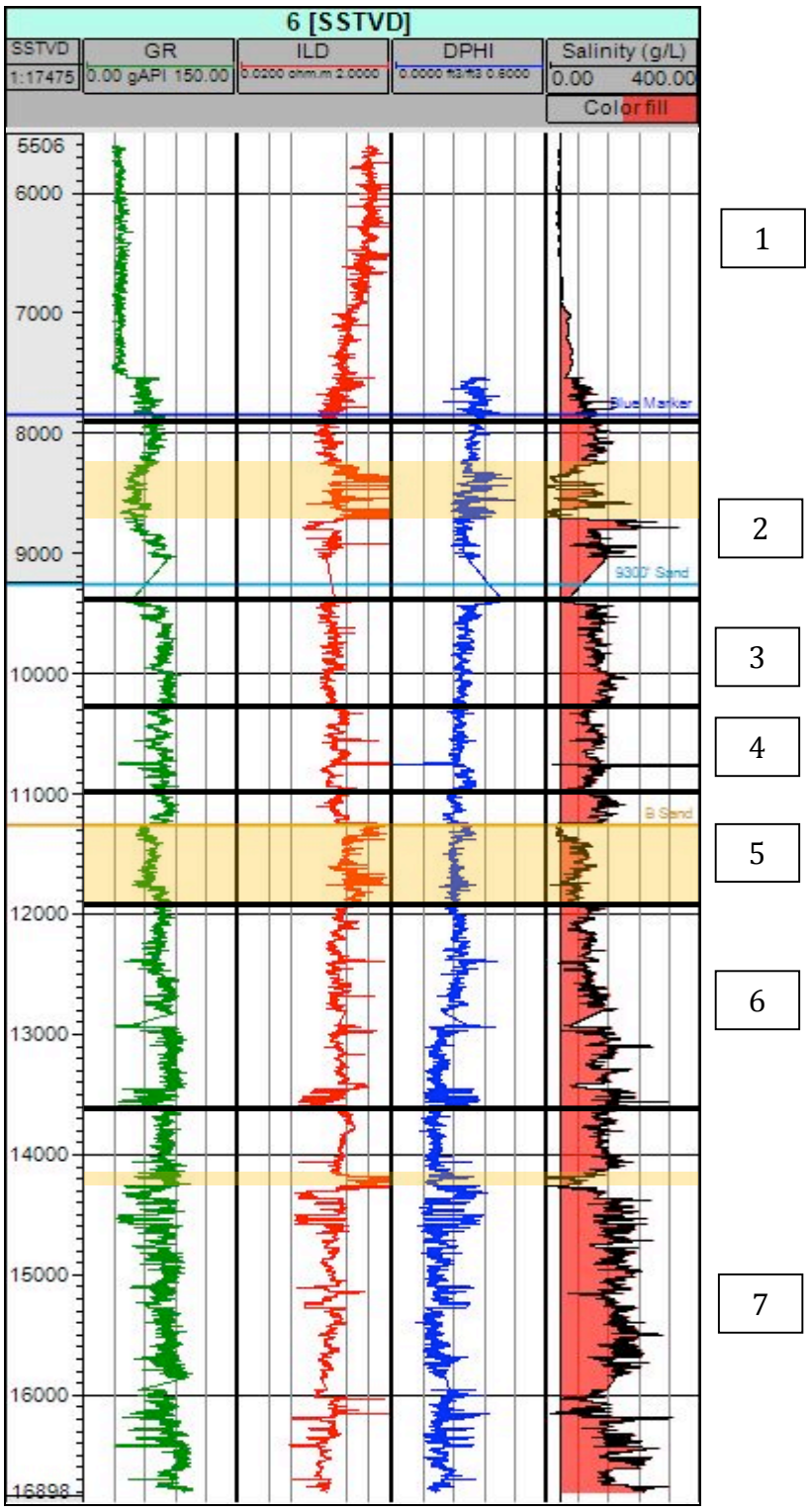

Figure 25. Well #6 salinity profile divided into zones separated by thick black horizontal lines. Logs from left to right are gamma ray, deep resistivity, density porosity and salinity. Shaded zones do not represent true estimate of salinity due to tool effects and hydrocarbon presence.

4.3 Southern section of study area

4.3.1 Overview

The wells in the southern section of the study area (Fig. 6) include the #2, #2ST1, #2ST3 and the #3. These wells have similar salinity profiles as the central section and the salinities range from approximately 35 g/L to 250 g/L. Well #2 had the most complete well log coverage of estimated salinity (Fig. 26) and will be discussed in detail in this section. The other wells in this section only had partial coverage of estimated salinity and are included in the discussions section.

4.3.2 Well #2 Salinity Profile

The #2 well ranges in salinity from approximately 35 g/L to 200 g/L (Fig. 28) and contains similar salinity trends as wells is other sections of the study area, specifically the #8 well. The first section is almost identical to all other wells and has salinity that gradually increases from 35 g/L to 80 g/L. Zone two is characterized by an increase in sand content and a range of salinity from 80 g/L to 120 g/L. This zone is followed by a salinity reversal in zone 3 where salinities decrease to approximately 60 g/L. The fourth zone contains alternating sand and shales with an overall increasing trend from 80 g/L to 160 g/L.

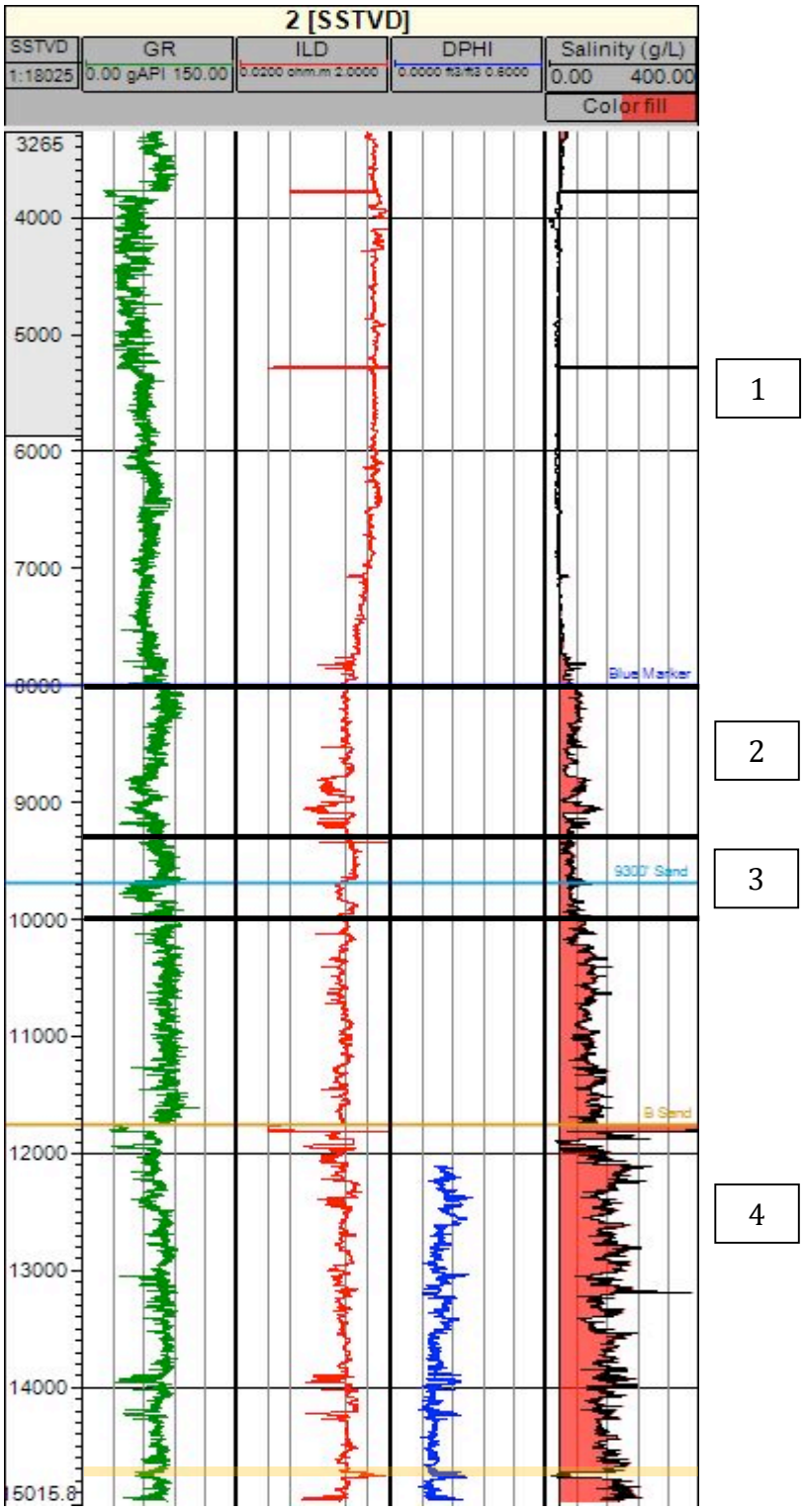

Figure 26. Well #2 salinity profile divided into zones separated by thick black horizontal lines. Logs from left to right are gamma ray, deep resistivity, density porosity and salinity. Shaded zone does not represent true estimate of salinity due to hydrocarbon presence.

CHAPTER 5. DISCUSSION

Variations in salinity have been observed in all three sections of the study area. Previous studies have shown that there are a number of mechanisms that can cause variations in salinity in the Northern Gulf Coast (Schmidt 1973, Funayama and Hanor 1995, Lin and Nunn 1997, Revil et al. 1998, Hanor 1999, Nikiel and Hanor 1999, Spears 2000, Bruno and Hanor 2003, Szalkowski and Hanor 2003, Little 2003, Hanor and Mercer 2010, Steen et al. 2011, McCammon 2012). Some of these mechanisms include compaction driven advection, migration of geopressured saline fluids up faults, salt dissolution and density driven brine migration, and shale dewatering. Each section will be discussed in turn as to how it compares to the others and make inferences about possible fluid flow pathways and compartmentalization.

5.1 Northern section variations in salinity

Bruno and Hanor (2003) found three hydrogeologic regimes existed in their study area around Bay Marchand dome on the continental shelf offshore Louisiana. They described a shallow hydropressured regime with salinities close to sea water, a middle hydrostatically pressured regime with hypersaline salinities and a deep overpressured regime with salinities consistent with normal marine waters or less. These three hydrogeologic regimes were also observed by Steen et al. (2011). In this study only a shallow hydropressured regime and a deep overpressured regime are observed. These two regimes are divided by the approximate position of the Blue Marker horizon described in the data and methods section. The shallow hydropressured regime has mean

sea water salinities, however the deeper overpressured regime has multiple salinity trends that are different than trends described by previous authors.

The salinity profiles of the #8, #8ST1 and the #1 (Figs. 27-29) wells provide the most complete stratigraphic depth coverage of salinity in the northern section of the field (Fig. 3). The #8ST2 and #5 (Figs. 30-31) have only short runs of salinity logs, but still help describe the hydrogeology of this section. The northern section of the study area has roughly normal marine salinity pore water down to a depth of about 8000'SSTVD, which coincides approximately with the onset of overpressure. The sediments found in this study area were all deposited in normal marine conditions therefore it is expected that the original salinity of pore waters should be equal to sea water salinity. This section correlates well to the shallow hydrogeologic regime characterized by normal marine salinity pore waters on the Louisiana continental shelf (Nikiel and Hanor (1999), Bruno and Hanor 2003, Steen et al. 2011). Hanor and Mercer (2010) reported a similar shallow hydrogeologic regime in the deeper water of the Green Canyon protraction area of the Gulf of Mexico. This shallow hydrogeologic regime is interpreted as original pore water unaffected by salt dissolution and brine migration up faults due to the depths of salt and migration pathway length based on seismic cross section (Fig. 32). Another possible explanation for this shallow hydrogeologic regime is that the sediments are too young to be altered by salt dissolution and migration.

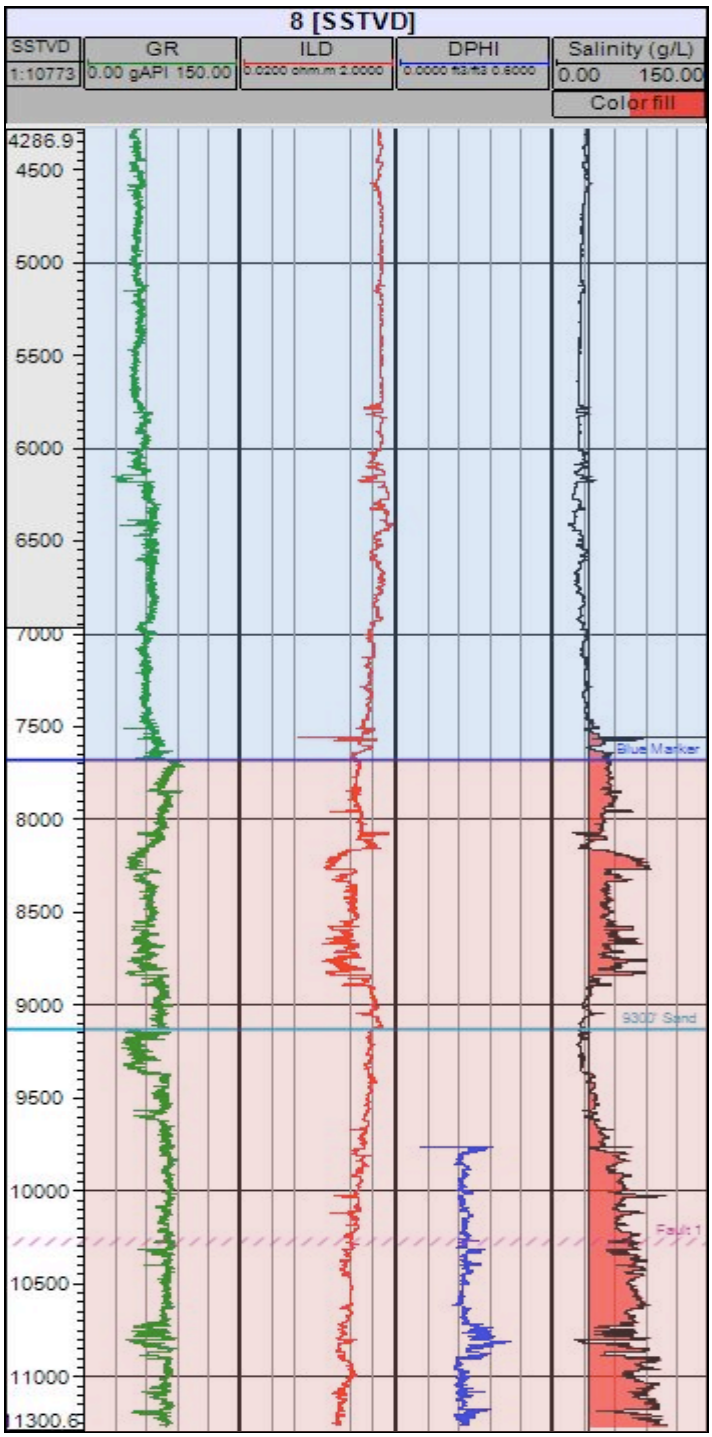

Figure 27. Salinity profile for the #8 well highlighting the hydropressured (blue box) and overpressured (red box) regimes.

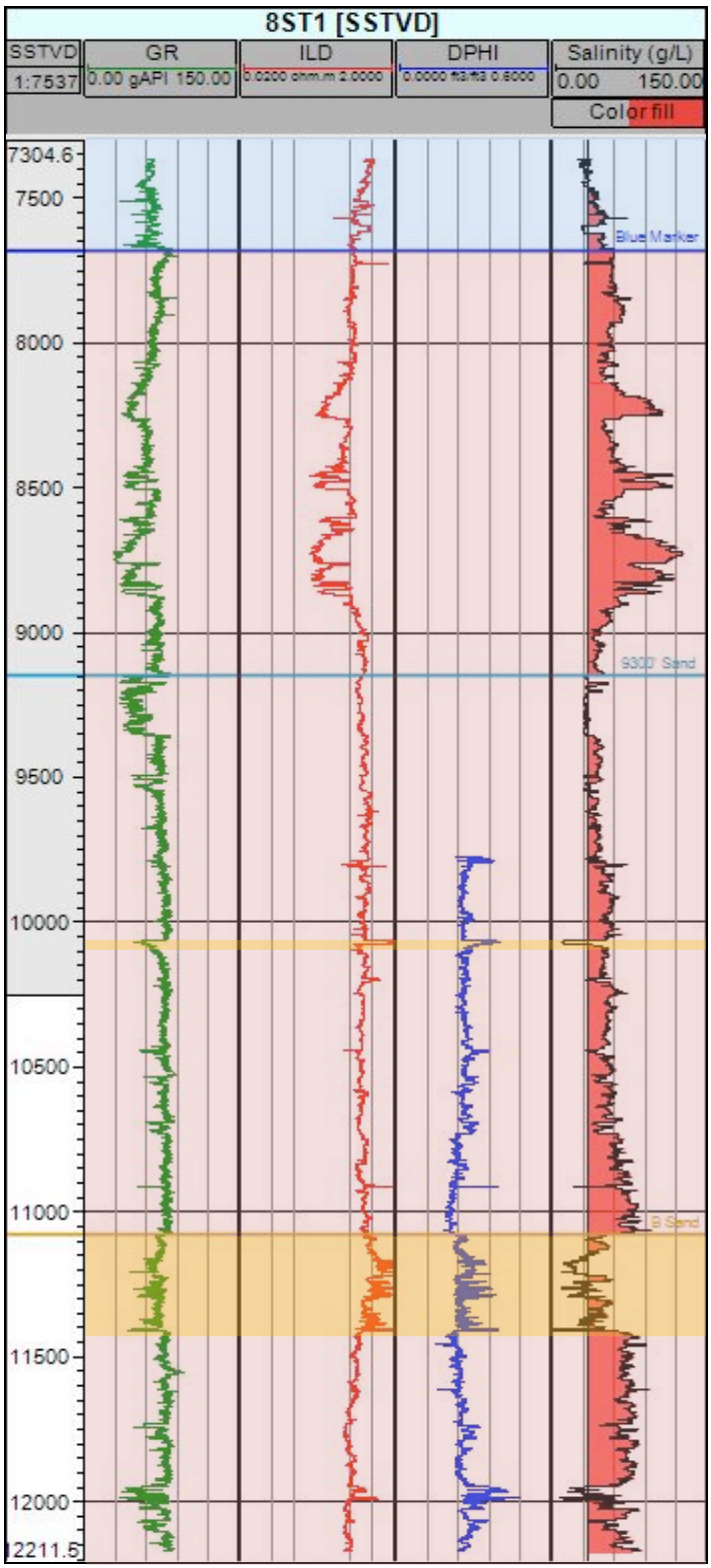

Figure 28. Salinity profile for the #8ST1 well highlighting the hydropressured (blue box) and overpressured (red box) regimes.

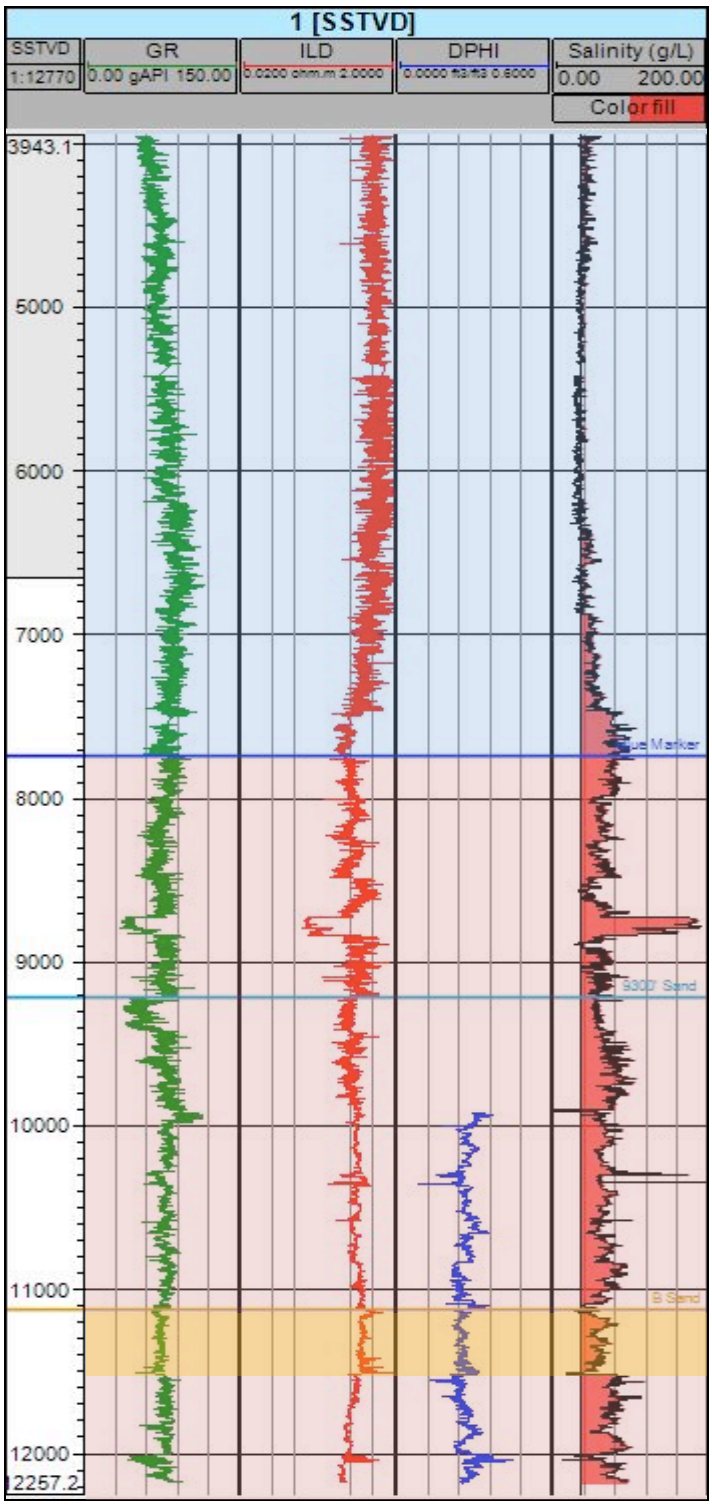

Figure 29. Salinity profile for the #1 well highlighting the hydropressured (blue box) and overpressured (red box) regimes.

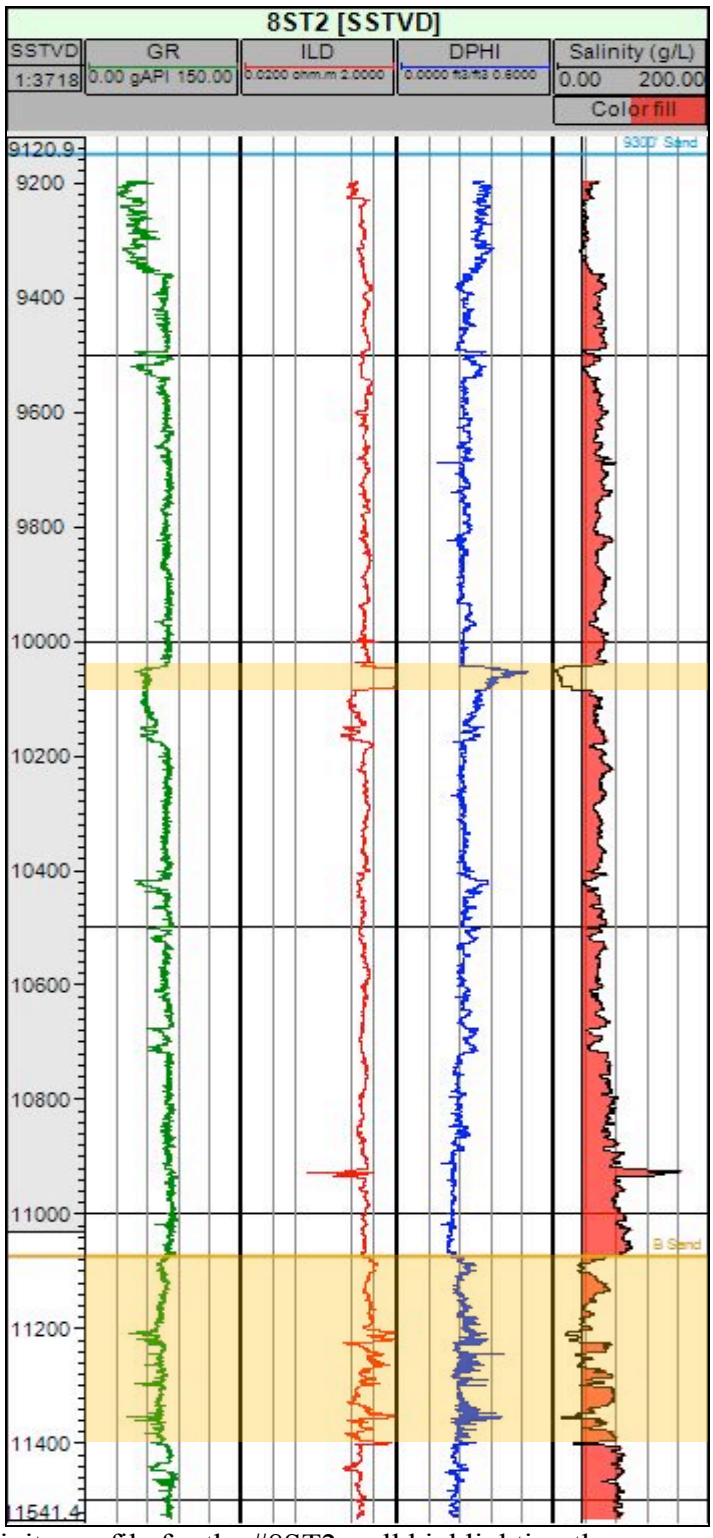

Figure 30. Salinity profile for the #8ST2 well highlighting the overpressured regime.

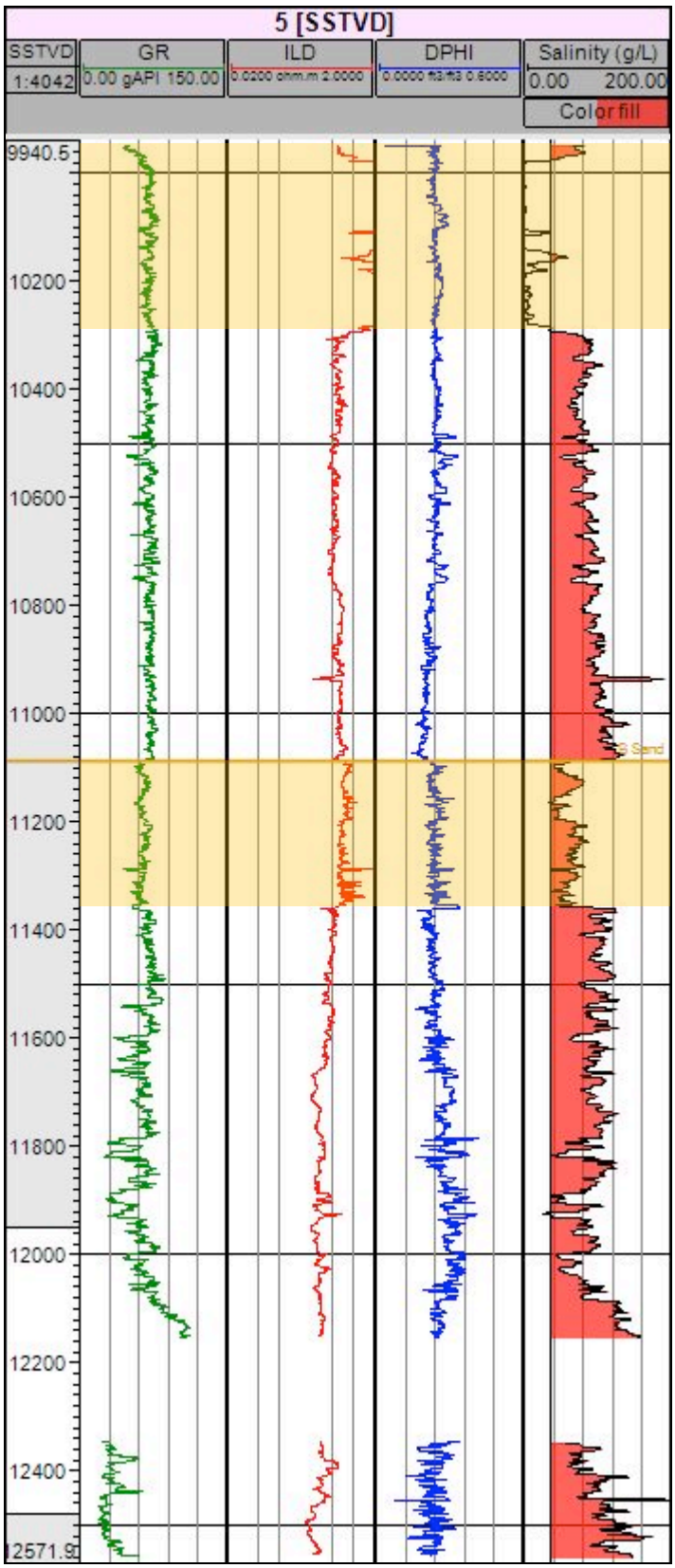

Figure 31. Salinity profile for the #5 well highlighting the overpressured regime.

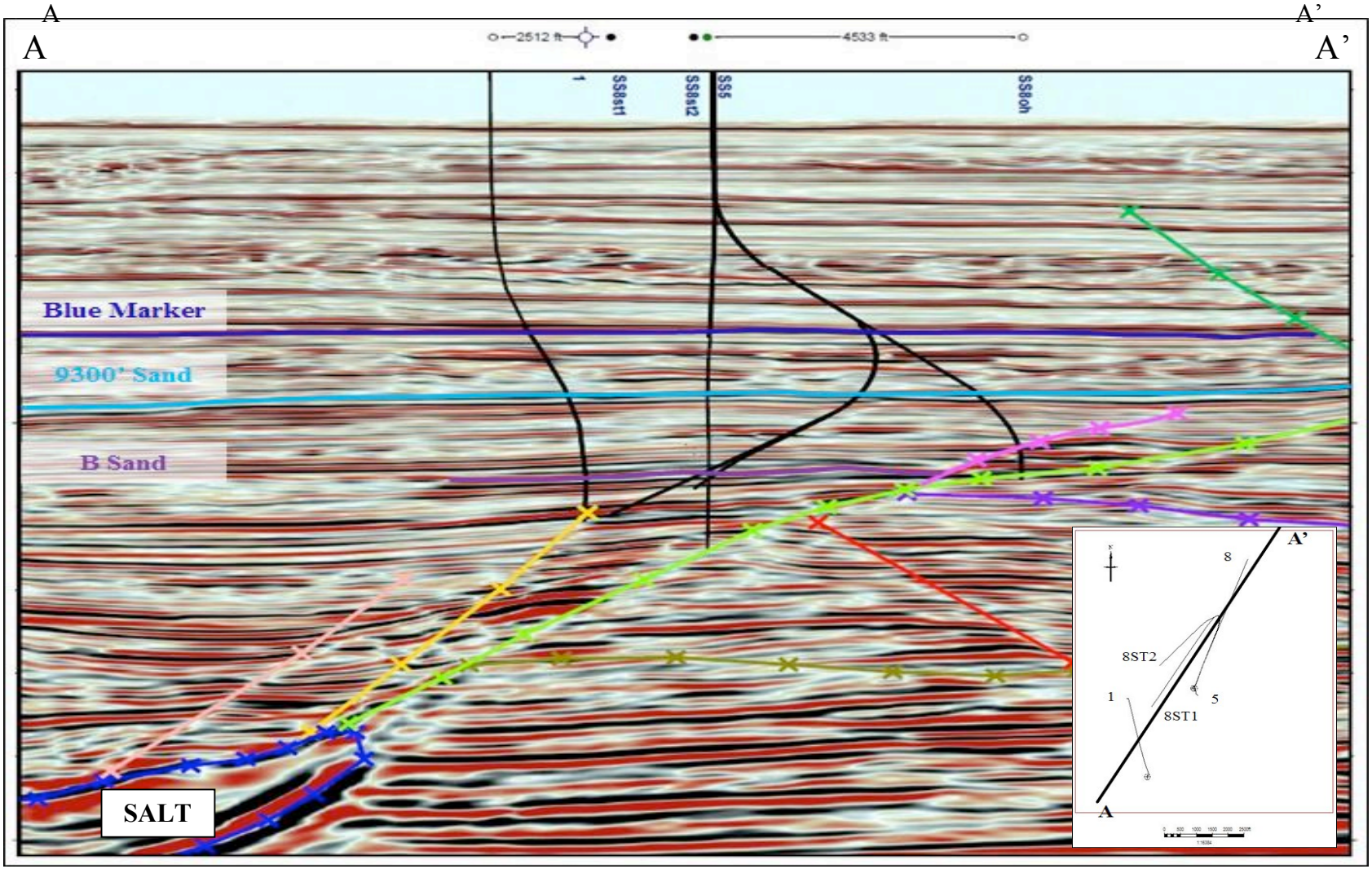

Figure 32. Seismic profile of northern section of study area illustrating hydropressured regime and overpressured regime . Blue Marker horizon separates the two regimes and is used for the structure map in figure 33. Wells are black lines with labels above bottom hole location. Colored lines with cross hatches are faults. (Seismic data courtesy of TGS).

A section with an elevated salinity is located just after the onset of overpressure in an interval that has a high sand to shale ratio. This interval is immediately underlain by a prominent salinity reversal and then a subsequent gradual increase of salinity until total depth is reached.

The overpressured regimes in the #8, #8ST1 and #1 wells contain a section with a high sand to shale ratio that has elevated salinities compared to intervals above and below. This interval is also not seen in previous studies such as Bruno and Hanor (2003) where they describe overpressured sections in their area as having approximately normal marine salinity. Based on structure contours mapped on the blue correlation marker located just above this interval these elevated salinities in the #8, #8ST1 and #1 well could be related to a known salt structure located in the northwest section of the Blue Marker horizon structure map (Fig. 33). Studies have shown that dissolution can occur at the salt sediment interface resulting in the formation of dense saline brines (Funayama and Hanor 1995, Nikiel and Hanor 1999, Bruno and Hanor 2003, Hanor and Mercer 2010, Steen et al. 2011). These brines have a higher density than normal salinity pore waters and this differential in pore water density can result in the down dip migration and mixing of pore waters. The migration of these saline fluids up the faults due to overpressure in figure 32 and into this interval was ruled out for this section of the field because of the orientation of the faults on the structure map (Fig. 33) and the complex migration pathway of multiple fault segments.

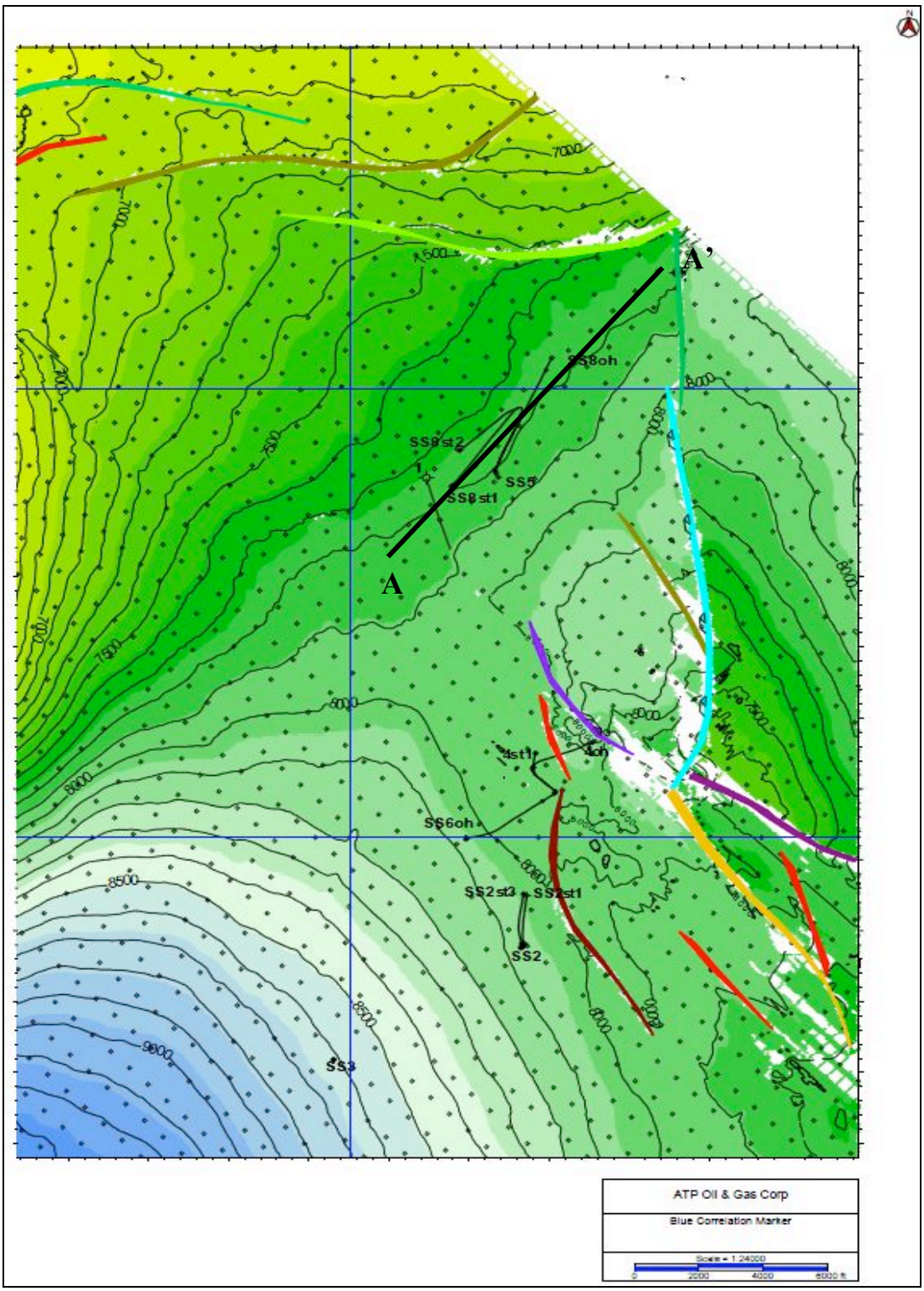

Figure 33. Structure contour map based on 3D seismic data of the Blue Marker horizon found in all wells within the study area. Contour interval is 100'. A-A' cross section line is seismic profile found in figure 32. Well paths are thin black lines. Colored polygons are faults. (Map created by Clark Walraven of ATP Oil and Gas).

The salinity profile just below this interval has salinities at or just below the salinity of normal marine water. Although there appears to be a hydrogeologic connection between the overlying permeable sediments and the salt sediment interface to the northwest, this interval doesn't appear to have that same connection. This lower salinity section is apparent in all of the wells within the northern section of the study area and is only slightly higher in salinity in the #1 well compared to the others. The reason that the #1 well has slightly higher salinities than the other wells may be due to its proximity to the salt structure to the northwest. The overall lower salinity compared to the overlying sediments can be attributed to the types of sediments that make up this section. This section corresponds to the stacked sequences discussed in chapter 2.3 where the bulk of the sediments are comprised of calcareous nannofossils and foraminifera. Based on sidewall core analysis provided by Crews et al. (2000) this interval was interpreted to have almost no connected porosity and permeabilities ranging from 0.6 to 0.8 md. The porosity and permeability for this section may vary from Crew et al. (2000) based on the salinity of this interval in other sections. If the porosity and permeability were similar to the study in Green Canyon by Crews et al. (2000) the salinity for this interval would be expected to be similar to normal sea water salinity due to limited connected porosity and very small permeabilities. Due to the elevated salinities in this interval in the study area there must be connected porosity with higher permeabilites than those seen in Crews et al. (2000).

Below the salinity reversal, the salinity profile for the rest of the wells slowly increases with depth reaching an average of 80 g/L which is similar to other studies. This slow increase in salinity with no large variations between sands and shales suggests that

these wells in the northern section of the study area are mostly unaffected by salt dissolution and brine migration, except for the sandy overpressured interval discussed previously. This is also apparent in seismic cross section (Fig. 31) where the depth to salt is greater than other sections of the study area and fault migration pathways are of substantial length. A structure contour map of the top of the B sand suggests that a density driven topographic flow is also unlikely due to the structure of the area (Fig. 34). Within the overpressure section there are sandy intervals that have lower salinities than adjacent shales (Fig. 35) suggesting that water has been released from the adjacent shales creating vertical compartmentalization due to overpressure (Schmidt 1973, Burst 1976).

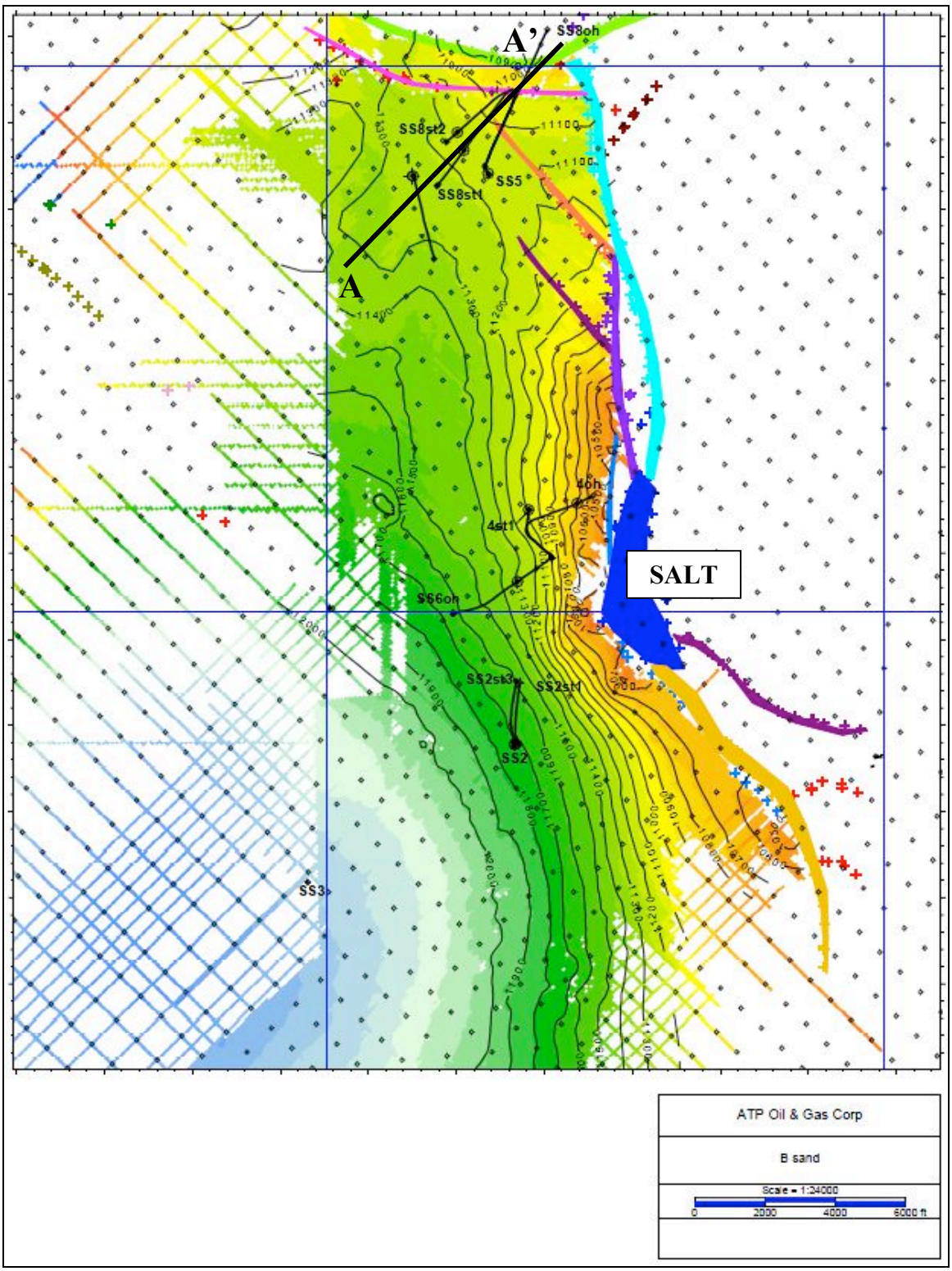

Figure 34. Structure contour map of the top of B Sand based on 3D seismic data. Contour interval is 100'. A-A' cross section line is seismic profile found in figure 32. Well paths are thin black lines. Blue polygon is salt and other colored polygons are faults. (Map created by Clark Walraven of ATP Oil and Gas).

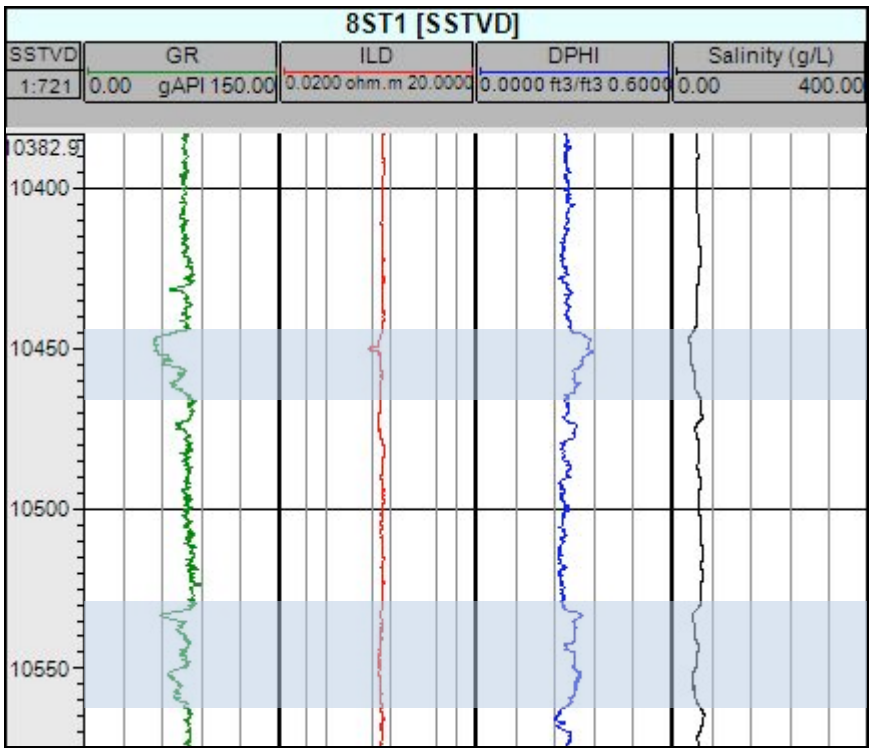

Figure. 35. Section of the #8ST1 well that shows fresher water sands (approx. 40 g/L) (blue boxes) compared to adjacent shales (approx. 70 g/L) suggesting vertical compartmentalization due to sediment dewatering in the overpressured zone.

5.2 Central section variations in salinity

The central section of the study area (Fig. 4) consists of the #6, #4, and #4ST1 wells (Figs. 36-38) that are in close proximity to a salt structure at depth (Fig. 39). The #6 and #4 wells provide the most stratigraphic depth coverage of calculated salinity and are discussed in detail here to illustrate the salinity profile of the central section of the study area compared to other areas. The #4 well has the most complete well log coverage of estimated salinity close to the sea floor surface and can be seen in figure 36. The #4 well has similar salinity characteristics as the wells in the northern section of the study area, but only in the hydropressured regime. The hydropressured regime in the #4 well is characterized by salinities that are approximately equal to that of normal marine water, but gradually increase near the onset of overpressure to approximately 160 g/L. The elevated salinities associated with the hydropressured regime in this section of the study

area are interpreted to be the result of salt dissolution and migration up fault planes to shallower depths (Fig. 39). This salinity trend is also apparent in the #6 well shown in figure 39.

The overpressured regime in the #4 and #6 wells is from approximately 8000' SSTVD until the total depth of each well. Within the overpressured section there is a portion of the well that experienced spiking in the resistivity tool due to drilling mud invasion, wellbore deviation effects and complicated shale/marl lithology. This section of the #4 well does not provide accurate results of estimated salinity, but part of this section represents accurate salinities in the #4ST1 well (Fig. 38). The section representing the interval between 9400' and 11800' SSTVD in the #4 well illustrates a complicated salinity profile that has multiple reversals of salinity. When this section of the well is projected onto a seismic cross section there appears to be multiple faults that intersect the well creating compartments with differing salinity (Fig. 39). The #6 and #4ST1 wells do not exhibit these salinity reversals suggesting the faulting that intersects the #4 well is due to its proximity to salt as shown in figure 39 and 40.

The overpressured regime in the #6 and #4ST1 wells exhibit similar salinities of approximately 160 g/L up until the end of the #4ST1 well at approximately 11500' SSTVD. The #6 well is the deepest well in the central section of the study area and penetrates stratigraphy that is also found in the southern section of the study area wells. The #6 well has an increase in sand lithologies near the base of the well that all exhibit lower salinity values than the shales immediately adjacent to them similar to the northern section of the study area and is interpreted to be the effect of sediment dewatering.

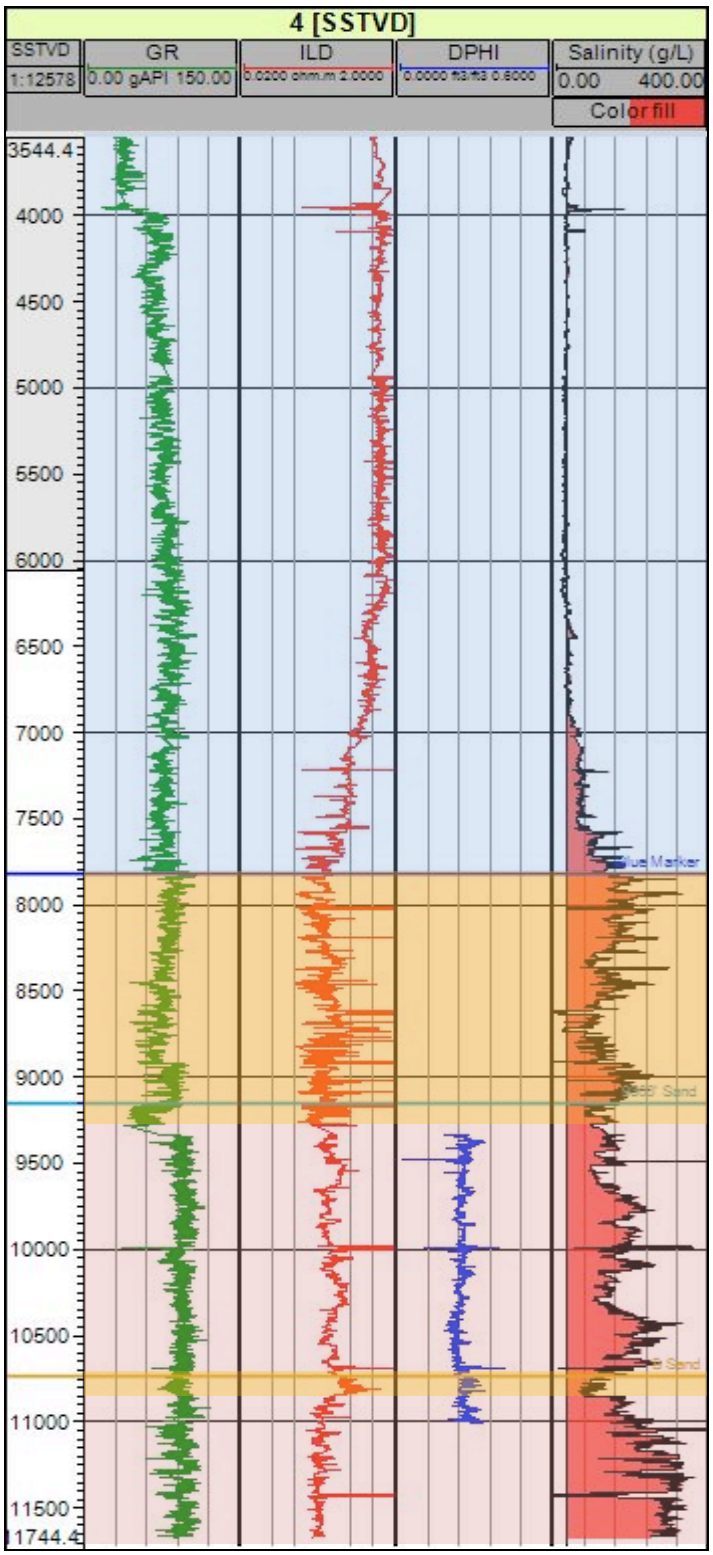

Figure 36. Salinity profile for the #4 well highlighting the hydropressured (blue box) and overpressured (red box) regimes. Blue line represents Blue Correlation marker used for structure contour map (Fig. 30). Orange line represents top of B Sand used for structure contour map (Fig. 31).

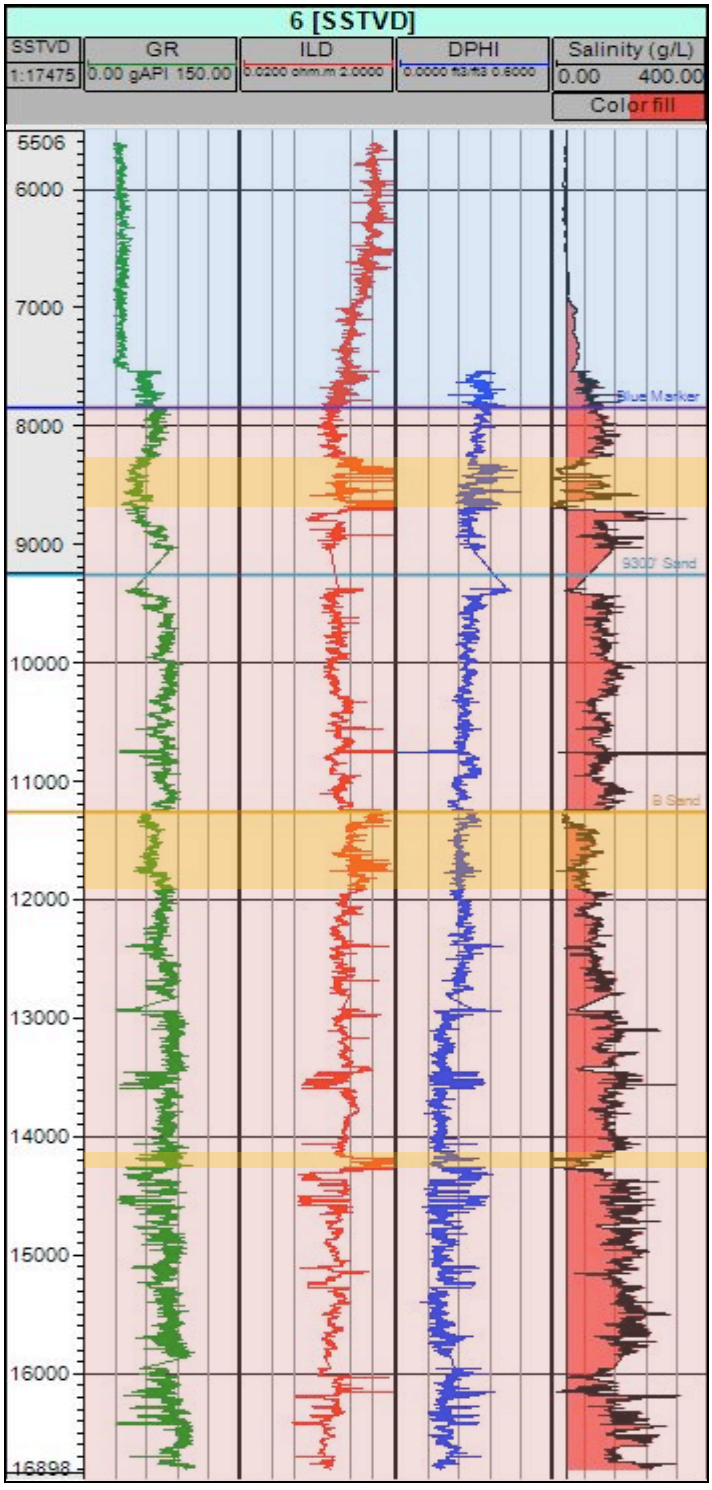

Figure 37. Salinity profile for the #6 well highlighting the hydropressured (blue box) and overpressured (red box) regimes. Blue line represents Blue Correlation marker used for structure contour map (Fig. 35). Orange line represents top of B Sand used for structure contour map (Fig. 36).

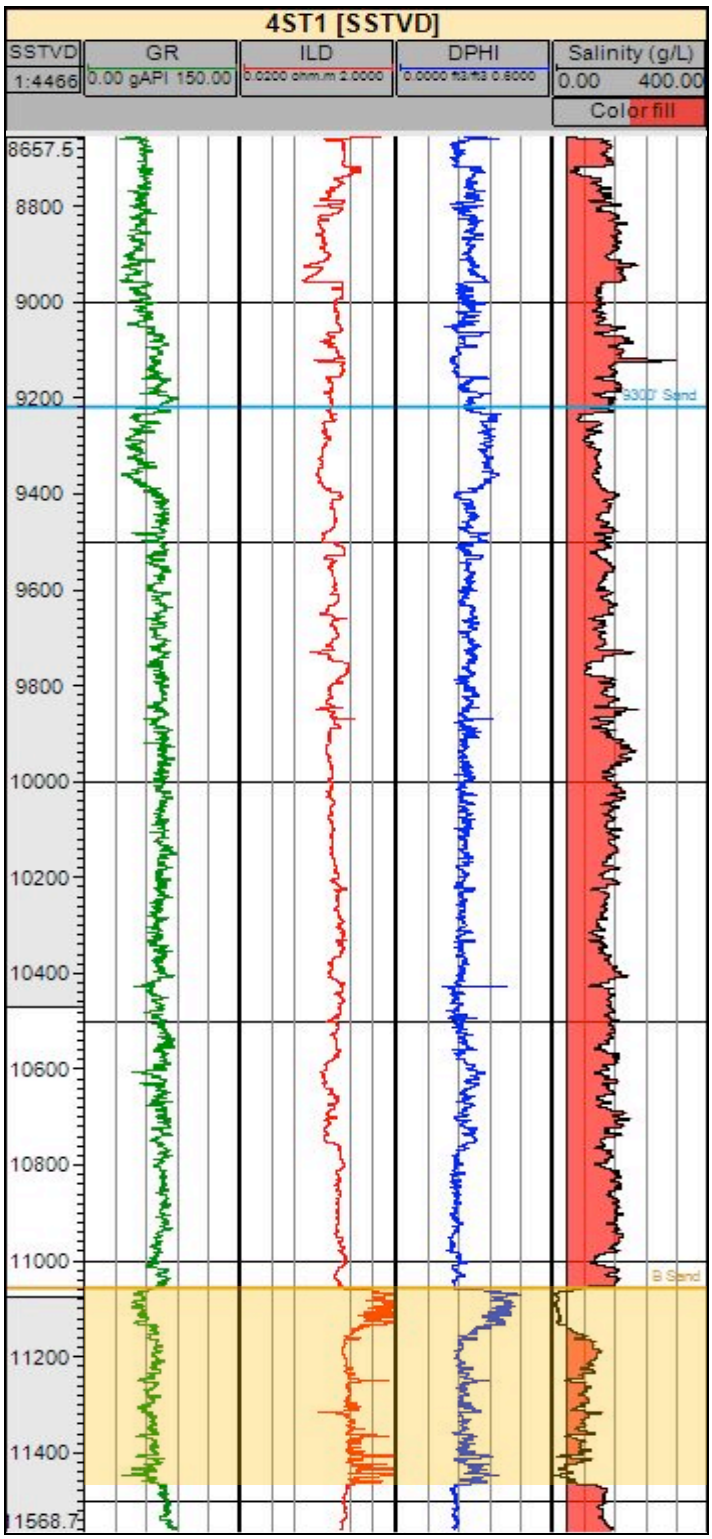

Figure 38. Salinity profile for the #4ST1 well highlighting the overpressured (red box) regime. Blue line represents Blue Correlation marker used for structure contour map (Fig. 35). Orange line represents top of B Sand used for structure contour map (Fig. 36).

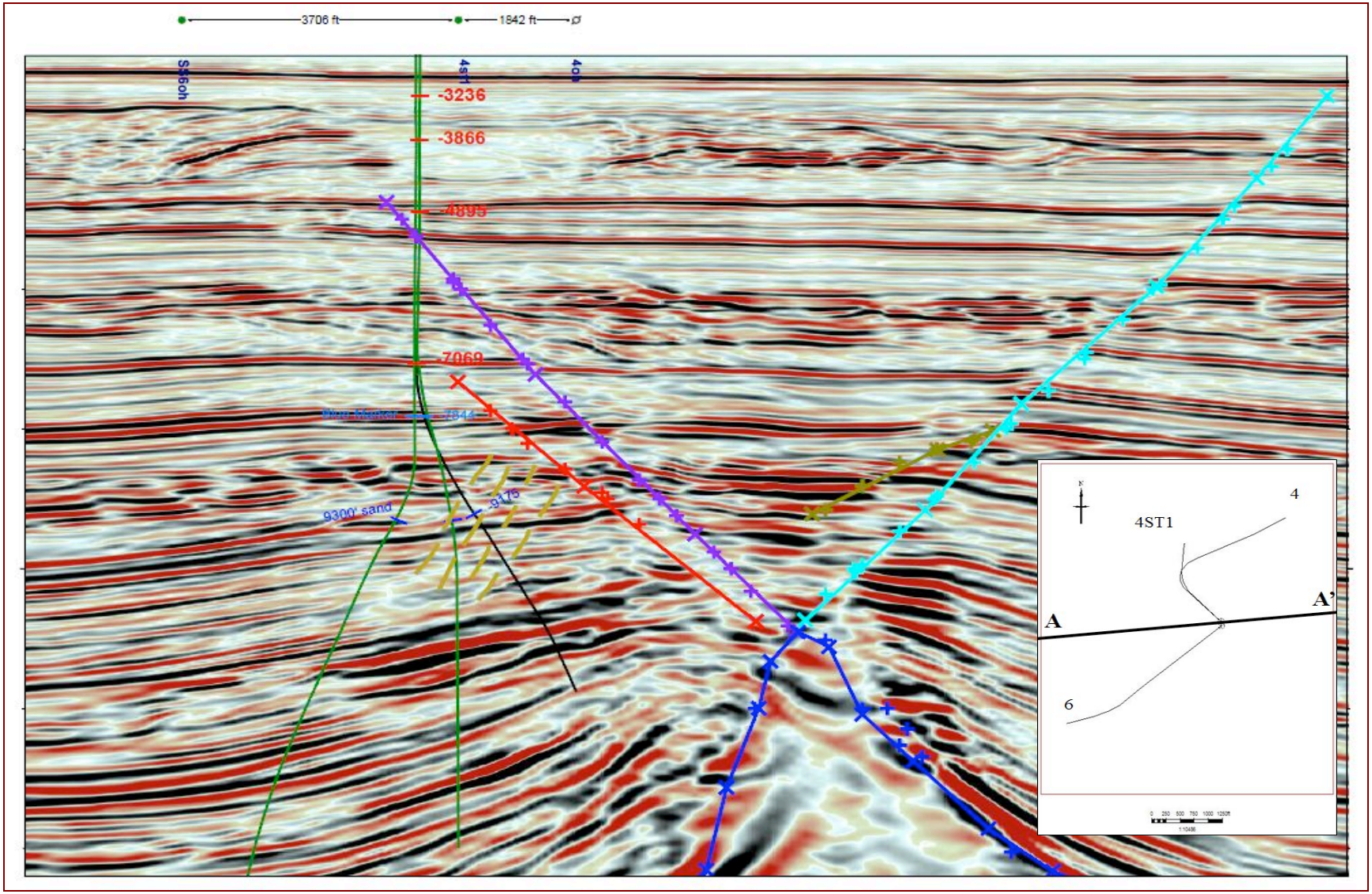

Figure 39. Seismic profile of central section of the study area illustrating complex faulting (brown dashed lines) around a salt structure (blue polygon). All depths are in SSTVD. (Seismic data courtesy of TGS).

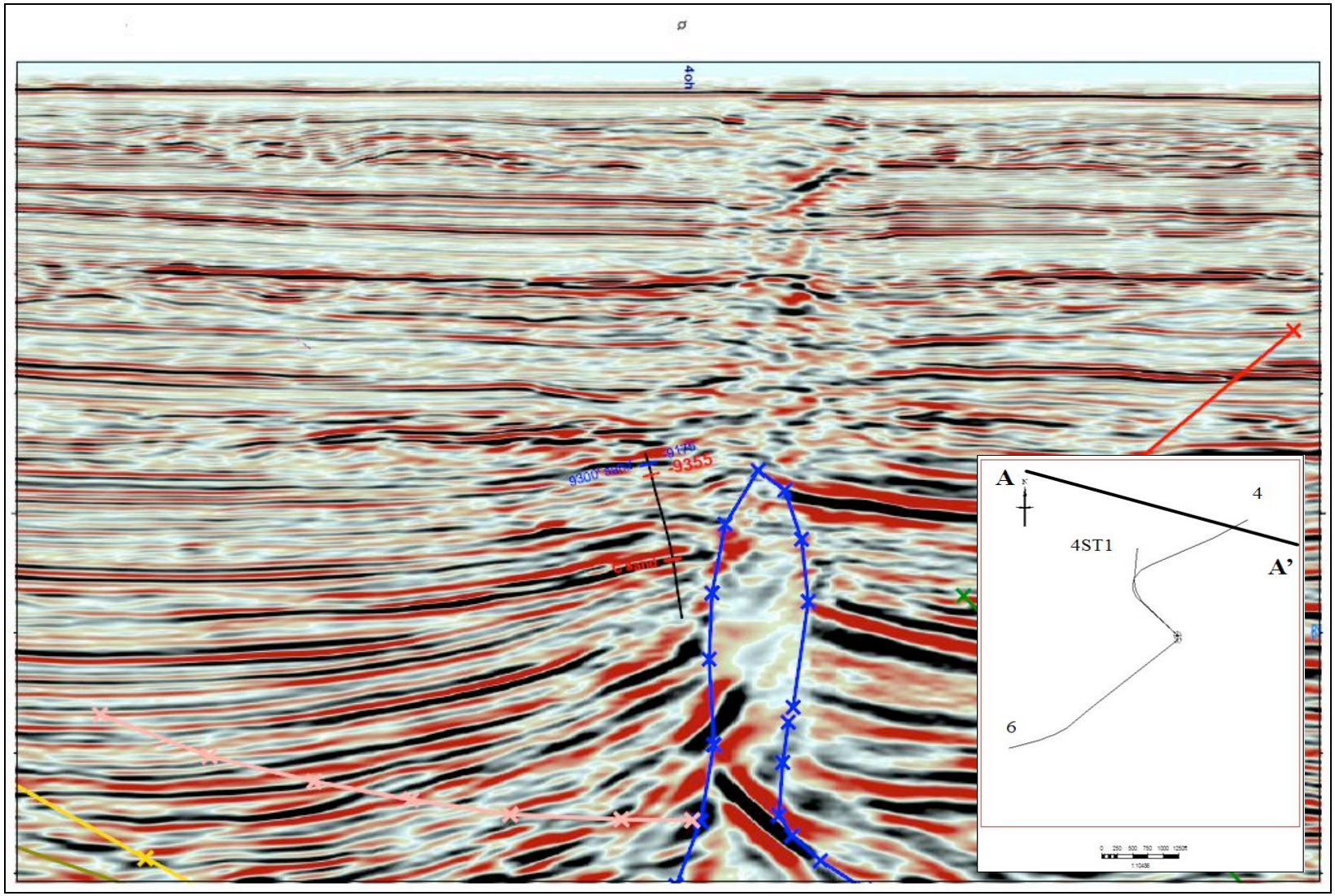

Figure 40. Sesimic cross section showing the #4 well and its proximity to salt (blue polygon). Chaotic seismic reflectors above salt indicate fluid migrating to the sea floor surface. This is also evident by the amplitude response of the sea floor surface (Fig. 41). All depths are in SSTVD. (Seismic courtesy of TGS).

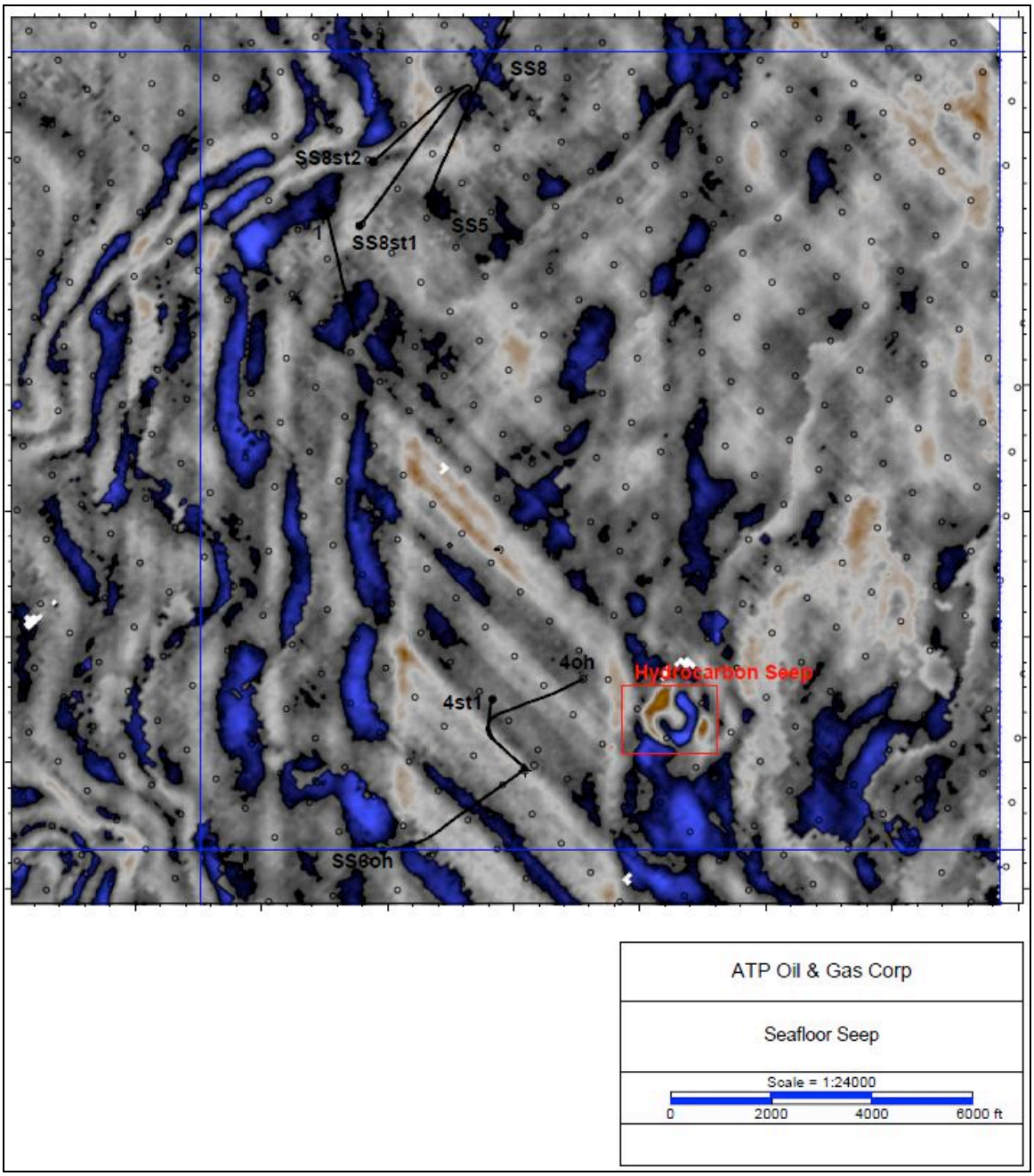

Figure 41. Depth slice (with amplitudes highlighted) of the sea floor surface illustrating hydrocarbon seep associated with salt structure and gas chimney shown in figure 40. (Map created by Clark Walraven of ATP Oil and Gas).

5.3 Southern section variations in salinity

The southern section of the study area (Fig. 5) consists of the #2, #2ST1, #2ST3 and #3 wells (Figs. 43-45). The #2 well has the most complete salinity profile for this

section of the study area and will be discussed in detail. The hydropressured regime in this well most closely resembles the wells in the northern section of the study area where the shallower sediments have not been affected by salt dissolution and brine migration.

The overpressured regime in this section of the study area also closely resembles the overpressured regime in the northern section of the study area. The #2 well contains elevated salinities in a sandy section just after the onset of overpressure similar to the northern section wells. This interval was previously interpreted for the northern section of the study area to be the result of brine migration from a salt structure to the northwest based on the interpreted blue correlation marker horizon structure map in figure 33. From the structure map it is clear that this could not be the case for the wells in the southern section of the study area because of the position of the wells in relation to the previously mentioned salt structure. If the downdip migration of brines is controlled by density differences and gravity the brines would migrate downdip perpendicular to structure contour lines. Instead these salinities could be the result of fluid migration up faults associated with the salt structure in the central section of the study area. The interpreted faults in Figure 33 cut this sandy interval and terminate near the top of the salt structure (Fig. 39). The #2 well also contains a salinity reversal below the high salinity section as seen in other sections.. These salinities are approximately the same as the wells in the central section of the study area suggesting that the central and southern sections are hydrogeologically connected. The rest of the #2 well closely resembles the other wells in this area and exhibits a gradual increase in salinity to approximately 160 g/L with intervals of sandier sediments having less than or equal to salinities as adjacent shales are observed and presumably is due to shale dewatering and mixing of fresher

waters from shales and saline pore waters found in sands. These intervals are best seen in the #2ST1 and #2ST3 (Figs. 42-43) which only illustrate part of the salinity profile for this section of the study area.

In all of the wells within the southern section of the study area a relatively thick hydrocarbon bearing sand is present near the bottom of each well. In the #2 well the sand is approximately 14,700' SSTVD and correlates to the cored sand section in the #6 well (Fig. 16). The wells in the southern section of the field show that this sand is a hydrocarbon bearing sand, but in the #6 well it is wet. The #6 well is located up dip of these wells, which means that in order for the sand in the #6 well to be wet there must be either a fault or some type of flow barrier that would allow hydrocarbons to accumulate in the southern section wells and not migrate up dip into the #6 well. This barrier to flow can be seen in seismic profile (Fig. 46) and is most likely some type of erosional feature due to the break in seismic reflector.

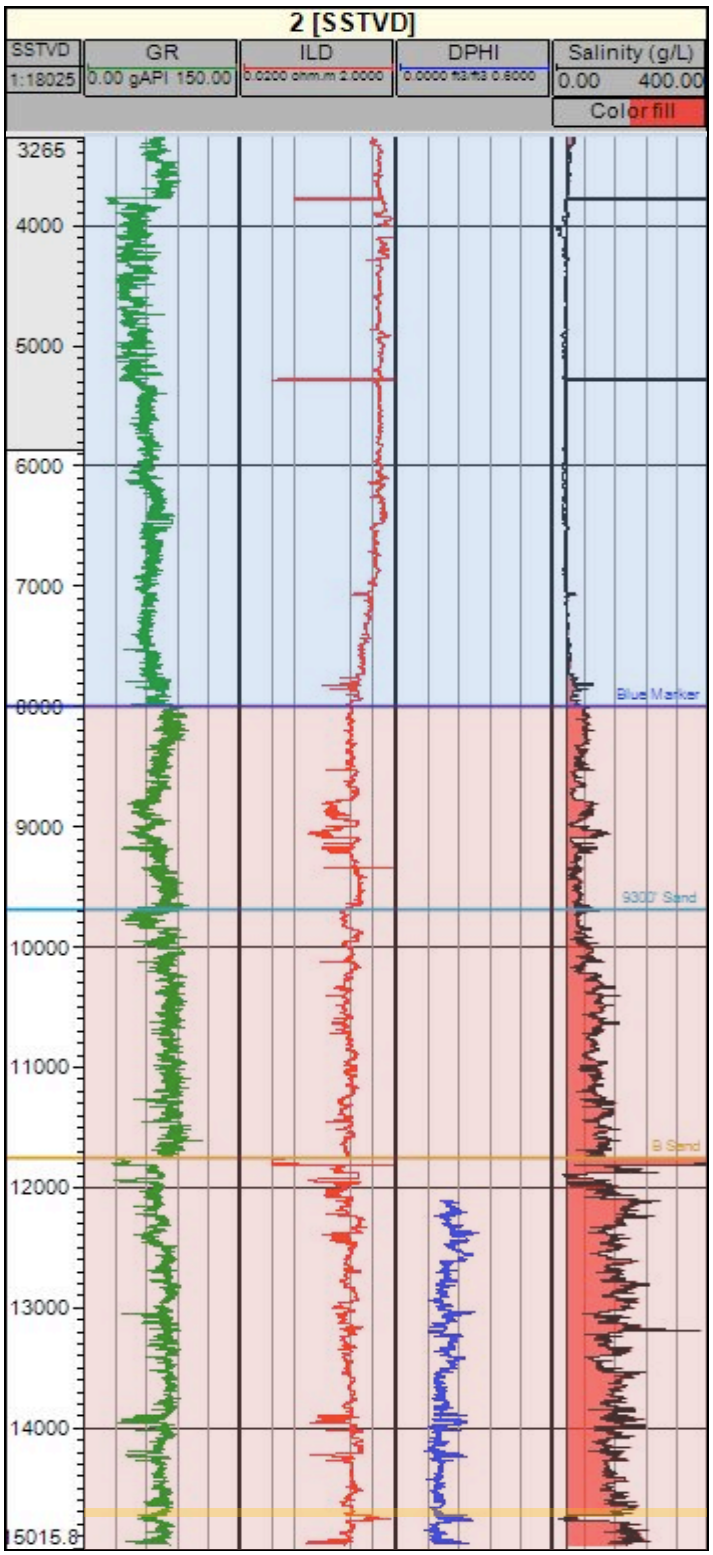

Figure 42. Salinity profile for the #2 well highlighting the hydropressured (blue box) and overpressured (red box) regimes. Blue line represents Blue Correlation marker used for structure contour map. Shaded interval represents hydrocarbon bearing sand interval discussed in previous section and correlates to the #6 cored interval (Fig. 16).

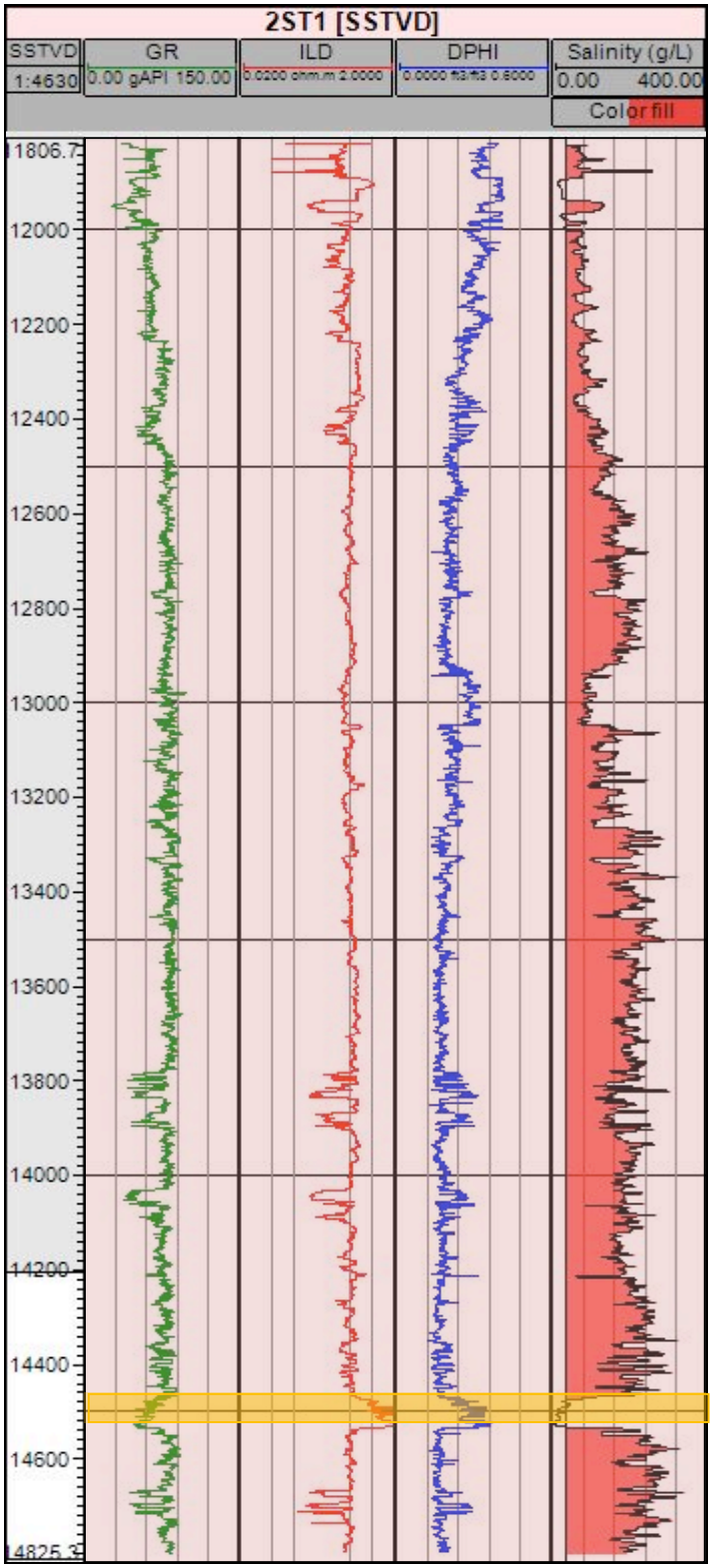

Figure 43. Salinity profile for the #2ST1 well highlighting the overpressured (red box) regime. Shaded interval represents hydrocarbon bearing sand interval discussed in previous section and correlates to the #6 cored interval (Fig. 16).

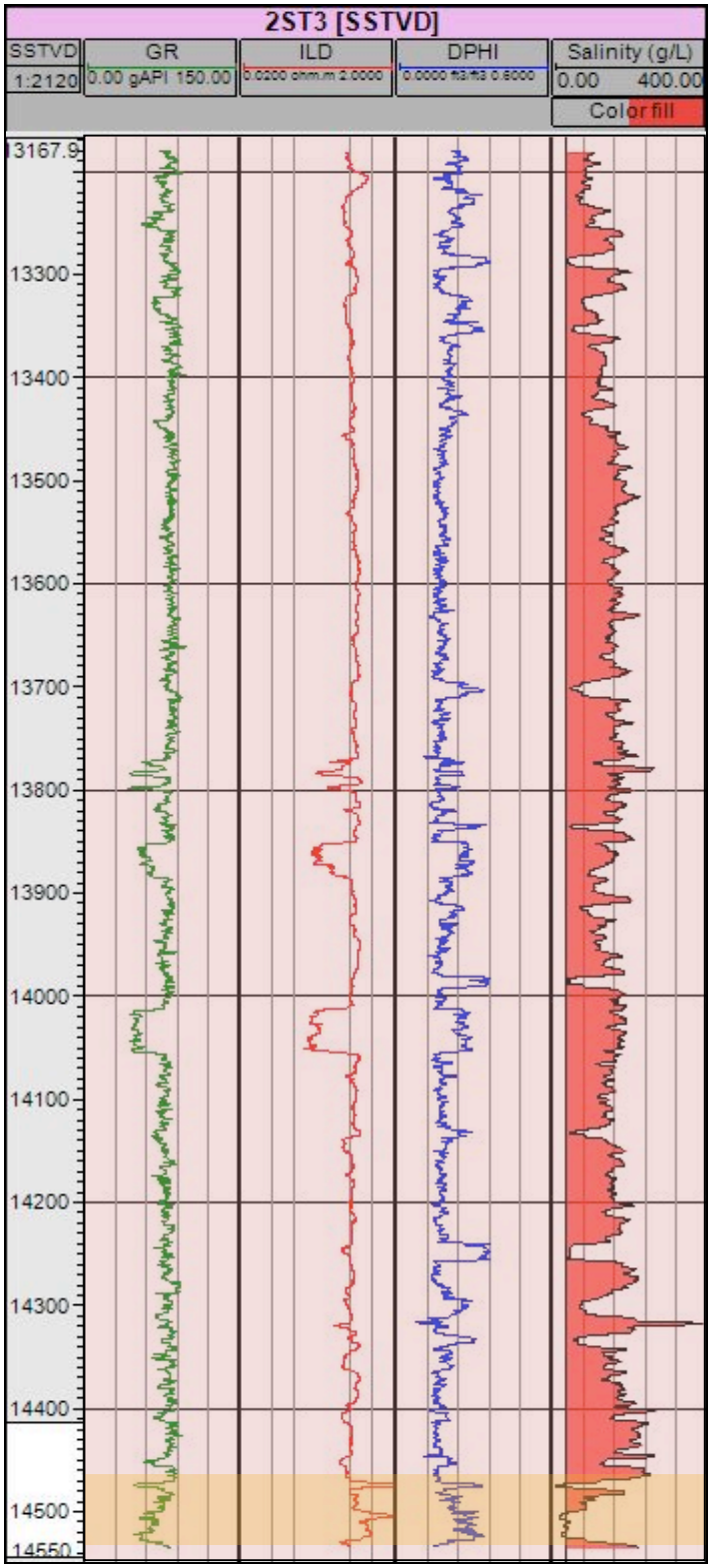

Figure 44. Salinity profile for the #2ST3 well highlighting the overpressured (red box) regime. Shaded interval represents hydrocarbon bearing sand interval discussed in previous section and correlates to the #6 cored interval (Fig. 16).

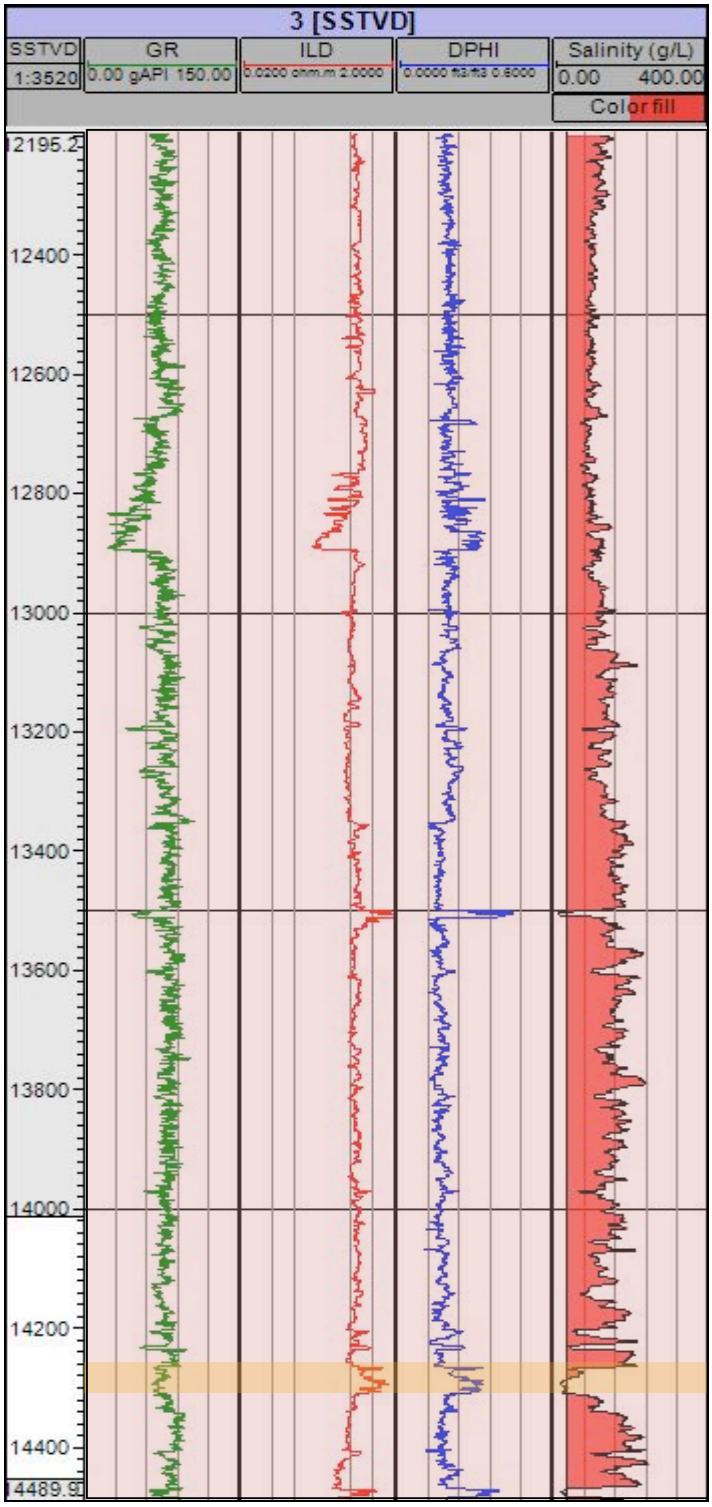

Figure 45. Salinity profile for the #3 well highlighting the overpressured (red box) regime. Shaded interval represents hydrocarbon bearing sand interval discussed in previous section and correlates to the #6 cored interval (Fig. 16).

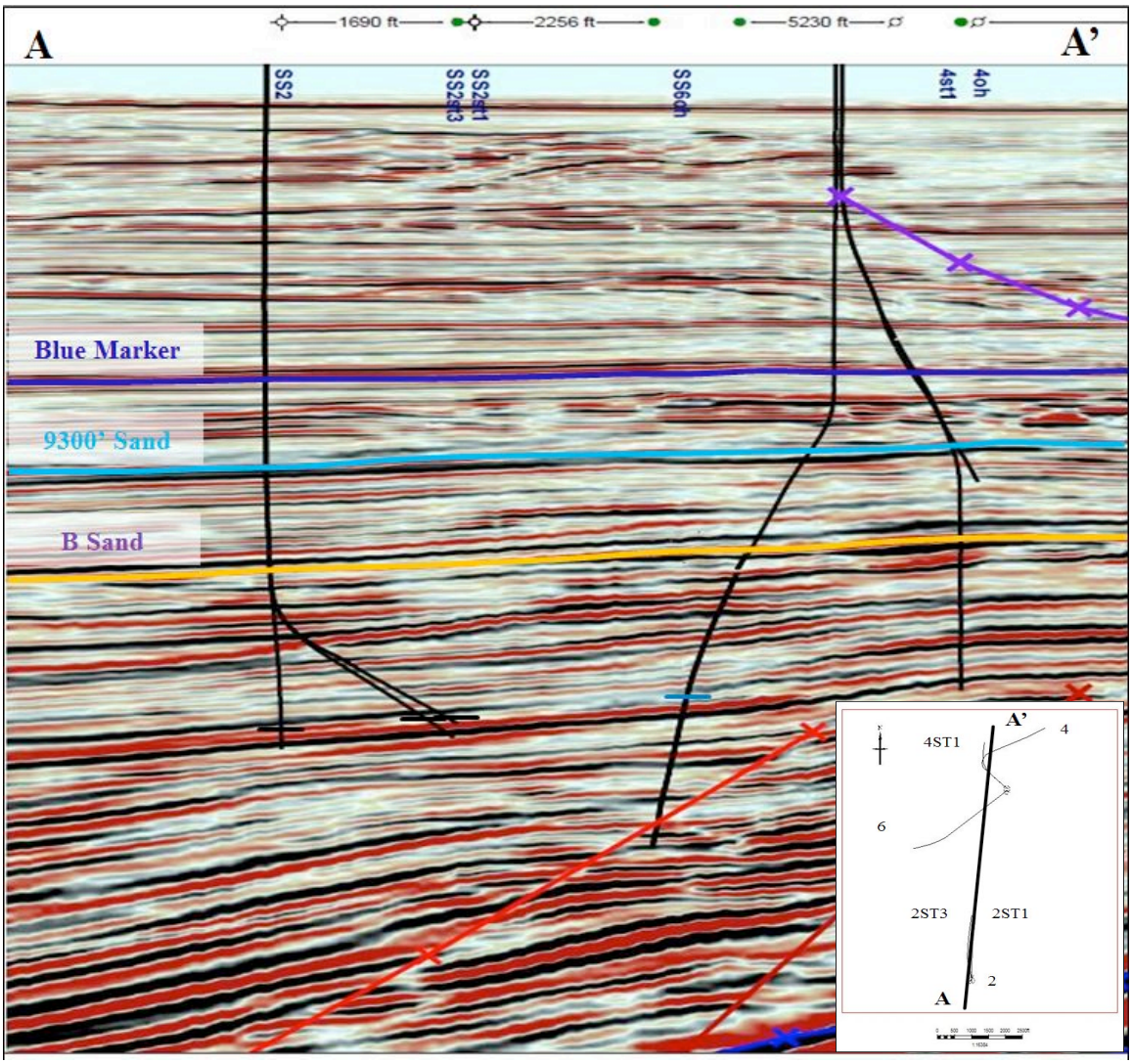

Figure 46. Seismic profile illustrating a break is the seismic reflector that corresponds to a hydrocarbon bearing sand in the southern section of the study area (black well picks) and a wet sand in the #6 well (light blue well picks). (Seismic courtesy of TGS).

CHAPTER 6. CONCLUSIONS

This study has demonstrated that the use of the Revil et al. (1998) method and the Waxman and Smits (1968) correction for hydrocarbons can be a useful method to analyze salinity variations in order to delineate fluid flow pathways and compartmentalization of pore fluids. Errors found in Revil et al. (1998) were corrected and validated the method with core data and well head salinity samples. Within the study area a shallow hydropressured zone with sea water salinity is underlain by a hypersaline geopressured zone. A middle hydrostatically pressured hypersaline zone found in other Gulf of Mexico studies was not observed here. This study was able to determine multiple fluid flow mechanisms such as downdip migration of dense brine fluids from salt structures as well as updip brine migration along fault planes and salt structures into shallower sediments due to overpressure as illustrated in the central and southern sections of the study area. Vertical compartmentalization of reservoirs was evident by the difference in pore fluid salinity of sands and adjacent shales as seen in Figure 35. Sands that exhibited fresher pore waters than adjacent shales were interpreted to be the result of sediment dewatering due to overpressure generation whereas shallower sands with higher salinities than adjacent shales suggested the migration of saline fluids not affected by sediment dewatering. Future work on analyzing variations in salinity should be done using high-resolution core data, well logs and fluid analysis from the RFT (repeat formation tester) tool or any other tool that samples formation fluids. The calibration of core data to well log data and fluid analyses is crucial when calibrating the Revil et al. (1998) method.

REFERENCES

Abid, Iftikhar, and Reinhard Hesse. "Illitizing Fluids as Precursors of Hydrocarbon Migration along Transfer and Boundary Faults of the Jeanned'Arc Basin Offshore Newfoundland, Canada." *Marine and Petroleum Geology* 24.4 (2007): 237-45.

Archie, G. E. "The Electrical Resistivity Log as an Aid in Determining Some Reservoir Characteristics." *Transactions of the AIME* 146.1 (1942): 54-62.

Beall, A. O. Jr., Fisher, A. G. 1969. Sedimentology. In Initial reports of the Deep Sea Drilling Project, Vol. 1, ed. M. Ewing et al. Washington DC: GPO. 672 pp.

Bray, R. B., and Jeffrey S. Hanor. "Spatial Variations in Subsurface Pore Fluid Properties in a Portion of Southeast Louisiana: Implications for Regional Fluid Flow and Solute Transport." *GCAGC Transactions* 40 (1990).

Bruno, R. S., and Jeffrey S. Hanor. "Large-Scale Fluid Migration Driven By Salt Dissolution, Bay Marchand Dome, Offshore Louisiana." *GCAGS/GCSSEPM Transactions* 53 (2003).

Buffler, R. T. "Early Evolution of the Gulf of Mexico Basin." *An Introduction to Central Gulf Coast Geology*. By Duncan Goldthwaite. [New Orleans]: New Orleans Geological Society, 1991. 1-15.

Burst, J. F. "Argillaceous Sediment Dewatering." *Annual Review of Earth and Planetary Sciences* 4.1 (1976): 293-318.

Bussian, A. E. "Electrical Conductance in a Porous Medium." *Geophysics* 48.9 (1983): 1258-268.

Crews, Jennifer R., Paul Weimer, Andrew J. Pulham, and Arthur S. Waterman. "Integrated Approach to Condensed Section Identification in Intraslope Basins, Pliocene-Pleistocene, Northern Gulf of Mexico." *AAPG Bulletin* 84.10 (2000): 1519-536.

Ehrenberg, S. N., and P. H. Nadeau. "Sandstone vs. Carbonate Petroleum Reservoirs: A Global Perspective on Porosity-depth and Porosity-permeability Relationships." *AAPG Bulletin* 89.4 (2005): 435-45.

Ehrenberg, S. N., P. H. Nadeau, and Ø. Steen. "A Megascale View of Reservoir Quality in Producing Sandstones from the Offshore Gulf of Mexico." *AAPG Bulletin* 92.2 (2008): 145-64.

Ehrenberg, S. N., P. H. Nadeau, and O. Steen. "Petroleum Reservoir Porosity versus Depth: Influence of Geological Age." *AAPG Bulletin* 93.10 (2009): 1281-296.

Ellis, Darwin V. *Well Logging for Earth Scientists*. New York: Elsevier, 1987.

Funayama, Masaaki, and Jeffrey S. Hanor. "Pore Water Salinity as a Tool for Evaluating Reservoir Continuity and Fluid Migration Pathways in the Wilcox Group of Central Louisiana: ABSTRACT." *AAPG Bulletin* 79 (1995).

Galloway, Wiliam E., Patricia E. Ganey-Curry, Xiang Li, and Richard T. Buffler. "Cenozoic Depositional History of the Gulf of Mexico Basin." *AAPG Bulletin* 84 (2000).

Hanor, J. S., and J. A. Mercer. "Spatial Variations in the Salinity of Pore Waters in Northern Deep Water Gulf of Mexico Sediments: Implications for Pathways and Mechanisms of Solute Transport." *Geofluids* 10 (2010): 83-93.

Honty, M., P. Uhlík, V. Sucha, M. Caplovicova, J. .. Franců, N. Clauer, and A. Biron. "Smectite-to-illite Alteration in Salt-bearing Bentonites (the East Slovak Basin)." *Clays and Clay Minerals* 52.5 (2004): 533-51.

Larionov, V. V., 1969, Borehole Radiometry: Moscow, U.S.S.R., Nedra

Lin, Guichang, and Jeffrey A. Nunn. "Evidence for Recent Migration of Geopressured Fluids along Faults in Eugene Island, Block 330 from Estimates of Pore Water Salinity." *AAPG Bulletin* 81 (1997).

Lin, Guichang, and Jeffrey A. Nunn. "Evidence for Recent Migration of Geopressured Fluids along Faults in Eugene Island, Block 330 from Estimates of Pore Water Salinity." *GCAGS Transactions* 47 (1997).

Little, Robert E. *An Investigation of a Salt Dome Environment at South Timbalier 54, Gulf of Mexico*. Thesis. Louisiana State University, 2003.

McCammon, Miles A. *Variations in Pore Water Salinities Above and Below Allochthonous Salt Sheets in the Deepwater Gulf of Mexico: Implications for Mechanisms of Solute Transport*. Thesis. Louisiana, 2012.

Nikiel, Amanda M., and Jeffrey S. Hanor. "Spatial Variations in Formation Water Salinities, South Pelto and South Timbalier Areas, Eastern Louisiana Continental Shelf ." *AAPG Bulletin* 83 (1999).

Overton, Harold L., and Aldo M. Zanier. "Hydratable Shales and the Salinity High Enigma." *Society Of Petroleum Engineers Paper No. 2989* (1970).

Pulham, Andrew J. "Variations in Slope Deposition, Pliocene-Pleistocene, Offshore Louisiana, Northeast Gulf of Mexico." *Siliclastic Sequence Stratigraphy: AAPG Memoir 58*. 199-234.

Revil, A., L. M. Cathles, S. Losh, and J. A. Nunn. "Electrical Conductivity in Shaly Sands with Geophysical Applications." *Journal of Geophysical Research* 103.B10 (1998): 23925-3936.

Salvador, Amos. "Late Triassic-Jurassic Paleogeography and Origin of Gulf of Mexico Basin." *AAPG Bulletin* 71 (1987).

Schmidt, Gene W. "Interstitial Water Composition and Geochemistry of Deep Gulf Coast Shales and Sandstones." *AAPG Bulletin* 57 (1973): 321-37.

Spears, Russel W., and Jeffrey A. Nunn. "Relationship between Overpressured Compartments and Spatial Variations in Pore Fluid Salinity in Sediments of South Marsh Island OCS 310, Offshore Louisiana." *AAPG Bulletin* 84 (2000).

Steen, Andrew K., Jeffrey A. Nunn, and Jeffrey S. Hanor. "Indications of Formation Water Flow and Compartmentalization on the Flank of a Salt Structure Derived from Salinity and Seismic Data." *Geofluids* (2011).

Szalkowski, D. Scott, and Jeffrey S. Hanor. "Spatial Variations in the Salinity of Produced Waters from Southwestern Louisiana." *GCAGS/GCSSEPM Transactions* 53 (2003).

Van Wagoner, J. C., H. W. Postmentier, R. M. Mitchum, P. R. Vail, J. F. Sarg, T. S. Loutit, and J. Hardenbol. "An Overview of the Fundamentals of Sequence Stratigraphy and Key Definitions." *Sea-Level Changes—An Integrated Approach, SEPM Special Publication* 42 (1988).

Waxman, M.h., and L.j.m. Smits. "Electrical Conductivities in Oil-Bearing Shaly Sands." *Society of Petroleum Engineers Journal* 8.2 (1968).

Weimer, Paul, Peter Varnai, Fadja M. Budhijanto, Zurilma M. Acosta, Rafael E. Martinez, Alonso F. Navarro, Mark G. Rowan, Barry C. McBride, Tomas Villamil, Claudia Arango, Jennifer R. Crews, and Andrew J. Pulham. "Sequence Stratigraphy of Pliocene and Pleistocene Turbidite Systems, Northern Green Canyon and Ewing Bank (Offshore Louisiana), Northern Gulf of Mexico." *AAPG Bulletin* 82 (1998).

APPENDIX: REVIL METHOD AND HYDROCARBON CORRECTION

The first step in the Revil et al. (1998) method is the calculation of the cation exchange capacity (CEC) for the clays present within the study area. This step involves information that is found in core analyses and from the gamma ray log. In order to properly calculate the CEC the clay mineralogy and volume percentages must be known. This information was obtained from cores that were taken in wells #4ST1 and #5 and the values can be seen in figures 47 and 48 respectively.

	MINERALOGY OF WHOLE ROCK SAMPLE (WEIGHT %)							MINERALOGY OF CLAY FRACTION (RELATIVE %)			
Depth (ft)	Qtz	Ksp	Plag	Cal	Dol	Pyr	Clay	Ill/Smec*	Ill&Mica	Kaol	Chl
11,451.8	65	10	15	0	1	1	8	61	26	9	3
11,465.4	65	10	16	1	1	0	8	64	24	8	4
11,467.8	68	8	16	0	1	0	8	62	27	7	5
11,468.5	71	8	14	0	1	0	5	69	20	7	5
11,781.5	56	11	17	0	1	1	14	58	30	7	5
11,807.3	77	7	7	1	0	1	8	60	24	10	7
11,821.3	73	10	13	0	0	0	5	55	29	9	7
Min:	56	7	7	0	0	0	5	55	20	7	3
Max:	77	11	17	1	1	1	14	69	30	10	7
Avg:	68	9	14	0	1	1	8	61	26	8	5

*Mixed-layer illite/smectite contains 75-80% smectite layer

KEY:

Qtz = Quartz
Ksp = K-feldspar
Plag = Plagioclase
Cal = Calcite
Dol = Dolomite
Pyr = Pyrite
Clay = Total Clay
Ill/Smec = Mixed-layer Illite/Smectite
Ill&Mica = Illite and Mica
Kaol = Kaolinite
Chl = Chlorite

Figure 47. Mineralogy of the whole rock sample and clay fraction determined by x-ray diffraction in the #4ST1 well. (courtesy of Core Laboratories Houston, Texas).

	MINERALOGY OF WHOLE ROCK SAMPLE (WEIGHT %)							MINERALOGY OF CLAY FRACTION (RELATIVE %)			
Depth (ft)	Qtz	Ksp	Plag	Dol	Pyr	Clin	Clay	Ill/Smec*	Ill&Mica	Kaol	Chl
11,246.7	69	9	15	1	0	1	7	55	33	6	6
11,383.25	71	7	14	0	0	3	5	59	30	7	5
11,383.5	75	9	11	1	0	2	3	49	37	5	9
11,417.65	64	8	15	1	0	5	7	55	32	7	6
11,419.3	60	8	16	1	1	5	10	56	29	8	7
11,445.5	73	7	11	1	1	2	7	53	31	9	7
Min:	60	7	11	0	0	1	3	49	29	5	5
Max:	75	9	16	1	1	5	10	59	37	9	9
Avg:	68	8	14	1	0	3	6	54	32	7	7

*Mixed-layer illite/smectite contains 80-85% smectite layer

KEY:

Qtz = Quartz
Ksp = K-feldspar
Plag = Plagioclase
Dol = Dolomite
Pyr = Pyrite
Clin = Clinoptilolite
Clay = Total Clay
Ill/Smec = Mixed-layer Illite/Smectite
Ill&Mica = Illite and Mica
Kaol = Kaolinite
Chl = Chlorite

Figure 48. Mineralogy of the whole rock sample and clay fraction determined by x-ray diffraction in the #5 well. (courtesy of Core Laboratories Houston, Texas).

The cation exchange capacity can be calculated using the equation

$$CEC = \varphi_w \sum_i \chi_i CEC_i \tag{1}$$

where CEC is the cation exchange capacity, φ_w is the clay weight fraction, χ_i is the relative fraction of each clay mineral type, and CEC_i is the cation exchange capacity of each clay mineral type. The CEC_i values for the clays found within this study area are documented in Thomas (1976) and listed here: $CEC_{kaolonite} \approx .03$ meq/g, $CEC_{chlorite} \approx .01$ meq/g, $CEC_{illite} \approx .09$ meq/g, $CEC_{smectite} \approx .8$ meq/g. The clay content and the CEC are important for this study because of the different electrical properties of each clay type. This difference is apparent in the values listed above when comparing the cation exchange capacity of smectite and illite.

The clay weight fraction of the rock used by Revil et al. (1998) (Eq. 2a) and in this study (Eq. 2b) are

$$\varphi_w = \frac{(\gamma_{\log} - \gamma_{sd})}{(\gamma_{sh} - \gamma_{sd})} \tag{2a}$$

$$\varphi_{Larinov} = .083(2^{(3.7\varphi_w)} - 1) \tag{2b}$$

where γ is the gamma ray value indicated on the log, γ_{sd} is the gamma ray value of clean sand (assumed to be 10 API units) and γ_{sh} is the gamma ray value of pure shale. The gamma ray values for pure shale were calculated using the experimental gamma ray values and clay type percentages. Assuming that the gamma ray log is only reading the clay portion of the rock, then a rock containing 100 percent clay will have a predictable gamma ray value based on the fractions of each clay mineral. Typical gamma ray values for clays are found in Ellis (1987) and listed here: kaolonite ≈ 80-130 API units, chlorite ≈ 180-250 API units, illite ≈ 250-300 API units, smectite ≈ 150-200 API units and the mixed layer clay values in this study area are approximately 170 API units . The equation to calculate the gamma ray value of pure shale for the study area is

$$\gamma_{sh} = \sum_i \chi_i \gamma_i \tag{3}$$

where γ_{sh} is the gamma ray value of pure shale, χ_i is the relative fraction of each clay mineral type and γ_I is the gamma ray value of each clay mineral type. Using the relative clay fractions from the #4ST1 well shown in figure 44 gamma ray value for pure shale is approximately 184 API units. Once the CEC has been calculated, it is possible to calculate Q_v, or the excess surface charge.

$$Q_v = \rho_g \left[\frac{1-\phi}{\phi}\right] CEC \tag{4}$$

where ρ_g is the grain density (2.65 g/m^3 for quartz), Φ is the porosity, and CEC is the cation exchange capacity calculated from equation 1. This excess surface charge is used to calculate the surface conductivity of the clay minerals.

The surface conductivity (σ_s) is calculated from the equation

$$\sigma_s = \left(\frac{2}{3}\right)\left[\frac{\phi}{1-\phi}\right] Z_s \beta_s Q_v \tag{5}$$

where Φ is the porosity, Z_s is the valence of the counterions ($Z_s = 1$ for Na^+), β_s is an equivalent surface mobility for the surface electrical conduction process ($\beta_s = 5.14 \times 10^{-9}$ m^2/sV at 25 °C) and Q_v is the excess surface charge calculated from equation 4. In equation 5, β_s must be corrected for temperature using the equation

$$\beta_s(T) = \beta_s(T_0)\left[1 + \upsilon_s\left(T - T_0\right)\right] \tag{6}$$

where β_s (T) is the equivalent surface mobility at a subsurface temperature (T) in °C, β_s (T_0) is the equivalent surface mobility at T_0 (25 °C) and υ_s is a coefficient approximately equivalent to .04 per °C for Na^+. The subsurface temperature (T) used in this equation is calculated using information from the well log headers to establish a geothermal gradient for each well within the study area and interpolating a temperature at a given true vertical depth.

The temperature that is used in the previous equation comes from the well log header bottom hole temperature (BHT) and is corrected for effects caused from the circulating drilling fluid used during the drilling process. As the fluid comes in contact with the rock formations it is heated and circulated through the mud system. Since the LWD tool is measuring the temperature of the mud, a correction must be made to account

for the difference between the mud temperature and the true formation temperature. For this study the Kehle (1971) correction was used which is an empirical correction that takes into account the BHT recorded in the well along with the true vertical depth (TVD) of the well. This correction was calculated with Gulf Coast data from depths of one to three kilometers, therefore it is appropriate for this study. The equation for the Kehle (1971) correction is

$$BHT_C = BHT - \left[\left(\left(8.819 * 10^{-12}\right) TVD^3\right) - \left(\left(2.143 * 10^{-8}\right) TVD^2\right) + \left(\left(4.375 * 10^{-3}\right) TVD\right) - 1.018\right] \quad (7)$$

where BHT_C is the corrected BHT in °F, BHT is the bottom hole temperature in °F located in the log header and TVD is the true vertical depth in feet of the recorded BHT. Once this correction is made the corrected BHT is used in conjunction with the sea floor temperature (6 °C) found in figure 46 to establish a geothermal gradient, which can then be used to interpolate temperatures throughout the length of the well. The geothermal gradient is calculated from

$$G = \frac{\left(BHT_C - T_{SF}\right)}{TVD} \quad (8)$$

where G is the geothermal gradient in °F/ft, BHT_C is the corrected bottom hole temperature in °F calculated in equation 7, T_{SF} is the sea floor surface temperature in °F, and TVD is the true vertical depth in feet from the sea floor. All temperatures were converted into degrees Celsius for use in the Revil et al. (1998) method.

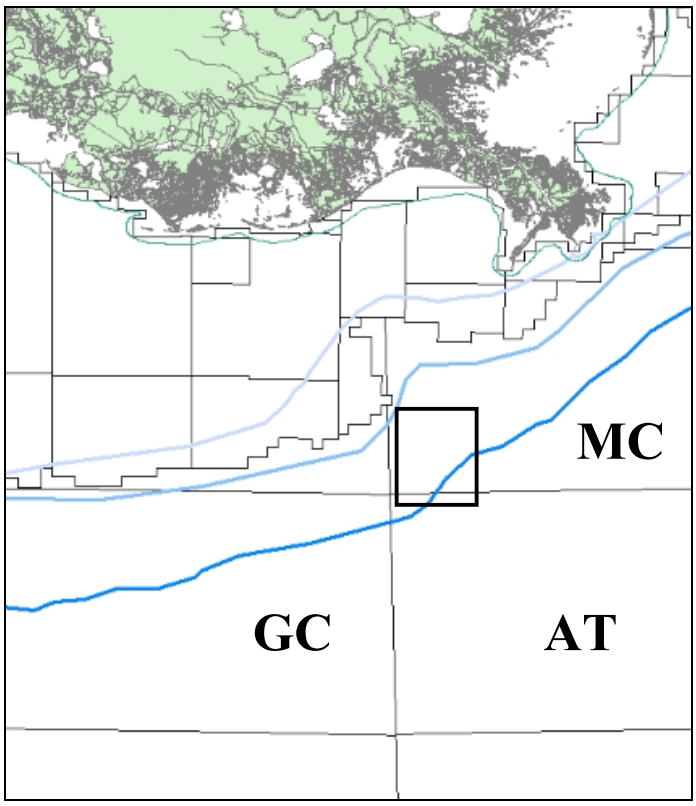

Figure 46. Seafloor temperature map of the Gulf of Mexico. The study area (black square) has seafloor temperatures of approximately 6°C (dark blue contour line). MC = Mississippi Canyon, AT = Atwater Valley, GC = Green Canyon (Data from USGS)

The next step in the Revil et al. (1998) method is to calculate the fluid conductivity. The fluid conductivity is a measure of the conductivity of the pore water within the formation and is related to the salinity of the formation fluid. The equation is

$$\sigma_f = (\sigma F) - 2(F-1)\sigma_s \tag{9}$$

where σ_f is the fluid conductivity, σ is the conductivity derived from the deep induction log, F is the formation resistivity factor and σ_s is the surface conductivity derived from equation 5. The formation resistivity factor is derived from Archie's (1942) law

$$\left(\frac{a}{F}\right) = \phi^m \tag{10}$$

where a is 0.81 (a simpler form equivalent to the Humble formula), F is the formation resistivity factor, Φ is the porosity, and m is the cementation exponent. The cementation exponent can be estimated based on lithology, but for this study it is calculated using

$$m = m_0 + \alpha Q_v \left[\frac{\phi}{1-\phi}\right] \tag{11}$$

where m is the cementation exponent, m_0 is the cementation exponent of a clean sand (assumed to be approximately 1.80), α is a coefficient that relates cementation exponent to CEC (approximately 1.80 mL/meq), Q_v is the excess surface charge calculated from equation 4, and Φ is the porosity. The fluid conductivity must be corrected for temperature with the equation

$$\sigma_f(T) = \sigma_f(T_0)\left[1 + \upsilon_f(T - T_0)\right] \tag{12}$$

where $\sigma_f(T)$ is the fluid conductivity corrected for temperature (T) in °C, $\sigma_f(T_0)$ is the fluid conductivity at 25 °C (T_0), and υ_f is a coefficient approximately equal to .023/°C. Fluid conductivity is approximately proportional to salinity and can be estimated with the equation

$$C_f = 0.56\left[\frac{\sigma_f(T)}{5}\right] \tag{13}$$

where C_f is the salinity in mol/L and $\sigma_f(T)$ is the fluid conductivity that was calculated in equation 12. For this study the salinity was converted from mol/L into g/L with the equation

$$Salinity = 58.443 C_f \tag{14}$$

where 58.443 is the conversion factor and C_f is the salinity calculated from equation 13. This estimated salinity calculation is primarily used for zones that are considered water

saturated or "wet" and not for zones that have both water and hydrocarbons within the pore space. When zones that are charged with hydrocarbons are encountered the Revil et al. (1998) method must be corrected for high resistivity values associated with hydrocarbons. Hydrocarbons have a higher resistivity value and act as an insulator within the pore space (Ellis 1987). Since the study area is a hydrocarbon producing field, many of the wells drilled encountered both water wet and hydrocarbon charged zones. Therefore, both the Revil et al. (1998) method and the Waxman and Smits (1968) correction for hydrocarbons must be used in order to properly evaluate "wet" zones and hydrocarbon bearing zones. Waxman and Smits (1968) proposed two corrections with equations

$$\phi^m = \phi^m S_w^n \tag{15}$$

$$Q_v = \frac{Q_v}{S_w} \tag{16}$$

where Φ is the porosity, m is the cementation exponent (equation 11), S_w was obtained from core analysis, n is the saturation exponent (assumed to be 2), and Q_v is the excess surface charge (equation 4). Once the corrections from Waxman and Smits (1968) have been calculated, the new values (Φ^m and Q_v) can be substituted into the Revil et al. (1998) method to calculate salinity.

VITA

William Daugherty was born in Gretna, Louisiana in June of 1986 to the parents of William Thomas and Susan Daugherty and the brother of Robert Daugherty. After living in New Orleans, Louisiana for six years William moved with his family to Jakarta, Indonesia where his father worked as a drilling engineer for Conoco. Two years later they moved to Dubai, United Arab Emirates where they resided for five years until moving to Houston, Texas. William Daugherty attended Cypress Falls High School for three years before transferring to Foster High School his senior year. Upon graduating high school in January 2004, William joined the United States Marine Corps as a machinegunner in the infantry and was deployed to Iraq in August 2004. After completing his tour in Iraq that ended in March 2005 William returned to the United States to finish his contract with the Marine Corps before he moved to Nashville, Tennessee. While in Nashville, Tennessee William completed his Bachelors of Science degree in Geosciences at Austin Peay State University and married Morgan Gates who he had met in high school. After their wedding, William and Morgan moved to Baton Rouge, Louisiana where William attended Louisiana State University to obtain a Masters of Science in Geology. Upon graduation William and Morgan Daugherty will be moving to Houston, Texas where William will be working for Devon Energy as a geologist.